SEARS FOUNDATION FOR MARINE RESEARCH
BINGHAM OCEANOGRAPHIC LABORATORY, YALE UNIVERSITY

JOURNAL OF
MARINE RESEARCH

VOLUME 16 1958 NUMBER 3

OBSERVATIONS OF SURFACE PHENOMENA IN OCEAN AND COASTAL WATERS NEAR JAPAN

By

KIYOMITSU KITANO

Tohoku Regional Fisheries Research Laboratory, Shiogama, Miyagi Prefecture, Japan

ABSTRACT

Surface phenomena of many kinds were observed from boats and aircraft over the Kuroshio Extension off the coast of Japan and from aircraft in the coastal area from Cape Inubo to Kinkazan. The distribution of these surface phenomena (both natural and artificial) have been correlated with observed oceanic conditions, principally areas of upwelling.

INTRODUCTION

The ocean surface is by no means monotonous due to changing light and color, different types of waves, slicks, streaks, rips, and concentrations of organic matter, bubbles, debris, and other drifting objects. Mariners and fishermen have observed these surface phenomena for centuries, and of recent years they have become a subject of considerable interest. A comprehensive study of the current rip was published in 1938 by Uda, and subsequently numerous American workers contributed valuable studies of natural slicks, surface films, streaks, and similar phenomena (Dietz and LaFond, 1950; Ewing, 1950; Stommel, 1951; Ford, *et al.*, 1952; von Arx, *et al.*, 1955; Cromwell and Reid, 1956).

The present paper reports observations of the distribution of various surface objects (natural and artificial) by skipjack fishermen in boats

and by Japanese oceanographers in aircraft over the Kuroshio Extension, and by observers in aircraft over the coastal area of Japan from Cape Inubo to Kinkazan. These observations have been correlated to some extent with observed oceanic conditions, but more detailed study remains for the future.

OBSERVATIONS BY SKIPJACK FISHERMEN

During summer 1956, skipjack fishermen, in their search for schools of these fish, observed and prepared detailed reports and sketches of the distribution of various kinds of surface phenomena and differences in sea color. Fig. 1 shows a compilation of their observations by

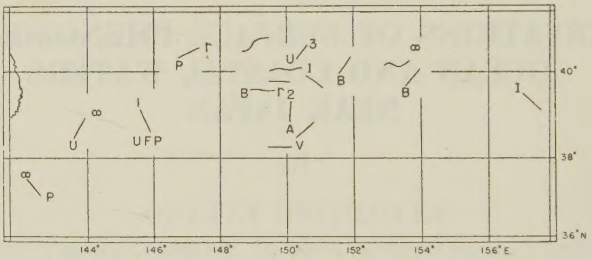

Figure 1. Solid lines show presumed direction of surface phenomena, based on original sketches by fishermen. B indicates biological aggregations; F, feathers; V, vortices; P, timbers and wood products; A, algae; U, bubbles; numerals, number of streaky slicks; r, several bands; ∞, countless number of surface phenomena.

latitude and longitude; B represents biological concentrations such as jellyfish, *Physalia*, etc.; F, feathers; V, vortices; P, wood products; A, algae; and U, bubbles. Most of these phenomena were accompanied by several bands of streaky slicks; a numeral indicates the number of slicks noted; r indicates several bands; ∞ indicates a vast area of countless patches. The presumed direction of a slick has been taken from the original sketches made by the fishermen. Their widths were frequently 10–40 m, but sometimes widths of 1000 m or more were reported. The slicks varied greatly in length, 1–10 km being reported most commonly. Temperature and color differences between the two sides of a slick were also observed; the color was mostly whitish-blue or greenish in the cold water and dark blue in the warm water. Surface phenomena were observed also at 164°E, 41°N, but these observations are not shown in Fig. 1.

Cold low-salinity water occurs on the northern edge of the Kuroshio Extension, a phenomenon parallel to that reported for the Gulf Stream (Ford, *et al.*, 1952). Fig. 2 shows the location of the Kuroshio

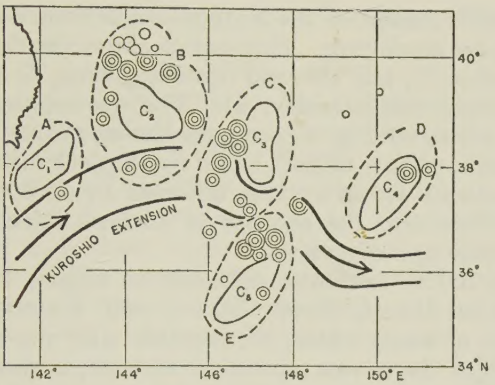

Figure 2. Surface phenomena relative to cold upwelling areas (C_1–C_5) adjacent to the Kuroshio Extension (heavy solid lines); a single circle indicates either few surface markings or a directional observation; a double circle indicates some surface objects; a triple circle indicates many or countless surface objects.

Extension together with its main axis as well as the cold upwelling areas on its northern boundary—C_1, C_2, C_3, C_4—and on its southern boundary—C_5. The data are based on isotherms observed at a depth of 100 m from 13 August to 13 September 1955 by the RYOFU-MARU. The circles indicate the location of surface phenomena observed by the skipjack boats from 4 June to 17 September; a single circle represents a directional observation, or indicates that the surface objects were few in number; a double circle denotes the fact that a number of objects were present; and a triple circle indicates many or even countless phenomena. Apparently the surface phenomena were essentially restricted to these cold areas, as the broken lines on the periphery of each upwelling area indicate.

A section of isotherms (Fig. 3) demonstrates further the correlation of zones of upwelling and surface phenomena. For this purpose iso-

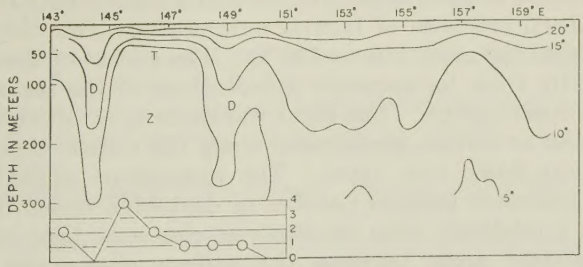

Figure 3. Sectional plane showing relationship of surface phenomena to upwelling. T, thermocline; Z, cold upwelling zone; and D, sharp thermal discontinuity. The lower left curve gives the number of areas of surface phenomena found at 39°30′–40°30′N.

therms along 40°N, taken by the KYOSEI-MARU from 31 July through 5 August 1950, are employed. This section shows clearly the elevation of the thermocline, T, and the cold upwelling zone, Z, surrounded by the sharp thermal discontinuity, D. The accompanying graph in the lower left corner of Fig. 3 correlates the upwelling area with the number of areas of surface objects found by skipjack fishermen (during their fishing season) within an area bounded by 39°30′–40°30′N and 143°–160°E. Note also the absence of surface objects from 151°–160°E, outside the upwelling area.

Fig. 4, with 100 m isotherms obtained in August 1954 by SOYO-MARU, KITAKAMI-MARU, RYOFU-MARU, and KAIYO-MARU NO. 4, shows a tongue of warm water, W, together with the cold upwelling area, C. Each of the circles represents surface phenomena noted by

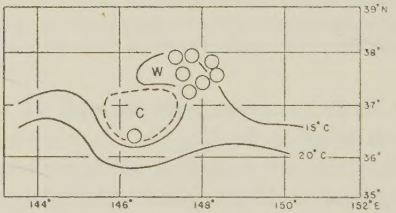

Figure 4. Surface phenomena in the area where warm water, W, comes into contact with cold water, C; based on 100 m isotherms. Circles indicate locations of surface phenomena.

skipjack fishermen during the 1954 fishing season. The relation of surface objects to this oceanographic complex seems to demonstrate that such oceanic conditions are favorable for a concentration of surface objects.

OBSERVATIONS FROM AIRCRAFT

Kuroshio Extension. A wide-angle time-lapse motion picture camera mounted in an aircraft was used in a survey on 29 May 1956 to detect visual evidence of frontal outcroppings over the Kuroshio Extension from the coast out to 144°E. The course of the flight was planned partly from temperature observations of the sea and partly from visual observations. The flight was made at an altitude of about 3000 feet, and as surface phenomena along the course were observed, the plane was flown over them. The phenomena appeared as ensembles of countless isolated patches of dark-blue midst the whitish blue sea; in a relatively calm sea these patches were light and ruffled. The intermittent areas between the surface phenomena probably arose from the same causes which created the shingling structure of the Gulf Stream noted by von Arx, *et al.*, (1955). Also, the coinci-

dental occurrence of upwellings and surface phenomena are assumed to be characteristic.

Cape Inubo to Kinkazan. On 20 May 1956 an aerial survey was carried out over the coastal sea area from Cape Inubo to Kinkazan, almost all of it along 142°E. The abundance of surface phenomena in the coastal area was striking. Most outstanding in this area were the long narrow bands which were frequently composed of bubbles and which were of a different color from the surrounding waters. The various objects in the coastal area were classified into seven major types: the single and concentrated; the single and scattered; the multiple and concentrated; the multiple and scattered; the crossed; the branched; and the showered [*sic*].

ACKNOWLEDGMENTS

Most of the cost of the aerial survey was paid from funds supplied by the Fishery Agency of the Agriculture and Forestry Ministry, by the Fishery Experiment Stations of the Ibaragi, Chiba, Fukushima, Miyagi, Iwate and Aomori Prefectural governments, and by the fishery industries; the support from all is gratefully acknowledged. I also wish to express my thanks: to Dr. K. Kimura for helpful suggestions; to Dr. Kimura and Mr. T. Kuroda for constant guidance during the aerial survey; to Dr. H. Stommel of the Woods Hole Oceanographic Institution; and to the crews of the many fishing boats who kindly made observations for this study.

REFERENCES

Cromwell, Townsend and J. L. Reid
1956. A study of oceanic fronts. Tellus, *8:* 94–101.
Dietz, R. S. and E. C. LaFond
1950. Natural slicks on the ocean. J. Mar. Res., *9:* 69–76.
Ewing, Gifford
1950. Slicks, surface films and internal waves. J. Mar. Res., *9:* 161–187.
Ford, W. L., J. R. Longard and R. E. Banks
1952. On the nature, occurrence and origin of cold low salinity water along the edge of the Gulf Stream. J. Mar. Res., *11:* 281–293.
Stommel, Henry
1951. Streaks on natural water surfaces. Weather, March 1951: 72–74.
Uda, M.
1938. Researches on "Siome" or current rip in the seas and oceans. Geophys. Mag., *11:* 307–372.
von Arx, W. S., D. F. Bumpus and W. S. Richardson
1955. On the fine-structure of the Gulf Stream front. Deep-sea Res., *3:* 46–65.

THE MIGRATION OF ADULT FEMALE BLUE CRABS, *CALLINECTES SAPIDUS* Rathbun, IN CHINCOTEAGUE BAY AND ADJACENT WATERS[1]

By

DAVID G. CARGO

Department of Research and Education
Chesapeake Biological Laboratory
Solomons, Maryland

ABSTRACT

A total of 392 adult female blue crabs were tagged at four different points in the Chincoteague Bay area from 31 July to 7 September 1953. Over a period including June 1954, about 25% were recaptured, mostly to the south of the release points. Only three had moved northward, and only two were recaptured outside the area; one in Delaware Bay and one at Oyster, Virginia. Factors that may influence their movements and some ecological considerations are discussed.

INTRODUCTION

The Chincoteague Bay area, composed of Chincoteague, Sinepuxent, Isle of Wight, and Assawoman Bays, is an estuarine system separated from the Atlantic Ocean by a series of narrow barrier islands with major inlets at Ocean City, Maryland, and Chincoteague, Virginia. An ecological study of this area was initiated in August 1951, primarily to determine the cause or causes of the marked decline in oyster production. The biology of the blue crab, *Callinectes sapidus* Rathbun, in these waters was included in this study since the crab is closely associated with the oyster communities and is, in itself, a valuable marine resource. The present paper deals with its migratory activities in these waters. Knowledge of its movements is necessary to an understanding of its life history and might aid in providing an estimate of the amount of recruitment and/or loss from the resident population. Ultimately, these studies might form a basis for necessary management practices that would avoid erroneous procedures based solely on findings in other estuaries.

[1] Contribution No. 121, Chesapeake Biological Laboratory, Maryland Department of Research and Education, Solomons, Maryland.

The pattern of movement of the blue crab in Chesapeake and Delaware bays has been the subject of extensive studies. In 1925 Fiedler (1930) tagged almost 1800 crabs in the Chesapeake area and recaptured 10.8%. Later Truitt (1936, 1937) tagged more than 4600 crabs, by several methods, in the same body of water. Although two of his methods failed to provide a large number of returns, results from the entire series were adequate to outline some of the patterns being followed by the crabs. From 1943 to 1946, Cronin released over 1300 crabs in the Chesapeake area. The bright red external tags used in this experiment provided a high (22.6%) rate of return. Cronin's data substantiated and refined the findings of Fiedler and Truitt, and in 1949 he summarized the results of various tagging observations. These workers determined that female crabs, after reaching maturity, move toward the mouth of Chesapeake Bay, wintering near the spawning area and moving into it during the spring. The males showed a nondirectional and random migratory pattern.

In Delaware Bay, Cronin (1952, 1954) tagged over 1100 crabs from 1952 to 1954. Returns from these releases indicated that the crabs there move widely, with no simple pattern, and that adult females move both up and down the estuary. No specific movement toward the capes was observed but, as Cronin pointed out, there is little crabbing conducted at the capes so that returns from that area would be limited.

There is no published information available concerning the movements of blue crabs inhabiting Chincoteague Bay and its adjacent waters. The direction of movement, the effects exerted by inlets, and any tendency they may have toward congregating or schooling during the winter are points to be considered. The discussion in this paper is based almost entirely on the results of tagging. It is unfortunate that adequate supplementary information on the habits and life history of the crab in Chincoteague Bay is not available.

ACKNOWLEDGMENTS

I should like to thank a number of people without whose help this study could not have been completed: Mr. Fred W. Sieling who supervised field operations; Mr. Eric Matthews who carried out most of the tagging and who collected other data throughout the study. The tag returns were handled through the United States Fish and Wildlife Service. Additional thanks are due Dr. R. V. Truitt and Dr. L. Eugene Cronin who gave encouragement and counsel and who helped in the preparation of the manuscript.

DESCRIPTION OF THE AREA

The Chincoteague Bay area covers about 120 square miles at mean low tide (Truitt, 1953). The shores of the embayments are characterized by low relief and support a typical saltmarsh succession consisting primarily of cordgrass, *Spartina alternifolia* Loisel. The bays, adequately described by Sieling and McGary (1952), are shallow, averaging about five feet in depth; and the bottom consists mostly of mud and sand. The watershed of the area amounts to only 205 square miles, thus providing little freshwater runoff. During certain periods of the summer, evaporation exceeds precipitation to such an extent that the central part of the bay may exhibit higher salinities (>35 ‰) than those found in the open ocean (McGary and Sieling, 1953). The effects of the two inlets are marked, causing a system of complex tides and currents which influence temperature and salinity distribution to some degree throughout the area. Tidal currents near the inlets provide an influx of ocean water accompanied by considerable flow while those portions of the bay remote from these inlets undergo little change from these tidal movements. The currents within most of Chincoteague Bay, primarily due to wind, are so slight (0.3 knots) that accurate measurements are difficult to obtain. Fig. 1 gives the surface salinity distribution from Ocean City to Chincoteague Inlet during the period of study.

METHODS AND MATERIALS

Tagging was limited to adult female crabs for two reasons: 1) Male crabs exhibit no recognizable indication of the attainment of maximum size whereas females do in that the triangular abdomen becomes broad and semicircular. By tagging such specimens, there was assurance that the tag would not be lost through molting. 2) There might be some indication of movement toward the spawning areas. The experimental animals were obtained through the co-operation of commercial crabbers who permitted the investigators to accompany them when fishing their gear. The crabs were tagged and released in the area where they were captured; this avoided displacement of tagged animals to another area and prevented the uncertain effects of holding them out of water for extended periods.

The red plastic strip tags used have been described by Cronin (1949). Each tag, prior to use, was provided with a two inch loop of soft stainless steel wire (.022 in.) at the left end and a straight length (about 5 in.) of the same wire at the other end. The tags were then arranged in numerical order on strips of masking tape in groups of 25 to facilitate recording at the time of tagging. The tag was applied

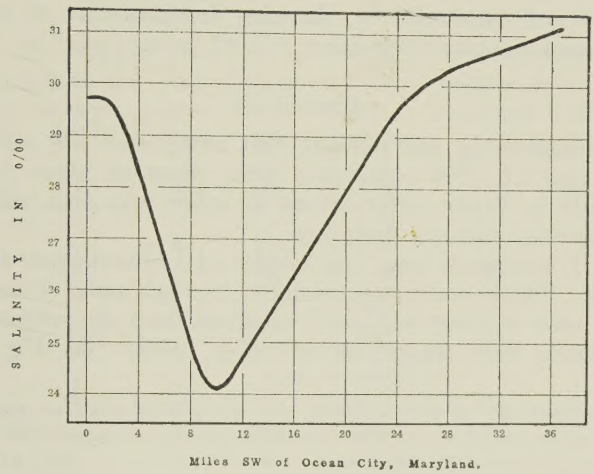

Figure 1. Graph of average salinity gradient from July 1953 through June 1954 in Chincoteague Bay.

simply by slipping the wire loop over the left lateral spine of the crab's carapace, stretching the tag snugly in a saddle fashion across the back and twisting the other length of wire around the right spine. This routine permits rapid tagging with a minimum of handling.

By releasing the tagged crabs at four well separated locations (noted below), variation was achieved with respect to the physical boundaries and to local hydrographic characteristics of the area. In addition, this practice served to subject tagged individuals to various levels of fishing pressure within the area. Several fishing methods were employed by crabbers during the period following the release of the crabs.

The returns were received in two ways. Fishermen who knew of the study often contacted an investigator in the field who obtained the necessary data and paid the reward of $1.00 per tag. Most crabbers, however, sent the tag to the U. S. Fish and Wildlife Service which then forwarded it and accompanying data to the Chesapeake Biological Laboratory at Solomons. A letter, enclosed with the reward, thanked the person for his co-operation, explained briefly the purpose of the study, and outlined when and where the crab had been tagged. This latter method of handling the returns is believed to be effective in avoiding a noncooperative attitude toward a laboratory in another state.

The release and recapture data were plotted on rough charts to facilitate analysis and interpretation. The following developments

were noted and considered: 1) distance and direction of movement, and 2) time of recapture and other related data.

RESULTS

Details concerning the releases and recaptures are set down in Tables I and II. No recaptures were reported after June 1954, which tends to verify observations in other estuaries that the life span of the blue crab is a short one.

Release I was made near the middle of Chincoteague Bay on 31 July 1953. These crabs were caught in crab pots (Cargo, 1954). Although none of these crabs were returned from the release location, 17 individuals were recaptured at other points (see Fig. 2a). Of

TABLE I. SUMMARY OF THE RELEASE AND RECAPTURE DATA OF ADULT FEMALE BLUE CRABS TAGGED IN CHINCOTEAGUE BAY DURING 1953

RELEASES				*RECAPTURES*	
Release	*Location*	*Date*	*Number tagged*	*Total number*	*Number with usable data**
I	Off Public Landing, Md.	31 July	98	23	19
II	Off Sandy Point, Md.	10 Aug.	102	24	24
III	Off White Rock, Md.	11 Sept.	97	27	22
IV	At Fenwick Island Light, Del.	17 Sept.	95	43	40
	TOTALS		392	117 or 29.8%	105 or 26.7%

* These returns provided adequate information on the location and date of recapture.

these, one had moved six nautical miles northward and was recaptured 10 months after release. The other 16 recaptured animals apparently moved in a southerly direction for distances ranging from two to ten nautical miles, and one individual presumably went out of the bay at Chincoteague, Virginia, since it was recaptured 3½ months later at Oyster, Virginia, 60 nautical miles from the point of release. These distances are given as direct routes since they obviously cannot represent the actual paths taken by the animals.

Release II took place on 10 August 1953 at Sandy Point in Sinepuxent Bay, a narrow extension of Chincoteague Bay to the north toward Ocean City. These crabs were caught by trotline (Cargo, 1954), and Fig. 2b shows the movement and location of recapture of 24 females. In this instance, most of the crabs were caught at or near the release point within 10 days. Nine migrated in a southerly direction and were not recaptured until April and May of 1954.

TABLE II. DETAILS OF RECAPTURE

Release I	*31 July 1953*			*Release III*	*11 September 1953*		
Date of recapture	*Distance in nautical miles*	*Direction*	*No. of days out*	*Date of recapture*	*Distance in nautical miles*	*Direction*	*No. of days out*
5/14/54	6	N	278	2/5/54	0	O	158
5/21/54	2	S	285	4/12/54	0	O	224
8/4/53	3	S	4	9/14/53	0	O	3
5/10/54	4	S	274	5/10/54	0	O	252
5/10/54	4	S	274	9/17/53	10	N	6
8/14/53	5	S	14	11/23/53	3	W	74
5/12/54	8	S	276	5/24/54	2	S	266
6/10/54	8	S	305	10/23/53	3	S	43
8/11/53	8	S	11	10/22/53	3	S	42
8/8/53	9	S	8	9/24/53	3	S	13
2/24/54	10	S	209	5/12/54	4	S	254
10/5/53	10	S	67	6/11/54	4	S	284
10/10/53	10	S	72	4/30/54	4	S	241
4/27/54	10	S	261	11/19/53	4	S	70
10/5/53	10	S	67	3/28/54	4	S	209
10/2/53	10	S	63	2/1/54	4	S	153
8/20/53	11	S	20	3/29/54	7	S	271
5/3/54	11	S	267	2/3/54	7	S	156
11/16/53	60	S	109	11/9/53	7	S	60
				3/23/54	7	S	204
				1/26/54	7	S	148
Release II	*10 August 1953*			*Release IV*	*17 September 1953*		
14 crabs	0	0	7 to 9	17 crabs	0	0	3 to 9
1/20/54	0	0	163	4/23/54	40	N	218
5/5/54	3	S	268	5/3/54	3	S	228
4/29/54	3	S	261	1/27/54	4	S	132
4/16/54	3	S	249	4/27/54	4	S	222
4/29/54	3	S	261	4/15/54	4	S	210
5/5/54	3	S	268	4/20/54	4	S	215
5/3/54	7	S	266	10/26/53	4	S	39
4/30/54	17	S	262	2/19/54	5	S	155
4/10/54	17	S	252	2/27/54	5	S	163
5/10/54	20	S	243	4/20/54	6	S	215
				2/18/54	6	S	154
				2/4/54	6	S	140
				1/28/54	6	S	133
				9/24/53	6	S	7
				2/1/54	6	S	138
				1/27/54	6	S	133
				2/11/54	15	S	147
				2/11/54	15	S	147
				5/23/54	20	S	248
				4/28/54	37	S	223
				*	6	S	*

* Date of recapture unreliable.

Release III was made at White Rock, a deep area (seven feet) in lower Chincoteague Bay. These crabs, secured by pots, were released on 11 September 1953. A few were caught shortly thereafter in the immediate area, and although one individual was recaptured about 10 nautical miles north of the release point, most recaptures were made to the south (see Fig. 2c).

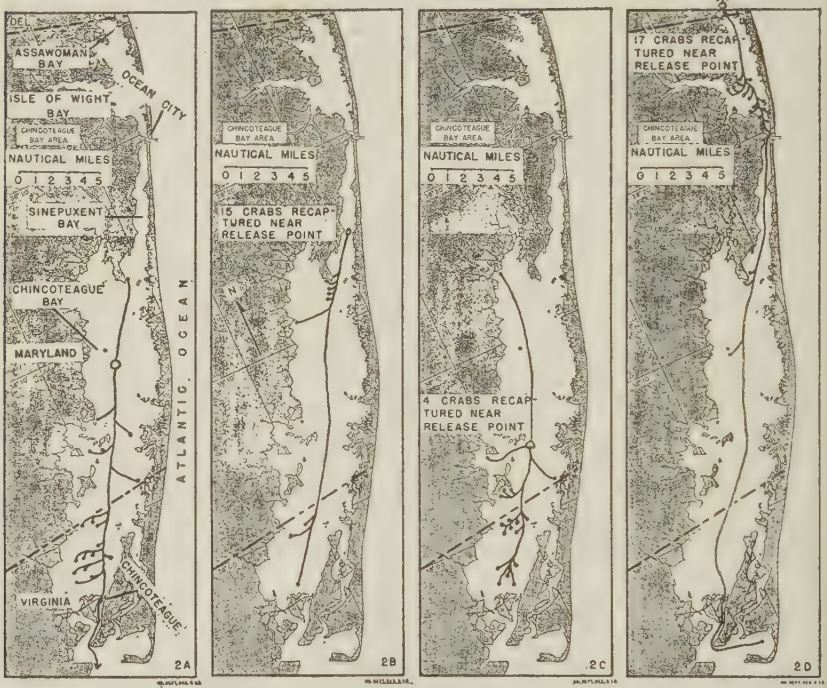

Figure 2. Charts showing locations of releases and recaptures. 2A. Release I. 2B. Release II 2C. Release III. 2D. Release IV. Releases indicated by open circles. Recaptures indicated by solid dots.

Release IV was made on 17 September 1953 at the extreme northern end of the area being studied. These crabs, caught on a trotline, were released in a narrow embayment just north of the Maryland-Delaware line. This release not only produced the largest number of returns but also provided some interesting data on crab movements. Except for the 17 that were returned from the immediate release area, most of the crabs moved southward, at least four bypassing the inlet at Ocean City. One of these was caught on 28 April 1954 at Assateague Cove at the extreme southern end of Chincoteague Bay, a distance of some 36 nautical miles. Another crab, which moved to

the north, was recaptured at Bower's Beach in Delaware Bay about seven months after release (Fig. 2d).

Twenty-eight tagged crabs were also released eight miles off Ocean City, Maryland, in a pilot experiment in which the crabs were obtained by hydraulic dredges fishing for surf clams. No returns were secured from this release.

Cronin (1949) pointed out the likelihood of a tag being overlooked if used internally, but it is apparent from this study that external tags may also be overlooked. If a tag is not observed at the time of recapture, then it is of little value in an experiment of this nature, since the data are frequently questionable. Several of these vividly colored tags were overlooked by crabbers and shippers and were subsequently returned from retail outlets in Chicago and New York. For purposes of this migratory study, recaptured animals that have escaped the notice of the crabber are lost and have not been included in the data presented.

DISCUSSION

Considerations of Techniques. This study has resulted in a return of about one third of the crabs tagged, which suggests that the watermen in the area are effectively fishing the available crop. The fact that the estuary is small and can be covered rather completely by the various gears probably contributes to this high percentage of returns. The returns of biological value amounted to 87% of the total returns. This is about average for external tags of this type (Cronin, 1949). Although it may be difficult, this percentage of usable tags might be increased somewhat by repeatedly publicizing the release date and by outlining briefly the purpose of the study and the necessity for returning all tags together with the information requested on the tag. Frequent personal contacts by field investigators during the course of a study may further increase the returns.

An interesting side light on tagging was observed during Release IV. While the first crabs taken were being tagged and returned to the water as quickly as possible, the crabber continued to fish his trotline in order to get an adequate number of additional specimens for a release. In the course of fishing, several of the newly tagged crabs were recaptured, and one individual was caught on three successive runs. This behavior suggests that the tagging experiment may have had little effect on a crab's subsequent reaction to a baited trotline or, perhaps, to his future well being.

It is evident that, since returns are dependent upon commercial fishing, the distribution of fishing pressure must have some effect upon the locale of these returns. This is important in analyses based

on clustered returns from one area. Crabbing in Chincoteague Bay is fairly homogeneously distributed because of its comparatively shallow depths. However, Figs. 2a, c and d show a clustering of returns just above Ocean City, Maryland, and in the southern part of Chincoteague Bay; both of these areas are close to centers of fishing activity. No specific evaluation of the influence of these factors was made during this study.

Considering the bias which can be exerted by such concentrations of fishing activity, it is possible that the clustering of returns might not have occurred if the fishing pressure had not been heavy in these areas. However, it is just as feasible to assume that the crabs would not have been recaptured there if they had not actually moved into the area, regardless of fishing pressure. Although the scattering of the released animals is probably somewhat more diffuse than the returns indicate, it is felt that the general picture of movement in a southward direction is valid. In this respect, crabs in the Chincoteague area appear to follow a pattern similar to that in Chesapeake Bay.

Biological Considerations. It is apparent that the adult female crabs present in late summer move in a generally southward direction during the subsequent eight to ten months. The salinity gradients in Chesapeake and Delaware Bays gradually increase from the headwaters to the mouth. In Chesapeake Bay, adult females move toward the more saline waters and some do likewise in Delaware Bay, although their pattern is less consistent than that of the Chesapeake. The Chincoteague females, according to our observations, move in a southerly direction regardless of salinity gradients. Releases I and III (see Figs. 2a, c) were made far enough down in the main part of the bay to be influenced by the high salinity water that enters through Chincoteague Inlet to the south. Likewise, Release IV was made at a location where saltier water enters to the south of the release point. In the case of Release II, however (see Figs. 2b, d), the high salinity water is to the north. If adult females are attracted toward high salinities, then it might be expected that the crabs released south of Ocean City Inlet in Sinepuxent Bay would travel northward. Such was not the case. As did the crabs of Releases I, III, and IV, those from Release II also traveled in a southward direction.

Graham and Beaven (1942) showed that the zoeae of *Callinectes* are concentrated near the mouth of Chesapeake Bay. Subsequently, Sandoz and Rogers (1944) determined that salinities in excess of 20‰ resulted in the successful hatching of blue crab eggs into "normal" first stage zoeae and that, at salinities below this, many prezoeae were

produced and the percent of hatching was materially reduced. Salinity was therefore considered to be an important controlling factor that influences the survival of blue crab larvae. Although the spawning area in Chincoteague has not been investigated, it is probable that the relatively high salinity in the bay permits spawning to occur throughout most of the area during summer months. Inconclusive evidence from larvae collections suggests that spawning is concentrated in the lower parts of Chincoteague Bay. This is supported by reports from commercial watermen who have observed a large number of "sponge" or egg-bearing crabs in that area, and in the southerly portions of Isle of Wight Bay as well.

The Chincoteague area differs considerably from Delaware and Chesapeake Bays in ecological and physiographic conditions, and such differences must be weighed and considered. If the movement or migration of adult female blue crabs is influenced by a salinity factor, then one might expect different patterns of migration in the different bodies of water. The lack of a continuous salinity gradient is likely to exert considerable effect upon the forces which determine or influence the migratory patterns of these crustaceans. A gradual increase in salinity from the headwaters to the mouth, as is found in Chesapeake and Delaware Bays, may serve as an orienting factor in determining the migratory patterns of animals in such areas. Although the hydrography of Chincoteague Bay does not follow this regular pattern, the net movement was southerly in most cases. The reasons for this response have not been determined. The inlet at Ocean City was not opened until 1933. This event probably had a marked effect upon the hydrography of the region, but the effects upon the fauna of the area have not been investigated.

The recovery of one individual from Delaware Bay is highly unusual. Previous tagging experiments have shown that crabs rarely move from one estuarine system to another (Porter 1956). The routes open to the crab in this case are rather limited. One possibility is that the crab first moved south to Ocean City and then out into the ocean and northward into Delaware Bay. At least two northern routes were open to it: one utilizes an inlet from the ocean a few miles north of the release point; the other involves a passage through two narrow canals to Lewes, Delaware, and thence directly into Delaware Bay. Any of these routes would necessitate a journey of at least 40 miles.

From these results, then, it appears that these populations do practice some limited migration between estuaries and that mixing is possible. This may have an effect on the morphometric characteristics of a population if the degree of intermixture ever becomes

greater than is indicated at present. The Chincoteague crabs ar significantly smaller than those of either the Delaware or Chesapeak populations (Porter 1955, 1956). If the size of crabs is geneticall determined, intermixture might result in either an increase or decreas of size in the estuaries involved.

The use of the inlet at Chincoteague by migrating crabs is no unusual, fishermen having reported that crabs frequently pass throug it. The coast line of the eastern shore of Virginia is broken an shallow and includes many islands so that this area does not diffe greatly from Chincoteague Bay in topography.

The inlet at Ocean City may have less influence on the movemen of crabs than Chincoteague Inlet. As shown in Fig. 2d, a few tagge crabs passed it and continued their migration down Sinepuxent Ba and even into Chincoteague Bay. This is probably part of a norma migration of adult females toward the assumed spawning area i lower Chincoteague Bay, but a considerable number of crabs fro Release IV were recaptured in the Isle of Wight Bay, where spawnin may also occur, since some were taken there late in the spring. Th statements of local watermen, that sponge crabs do occur there i fair numbers, supports this theory. No data are available on th quantity or quality of the crabs outside the inlet. Crabs exist i shallow ocean waters along the coastal areas within their geographi range, but they have not been utilized in commercial numbers fro such waters by Maryland crabbers. Recent hydrographic investi gations (Sieling 1957) have shown that intrusion of saline ocean wate through the inlet at Ocean City raises the salinity in the lower pa of Isle of Wight Bay and in the upper part of Sinepuxent Bay, bu the effect of this intrusion on the movements of crabs is not clea Further study of the ecological relationships between the crabs an this exchange of water would be of interest and might prove of valu as a basis for future investigations.

REFERENCES

Cargo, D. G.

1954. Maryland commercial fishing gears. III. The crab gears. Chesapeak Biol. Lab., (Educ.) No. 36; 18 pp.

Cronin, L. E.

1949. Comparison of methods of tagging the blue crab. Ecology, *30* (3): 39 394.

1952. Blue crab studies *in* Annu. Rep. Mar. Lab., Dept. Biol. Sci., Univ. Del ware. Publ. 1: 44–47.

1954. Blue crab studies *in* Bienn. Rep. Mar. Lab., Dept. Biol. Sci., Univ. Del ware, Publ. 2: 65–70.

FIEDLER, R. H.
1930. Solving the question of crab migrations. Fish. Gaz., *47:* 18–21.
GRAHAM, J. G. AND G. F. BEAVEN
1942. Experimental sponge crab planting and crab larvae distribution in the region of Crisfield, Maryland. Publ. Chesapeake Biol. Lab., No. 52; 18 pp.
MCGARY, J. W. AND F. W. SIELING
1953. Chemical and physical data, Chincoteague Bay area, July 1943 to June 1953. Data Rep. Chesapeake Bay Inst., 15, Ref. 53–10; 169 pp.
PORTER, H. J.
1955. Variation in the morphometry of adult female blue crabs, Callinectes sapidus Rathbun. M. S. Thesis, Univ. Delaware; 69 pp.
1956. Delaware blue crab. Est. Bull. Mar. Lab., Univ. Delaware.
SANDOZ, MILDRED AND ROSALIE ROGERS
1944. The effect of environmental factors on hatching, moulting, and survival of zoea larvae of the blue crab, Callinectes sapidus Rathbun. Ecology, *25* (2): 216–228.
SIELING, F. W. AND J. W. MCGARY
1952. Preliminary report on the Chincoteague Bay survey. Nat. Shellfish. Ass., 1952: 194–197.
SIELING, F. W.
1957. Chemical and physical data, Chincoteague Bay area, June 1953–December 1956. Chesapeake Biol. Lab., Ref. 57–25: 93 pp.
TRUITT, R. V.
1936. Rep. Chesapeake Biol. Lab., 1936: 2–5.
1937. Crab tagging operations. Chesapeake Biol. Lab., mimeo, 4 pp.
1953. Annu. Rep. Chesapeake Biol. Lab., (Educ.) No. 31: 22–23, 25–27.

SOLUBLE IRON IN COASTAL WATERS[1]

By

TAIVO LAEVASTU[2] AND THOMAS G. THOMPSON

Department of Oceanography, University of Washington
Seattle, Washington

ABSTRACT

Soluble iron, defined as the amount of the element found in a unit volume of mill pore-filtered sea water, after oxidation of organic matter, has been determined o samples collected in inshore waters of the State of Washington. After filtration th samples were oxidized. The particulate matter and its iron content were also dete mined. Bathophenanthrolene was the reagent used.

Analyses showed a variation in soluble iron ranging from 5.5 to 32 μg/l; the pa ticulate matter varied from 700 to 2,000 μg/l and contained from 2.8 to 13.3% o iron. While the general conclusions on the distribution of iron in the waters of th State of Washington may be valid, such values for soluble iron are high in the ligh of recent studies by Lewis and Goldberg.

INTRODUCTION

In earlier studies on the occurrence of iron in sea water (Thompso and Bremner, 1935a, 1935b), Whatman No. 42 filter paper was use to remove suspended matter, and the iron, determined in the filtrat after oxidation of organic matter, was considered as soluble iron However, Armstrong and Atkins (1950) stated that such filters wi permit the passage of about 4% of the suspended matter. Subse quently Goldberg *et al.* (1952) and Fox *et al.* (1953) demonstrate that HA millipore filters were preferable for removing suspende matter. Accordingly, Lewis and Goldberg (1954) defined solubl iron as the amount found in a unit volume of sea water which had bee passed through a millipore filter. Unpublished data by T. Laevast and C. A. Barnes indicate considerable variation in the amounts o particulate matter retained by fine filter papers such as Whatma No. 42; these investigators often obtained values higher than the 4% suspended matter noted by Armstrong and Atkins as passing throug the filter. Observations by Laevastu and Barnes on the use of milli pore filters were in agreement with those of Goldberg *et al.* and Fo

[1] Contribution No. 222 from the Department of Oceanography, University o Washington, Seattle, Washington.

[2] Present address: Food and Agriculture Organization of the United Nations, Via delle Terme di Caracalla, Rome, Italy.

et al. Thus, the definition of soluble iron as given by Lewis and Goldberg is preferred to that given earlier by Thompson and Bremner.

Lewis and Goldberg showed that particulate iron varied considerably in waters of the North Pacific; they also implied that soluble iron is rather uniformly dispersed in oceanic and coastal waters. Thompson and Bremner showed a decided seasonal variation in soluble iron, the range being from 14.5 μg during the spring and summer months to 41.8 μg for the fall and winter months. Thus, these data show a marked variance from those of Lewis and Goldberg. Furthermore, Lewis and Goldberg found that soluble iron in California coastal waters was 3.4 μg while Thompson and Bremner reported 6.1 μg soluble iron for waters some 100 miles off the coast of the State of Washington. Considering the differences noted, re-examination of the occurrence of soluble iron in the sea waters of Washington seemed desirable. The same method as that employed by Lewis and Goldberg was used.

METHOD OF ANALYSIS

Determination of Soluble Iron and Particulate Iron. The method of Lewis and Goldberg was applied in the present study with the exception of the following minor changes: (1) Because of the relatively large blank corrections due to the iron content of the perchloric acid, sea water samples of 200 ml or more were used; these had been filtered through HA millipore filters. (2) Both particulate iron and soluble iron were determined by the bathophenanthrolene method.

Determination of Particulate Matter. Millipore filters, HA type, were dried at 20°C in a vacuum desiccator containing a solution of sulfuric acid which had a water vapor pressure equivalent to 60% of the relative humidity. Each filter was weighed to constant weight after it had been dried and 1.5 liters of freshly collected sea water were passed through it. The filter and the particulate matter retained by it were washed with distilled water to remove all soluble salts, after which the filter was again dried in a vacuum desiccator to constant weight. The difference in weight gave the total particulate matter which was further checked by an optical method to be described in a future paper by one of us (TL).

The particulate matter and the millipore filter, after weighing, were digested with perchloric acid as described by Lewis and Goldberg; the resulting solution was then diluted to 100 ml with iron-free distilled water, and 10 ml aliquots were taken for analysis with the bathophenanthrolene reagent.

Collection of Samples. Surface samples were collected with a plastic bucket and subsurface samples with a nonmetallic water sampler described by Thompson and Chow (1955); thus, the possibility of contamination from extraneous particles containing iron or iron rust was eliminated. The plastic bucket and the sampler were washed occasionally with dilute hydrochloric acid and rinsed with distilled water. Samples were prepared for analysis immediately after collection. All samples ranged from 16.0 to 16.8 Cl‰, except the surface sample at Brown Point which had a chlorinity of 14.0‰.

Errors that may occur in iron analyses if samples are stored in glass bottles have been described by Goldberg (1952). Armstrong (1957) calls attention to the deposition of ferruginous matter on polyethylene exposed repeatedly to sea water, and this observation has been confirmed by us.

DISCUSSION OF RESULTS

Results of analyses are shown in Table I. The soluble iron content varied from 5.5 to 32 μg/l with an average of 17.8 μg for all stations. These values are about 40% less than those reported by Thompson and Bremner, who used Whatman No. 42 filter paper; on the other hand, these are much greater than the 3.4 μg iron values given by Lewis and Goldberg. Armstrong reports values of 4 to 8 μg soluble iron per liter.

Suspended or particulate matter in the samples ranged from 700 to 2,000 μg/l, the mean being 1,440 μg. The iron content of this material varied from 51 to 163 μg/l, with a mean of 114 μg, or, from 2.8 to 13.3%, with a mean of 6.8%. Armstrong and Atkins also found considerable fluctuations in the iron content of suspended material. However, their values were obtained after the particulates had been ignited. Such ignition caused the destruction of organic matter and produced other chemical changes. Their mean value was 10.5%; this is higher, as would be expected due to ignition, than our value for air-dried material.

Samples of millipore-filtered sea water were analyzed for soluble iron both with and without oxidation with perchloric acid. The data shown in Table II, demonstrate that only 25% of the total soluble iron is determinable on the nonoxidized samples. The undeterminable iron in such waters exists largely in the form of ferruginous organic complexes which will not react with reagents used for the estimation of iron. Such reactions will readily occur upon the destruction of the complexes by oxidation.

Simons *et al.* (1953) determined soluble iron in offshore waters in the western Atlantic by using Whatman No. 42 filters to remove

TABLE I. Analyses of sea water samples for particulate matter, particulate iron, and soluble iron

15 March 1955

Location, including Latitude and Longitude	*Depth* (*m*)	*Particulates dry* (*μg/L*)	*Particulate iron* (*μg/L*)	*Iron in dry particulates* (%)	*Soluble iron* (*μg/L*)
Strait of Juan de Fuca					
Green Point	0	1,500	93	6.2	5.5
48°10′ N, 123°19′ W	100	1,850	111	6.0	27.0
Admiralty Inlet					
Port Townsend					
48°8′ N, 122°45′ W	0	—	—	—	9.0
Point No Point					
47°54′ N, 122°30′ W	100	1,100	53	4.8	29.0
Hood Canal					
Brown Point	0	2,000	125	6.2	24.0
47°45′ N, 122°45′ W	100	1,800	51	2.8	32.0
Tabook Point					
47°45′ N, 122°50′ W	100	1,100	108	9.8	9.0
Tekiu Point	100	700	93	13.3	15.0
47°35′ N, 122°59′ W	0	—	—	—	15.5
Tahuya River					
47°22′ N, 122°56′ W	0	1,600	163	10.2	13.0
Lynch Cove					
47°25′ N, 122°56′ W	0	—	—	—	7.5
Puget Sound					
Alki Point	0	1,000	60	6.0	11.0
47°35′ N, 122°26′ W	100	1,600	88	5.5	32.0
Gordon Point					
47°10′ N, 122°39′ W	0	1,550	59	3.8	20.0
Mean		1,440	114.1	6.78	17.8

TABLE II. Soluble iron, determined (A) without oxidation and (B) after oxidation with perchloric acid

15 March 1955

Place of collection	*Depth* (*m*)	*A* (*Fe. μg/L*)	*B* (*Fe. μg/L*)
Brown Point	0	5.7	24
Alki Point	0	5.7	11
Alki Point	100	4.0	32
Lynch Cove	0	2.8	7.5
Tekiu Point	0	2.5	15.5
Port Townsend	0	2.0	9.0
Mean		3.8	16.5

suspended matter and by using o-phenanthroline as the reagent fo estimating iron. They made no attempt to destroy the organi matter by oxidation. Their values for soluble iron are thus very lo and are in agreement with those shown in Table II for analyses mad when the samples were not treated with perchloric acid.

Cooper (1948) has discussed the various forms in which iron ma occur in sea water, and recently Armstrong has studied methods fo treatment of sea water samples so that the total soluble iron can b determined.

Iron analyses, compiled by Lewis and Goldberg from differen oceanic areas by previous investigators, show a wide range of vari ability. The anomalies may be attributed partially to differen methods of analyses and possibly to improper treatment and storag of samples; nevertheless, the results of individual investigators indi cate that a wide range of iron concentrations may actually exist.

Fleming (1948) has described the differences that may exist betwee coastal and offshore waters. He stressed the great range and vari ability of conditions for inshore waters and thus suggested the possi bility of considerable regional as well as seasonal variation. It i believed that such variations may be reflected in the large difference in the quantities of particulate as well as soluble iron. This is sub stantiated by Vinogradov (1944), who states that the concentratio of iron as well as that of other trace elements may show large range not only as to area but also as to depth.

Data presented herein and data previously reported for waters o the coasts of the State of Washington, British Columbia, and south eastern Alaska (Thompson and Bremner, 1935b) show considerabl fluctuations of particulate and soluble iron. Both forms of iron ten to increase with depth, and organic matter plays an important role i regulating the concentration of soluble iron.

The greater concentration of soluble iron in coastal and inshor waters may be attributed to the higher production of organic matte in these areas; to the halmirolysis of particulate matter; to the bio logical assimilation of the iron in particulates, which, on later deca of organisms, returns iron in soluble form to sea water; and to drain age from adjacent land areas.

The removal of iron from sea water may be attributed to precipita tion as hydrated ferric hydroxide or as hydrosols after decompositio of organic complexes; to scavenging by calcium carbonate, clay min erals and biogen suspended matter; and to biological assimilation Volcanic submarine activity may cause local differences, especially i deep water, as shown by Buljan (1954).

Knowing the amount of particulate iron present in oceanic water

TABLE III. DISTRIBUTION OF SOLUBLE IRON IN WATERS AT DIFFEENT DEPTHS IN SOUTHERN PUGET SOUND

28 May 1955

Location	*Depth* (*m*)	*Soluble iron* (*μg/L*)
Whitman's Cove		
Lat. 47°13′ N	0	4.7
Long. 122°48.8′ W	5	3.5
	10	6.7
	20	9.0
	30	8.5
	40	7.0
Devil's Head		
Lat. 47°10.0′ N	0	6.7
Long. 122°47.3′ W	5	5.7
	10	12.0
	25	6.3
	50	6.7
	75	8.0

nd the percentage of iron in suspended matter, it may be possible to stimate the amount of suspended matter and to aid in the solution f the problem brought into being by the controversies of Kullenberg 1953) and Arrhenius (1954) concerning the deposition of deep sea ediments. While the amount of data may be considered meager nd from widely different sources, a computation indicates an interest-ng situation. By using the Lewis and Goldberg values for the mount of particulate iron (4.5 μg/l) as representative for Pacific ceanic waters as well as the mean value of 6.8% for the iron in sus-ended matter (see Table I), computation gives 66 μg/l of suspended natter for offshore waters. This value is relatively close to that of 6 μg/l which Kullenberg obtained by direct measurement.

For the treatment of sea water samples for iron analysis, it is the pinion of the present authors that the use of sulfuric acid, as outlined y Thompson and Bremner (1935a), is to be preferred to that of erchloric acid. The former reagent can be prepared or secured ractically free of iron; the latter reagent has certain advantages, ut the high blank determinations for iron makes its use less desirable. s indicated by Armstrong, phenanthroline is the preferred reagent or the estimation of iron.

REFERENCES

ARMSTRONG, F. A. J.
1957. The iron content of sea water. J. Mar. biol. Ass. U. K., *36:* 509–517.
ARMSTRONG, F. A. J. AND W. R. G. ATKINS
1950. The suspended matter of sea water. J. Mar. biol. Ass. U. K., *29:* 139–143
ARRENHIUS, GUSTAF
1954. Origin and accumulation of aluminosilicates in the ocean. Tellus, *6:* 215–220.
BULJAN, MILJENKO
1954. The nutrient salts in the Adriatic waters. Acta Adriat., *5:* 3–15.
COOPER, L. H. N.
1948. The distribution of iron in the waters of the western English Channel. J. Mar. biol. Ass. U. K., *27:* 279–313.
FLEMING, R. H.
1948. Physical characteristics of inshore environment. J. mar. Res., *7:* 483–489
FOX, D. L., C. H. OPPENHEIMER AND J. S. KITTREDGE
1953. Microfiltration in oceanographic research. II. Retention of colloidal micelles by adsorptive filters and by filter-feeding invertebrates; proportions of dispersed organic to dispersed inorganic matter and to organic solutes. J. mar. Res., *12:* 233–243.
GOLDBERG, E. D.
1952. Iron assimilation by marine diatoms. Biol. Bull. Woods Hole, *102:* 243–248.
GOLDBERG, E. D., M. BAKER AND D. L. FOX
1952. Microfiltration in oceanographic research. I. Marine sampling with the molecular filter. J. mar. Res., *11:* 194–204.
KULLENBERG, B.
1953. Absolute chronology of deep sea sediments and deposition of clay on the ocean floor. Tellus, *5:* 302–305.
LEWIS, G. J. AND E. D. GOLDBERG
1954. Iron in marine waters. J. mar. Res., *13:* 183–197.
SIMONS, H. L., P. H. MONAGHAN AND M. S. TAGGART, JR.
1953. Aluminum and iron in Atlantic and Gulf of Mexico surface water. Anal. Chem., *25:* 989–990.
THOMPSON, T. G. AND R. W. BREMNER
1935a. The determination of iron in sea water. J. Cons. int. Explor. Mer, *10:* 33–38.
1935b. The occurrence of iron in waters of the Northeast Pacific Ocean. J. Cons. int. Explor. Mer, *10:* 39–47.
THOMPSON, T. G. AND T. J. CHOW
1955. A non-metallic water sampler. Deep-Sea Res., *2:* 200–203.
VINOGRADOV, A. P.
1944. Geochemistry of the scattered rarer elements in sea water. Uspekhi Khimii, *13:* 3–34.

MEASUREMENTS OF SLOPES OF HIGH-FREQUENCY WIND WAVES[1]

By

CHARLES S. COX

University of California
Scripps Institution of Oceanography
La Jolla, California

ABSTRACT

Water-surface slopes due to wind waves have been measured in a laboratory wind-wave tunnel. In all measurements, nonlinear effects are important for high-frequency wind waves; nonlinear effects noted are: increase of phase velocity due to finite amplitude of gravity waves, trapping of ripples on the leading slope of gravity wavelets, and limitation of slopes after the explosive growth of waves beyond a critical fetch.

The mean square water-surface slope observed in the tunnel showed a complicated behavior as a function of wind speed. The slope increases rapidly above a sharply defined minimum wind speed for wave generation; the minimum wind speed decreases with increasing fetch. There is no large effect of air-water temperature difference.

The frequency spectrum of slopes shows (for light winds) two peaks separated by a minimum near the frequency corresponding to waves of minimum-phase velocity. As the wind increases, the frequency difference between peaks tends to increase.

Measurements at three frequencies have shown changes of phase velocities of ripples as a function of wind speed that amount to as much as 30% of the theoretical phase velocity appropriate to still water and no wind; much smaller changes are noted for gravity waves. In general, the highest velocities are associated with the strongest winds.

Comparisons with Jeffreys' (1924–25) and Phillips' (1957) theories of wave generation show disagreements at short fetches.

1. INTRODUCTION

The friction of wind blowing over the sea presents an unusually difficult subject to discuss because the roughness of the surface is not

[1] Contribution from Scripps Institution of Oceanography, New Series.

This article by Dr. Cox and the one by Dr. Phillips which follows, both pertinent to the same area of interest, were submitted at approximately the same time, and since it is the policy of this Journal to encourage discussion, I asked each author if he would be willing to prepare a constructive comment on the other's article. Both authors gladly agreed to my proposal, and the Comments which appear after each article resulted. To each author, many thanks.

Y. H. Olsen

only caused by but is the cause of the pattern of flow in the air above the surface and in the water beneath. There have been several attempts to deduce properties of the large roughness elements (ocean waves) from various *ad hoc* hypotheses concerning the nature of the interactions between wind and water, but no great success has attended these efforts. (See Ursell, 1956; 216–248, for a discussion of these attempts and their limitations.) It is with the hope of finding some of the effective forces that a study has been made of the smallest roughness elements on the sea surface: high-frequency waves and ripples.

The first problem is to describe in some way, statistical or otherwise, typical shapes of the sea surface and to find how this shape changes with time. In representing the shape of the water surface, it has been found convenient to use the *slope* of the water surface rather than the more usual *elevation from mean water level* as the parameter to be studied. This is done because high-frequency waves, although of low elevation, have large slopes. It also turns out that rather simple apparatus can be used to detect slopes of the water surface.

Suppose that the elevation of the water surface is $z(x, y)$, where the horizontal axes x, y are directed toward the mean direction of the wind and cross wind, respectively. Then

$$s_x \equiv \frac{\partial z}{\partial x}, \quad s_y \equiv \frac{\partial z}{\partial y}$$

represent the up-down wind and cross-wind components of slope, respectively. In the experiments to be described below, the principal emphasis has been laid upon measurements of the up-down wind component of slope in time and space.

2. APPARATUS

Wind waves were produced in a wind-water tunnel (Fig. 1). A centrifugal blower driven by a ¾-hp motor draws air at speeds up to 12 m sec^{-1} through the tunnel. Observations of waves are made through any of the glass ports by means of the photocell telescopes illustrated in large scale. For measurements at a single point on the water surface, a single telescope is used; for simultaneous measurements at two points, two telescopes are used.

The optical principle upon which slopes are measured is that of refraction of light at the air-water interface. Consider a bundle of rays which passes through the pinhole and terminates on the sensitive surface of the photocell. Since the telescope is focussed on the water surface, all of the rays must have passed through, and been refracted at,

a small spot on the water surface. The region of origin of rays on the "wedge" (cross-section indicated at 8, Fig. 1) then depends primarily on the up- or down-wind component of tilt of the water surface at this spot. The wedge was so constructed that its transmission of light varied linearly from almost nil at the thick end to almost unity at the thin end. Hence brightness of light entering the photocell was proportional to the up-down wind component of slope of the water surface. By rotating the wedge 90° around a vertical axis, the cross-wind component of slope could be measured.

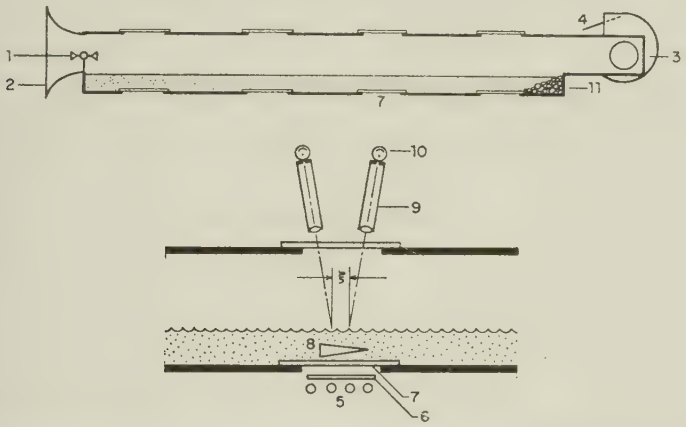

Figure 1. Wind and water tunnel for measurements of slopes of waves generated by wind. The stippled area in the lower third of the tank indicates water. The cross-sectional area of the air passage is 26.3 by 26.3 cm. The dimensions of the water channel are: 14 cm (depth), 26.3 cm (breadth), 1.1 m (length). Numerals refer to the following details: 1, cup anemometer; 2, entrance nozzle; 3, suction centrifugal fan; 4, damper for controlling wind speed; 11, gravel beach for absorbing waves. On an enlarged scale are shown: 5, light source composed of four cylindrical incandescent light bulbs operated on direct current; 6, diffusing glass; 7, plate glass windows (top and bottom of tank); 8, hollow wedge filled with inky water (placed directly upon or beneath lower plate glass window but here shown raised for clarity); 9, telescope tube which focusses an image of water surface on a pinhole directly in front of photocell; 10, photocell.

There are a number of features of this technique which make it less than ideal. The most serious fault is that the brightness registered by the phototube is affected to some extent by the elevation of the water surface above the wedge; for example, as the crest of a large wave comes into the field of view, the rate of change of brightness with respect to slope is increased above its mean value because rays traced back from the water surface have a longer than average distance to travel between wedge and water surface. Thus the effect is a change of scale between slopes measured near the crest of waves and near the troughs. It can be shown that the change of scale is to the mean scale

as the change of depth of water is to the mean depth from water sur face to wedge. At the highest wind speeds (12 m sec^{-1}) one may esti mate the changes of scale as $\pm 20\%$ of the mean scale; at lowe wind speeds the changes become rapidly smaller so that at 8 m sec the changes of scale are estimated at $\pm 5\%$.

Second, for angles of slope greater in magnitude than 40°, the bright ness is not linearly related to slope. For angles less than 40° th maximum departure from linearity is found to be about 5%.

Third, the brightness depends slightly on *cross-wind* components o slope as well as on the intended (up/down-wind) component. Thi effect is expected to be negligible compared to the larger errors men tioned above.

A final difficulty is brought about by scattered light which enters th photocell and causes spurious signals (generally of lower frequency tha the intended signal); this is reduced by painting the interior of th photocell telescope tubes dull black.

The wind speed in the tank was measured by a cup anemometer i the entrance nozzle. It was calibrated by comparison with a pro peller vane anemometer with a National Bureau of Standards calibra tion. The position of the anemometer in a section where the air flo is uniform ensures that it measures the *mean flow* through the tunne

Measurements of air temperature, wet bulb temperature, and wate temperature were made adjacent to the anemometer by mercury-in glass thermometers.

Surface tension measurements *in situ* were made with a De Nou ring tensiometer only when the air blower was not operating. Som attention was paid to the question of surface films on the water, sinc these are known to affect wave generation markedly (see Keulega 1951; Van Dorn, 1953; Cox and Munk, 1954). It was found that, b continuous draining through an overflow trough at the lee end of th tank, the surface could be kept clean. This was confirmed by measure ments of surface tension. Without draining, the surface film woul be compressed to the lee end of the tank by strong winds; when th wind ceased it would then expand rapidly in a few seconds over th entire tank. With continuous draining, the process of reformation o the surface film took several minutes.

2.1 Wave Length Response of System. The finite dimensions of th spot on the water through which all rays pass on their way to the photo cell form a "low-pass" filter to the signal. Slopes due to waves o length much less than the diameter of the spot are not effective i causing variations of brightness on the photocell; conversely, slope

ue to waves much longer than the diameter of the spot are properly ecorded.

The size of the spot on the water is determined by three factors: 1) size of pinhole in telescope divided by magnification ratio between bject and image; (2) degree of malfocussing (caused by rise and fall f waves); (3) perfection of lens in telescope. These factors were stimated separately. For observations of mean square slope (Section 3.1), the effective spot size was 2.0 mm in diameter. An improved lens system was used for observations of the frequency spectrum f slopes; the effective spot diameter was 0.7 mm.

Suppose that the spot radius is r_0 and that all light transmitted hrough the spot contributes equally to the signal. Suppose further hat a wave of slope $s = s_0 \cos(kx - \omega t)$ crosses the field of view entered at $r = x \cos\theta = 0$ in an arbitrary direction x and that the rightness is proportional to s plus a constant. Then the photocell urrent is proportional to a constant plus

$$\int_0^{r_0} \int_{-\pi}^{\pi} s_0 \cos(kr\cos\theta - \omega t)\, r\, dr\, d\theta = 2\pi \int_0^{r_0} s_0 r J_0(kr)\, dr \cos\omega t$$

$$= \text{const}\, s_0 \frac{J_1(kr_0)}{kr_0} \cos\omega t\ ,$$

here J_0 and J_1 are Bessel's functions in standard notation. The ean square output is therefore proportional to $\left[2\frac{J_1(kr_0)}{kr_0}\right]^2$. This uantity lies between 1.00 and 0.90 for wave lengths $\lambda = 2\pi/k > 6.8\, r_0$. or $\lambda = 1.7\, r_0$ the output vanishes, and for smaller wave lengths the utput remains always below .017. For values $2r_0 = 2.0$, 0.7 mm as bove, the wave length of 90% response is $\lambda = 6.8$, 2.4 mm. These orrespond (according to the usual theory of infinitesimal waves on till water) to frequencies of 42, 190 cps.

2.2 Calibration. A rectangular block of lucite supported on a orizontal axle, with its upper surface just above water level, is used o calibrate the slope-measuring system. When the block is rotated bout its axle, the phototube registers a change of light intensity as hough the water surface were tilted. In practice the lucite block is scillated by a motor through a 24-degree arc and the phototube out- ut is recorded.

2.3 Measurements of Phase Velocities. Here two photocell pickups re used. One is fixed while the other is mounted on a movable car- age so that the distance, ξ (Fig. 1), which separates the two fields of

TABLE I

Fetch (*m*)	*Temperature* (°C)		*Wind speed* (*m sec*$^{-1}$)	*Mean square slope*
	Air	*Water*		
1.47	23.8	22.1	4.18	0.0186
	24.2	21.8	5.63	0.0358
	24.4	21.8	2.99	0.00115
	24.6	21.7	6.83	0.0440
	24.5	21.7	7.90	0.0458
	24.7	21.6	9.29	0.0483
	25.0	21.4	10.40	0.0508
	23.9	21.3	12.17	0.0733
	24.0	21.6	4.92	0.0268
2.14	22.2	19.9	4.69	0.0332
	22.0	19.8	3.88	0.0256
	23.4	19.8	3.49	0.0176
	23.4	19.9	2.39	0.0000
	—	—	3.13	0.0126
	23.4	20.0	4.25	0.0286
	22.2	19.6	12.12	0.0885
	23.4	19.6	11.67	0.0772
	22.1	19.8	9.34	0.0598
	21.9	19.1	10.52	0.0622
	—	—	10.94	0.0670
	23.8	19.3	8.65	0.0585
	—	—	7.84	0.0564
	—	—	6.99	0.0522
	22.2	—	6.07	0.0439
	23.7	19.7	5.42	0.0381
	—	—	4.57	0.0281
3.20	—	—	12.04	0.0836
	23.0	—	11.78	0.0796
	—	—	11.45	0.0752
	23.3	—	10.86	0.0679
	23.3	—	10.25	0.0587
	23.2	—	9.48	0.0571
	23.8	—	8.20	0.0535
	23.6	—	7.57	0.0500
	23.7	—	7.07	0.0491
	23.8	—	6.43	0.0471
	23.9	—	5.22	0.0383
	23.6	—	5.99	0.0456
	—	—	4.73	0.0347
	24.2	—	4.44	0.0364
	24.0	20.6	3.79	0.0262
	23.7	19.9	3.11	0.0165
	24.6	20.0	2.73	0.00724
	22.8	20.1	2.39	0.00096
	—	—	2.28	0.00161

iew can be varied. The electrical output signals are sent first hrough two narrow-band electrical filters tuned as nearly as possible o the same frequency and then to a correlator which measures the nean product of the filtered signals. The correlation shows a nearly inusoidal variation as ξ is varied. The wavelength of the sinusoidal ariation is the apparent wavelength of the water waves having the ame frequency as the filters. The apparent wavelength needs cor- ection for the fact that the direction of propagation of the waves is ot always parallel to ξ. The corrected wavelength multiplied by the requency of the filtered disturbance yields the phase velocity.

3. LABORATORY MEASUREMENTS

3.1 Mean Square Slope. Mean square slopes were measured by assing the electrical output from a single photocell telescope to a quaring and averaging circuit. Data, recorded for three fetches Fig. 2; Table I), show that below a certain wind speed, U_0, the mean quare slope is extremely small; above this speed, however, the mean quare slope increases very rapidly with wind speed at first, then more lowly, and finally more rapidly again. The magnitude of U_0, defined y extrapolating the mean square slope curve linearly to the abscissa, aries with fetch as shown in Table II.

TABLE II

Fetch (m)	U_0 *(m sec*$^{-1}$*)*
1.47	2.9
2.14	2.5
3.20	2.3

Using data from the three fetches, one can get a rough idea of the hange of mean square slope with fetch. In Fig. 3 the data shown as ircled points have been found from intersections of the freehand urves in Fig. 2 with lines of constant wind velocity. Although these ata are sparse, they suggest that there is a sharply defined *critical tch* for winds in the range 2.4 to 3.2 m sec^{-1}, above which the mean quare slope increases rapidly from a very low value.

An attempt was made to find a variation of mean square slope with hanges of air-water temperature difference. The tank water tem- erature was varied by heating and cooling while the air temperature as uncontrolled. The data are summarized in Table III. Here $s_x^2\rangle$ is reported relative to its value under "normal" conditions group 2 in Table III). All measurements were made at a fetch of 14 m.

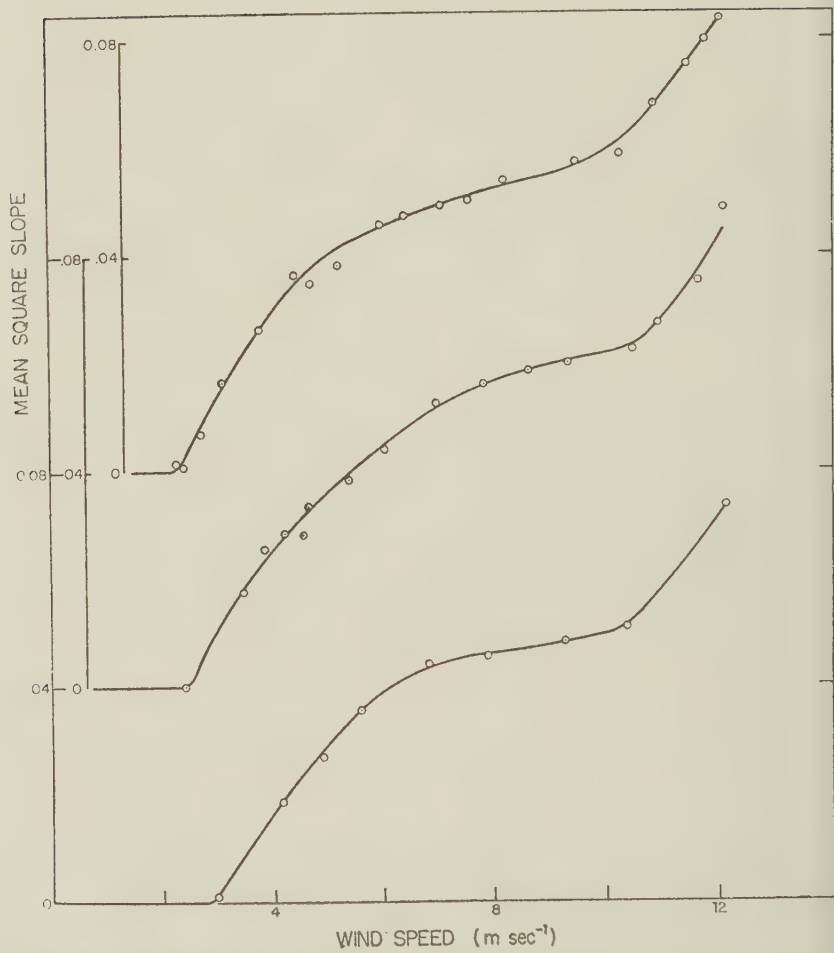

Figure 2. Mean square value ($\langle s_x^2 \rangle$) of up/down-wind slope component as a function of wind speed The three curves refer to fetches of 3.20 m (upper curve), 2.14 m (middle), and 1.47 m (lower). Th curves have been separated vertically for clarity.

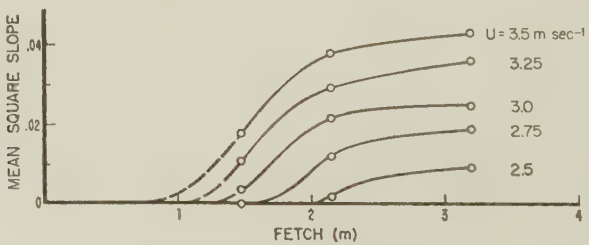

Figure 3. Relation of mean square water surface slopes to fetch for various wind speeds, *U*. Th circled points have been estimated by reading off selected values of the smooth curves shown in Fig The dotted lines are extrapolated.

TABLE III

Group	*Wind speed* ($m\ sec^{-1}$)	*Temperatures (°C)* — *Air* — *Wet bulb*	*Air* — *Dry bulb*	*Water*	*Relative mean square slope*
1	4.52	22.1	25.0	29.5	1.04
(hot)	7.73	21.8	26.6	29.5	0.93
	11.71	22.0	26.2	29.2	0.98
2	4.54	20.8	25.6	22.3	1.00
(normal)	7.69	—	—	—	1.00
	11.79	21.0	25.1	22.2	1.00
3	4.68	20.1	25.6	14.9	1.17
(cold)	7.90	20.0	25.6	15.5	0.94
	11.67	20.0	24.9	20.4	1.05
4	4.52	—	—	9.4	1.01
(very cold)	7.76	19.2	24.4	8.9	0.84
	11.69	19.0	24.6	10.0	0.85

From these observations no consistent change of mean square slope with water temperature is apparent.

3.2 Frequency Spectrum of Slope. The signal at 2.14 m fetch from a single phototube telescope, recorded on magnetic tape and played back at a speed 37.5 times higher than the recorded speed, was analyzed on a spectrum analyzer of the analogue type (Fig. 4). Calibration of the analyzer was carried out by impressing on the same tape a "white noise" (*i.e.*, a signal of uniform spectral intensity) produced by the shot effect in a multiplier phototube exposed to steady light. By comparing the spectrum of the white noise with sine-wave signals passed through the same system, it was found that the multiplier phototube output yielded a uniform spectral intensity (within the probable error of measurement, $\pm \frac{1}{2}$ db) from high frequencies down to 1 cps. Schwantes *et al.* (1956) have demonstrated with greater precision that some multiplier phototubes yield a uniform noise intensity above 1 cps.

Calibration in terms of real units of slope was performed as indicated in Section 2.2.

The frequency analyzer consists of 30 band-pass filters spaced one-third octave apart (frequency ratio between bands = 1.23). The effective width of each filter band is also one-third octave. Each datum reported by the analyzer is then proportional to the total spectral intensity integrated over the band passed by one filter.

The input to the spectrum analyzer is composed of two parts: (1) a noise spectrum compounded of multiplier phototube shot noise and stray electrical pickup (mostly 60 cps noise introduced in the analyzer which shows up as a peak at 60/37.5 cps = 1.7 cps in Fig. 4) and (2)

signal proportional to the spectrum of s_x. The shot noise is "white" and hence can easily be removed if its intensity is known at any frequency. The observations at low wind speed (3.2 m sec^{-1}) show a high-frequency tail from 170 to 540 cps of uniform intensity. It is assumed that this is the photomultiplier noise and that the same noise

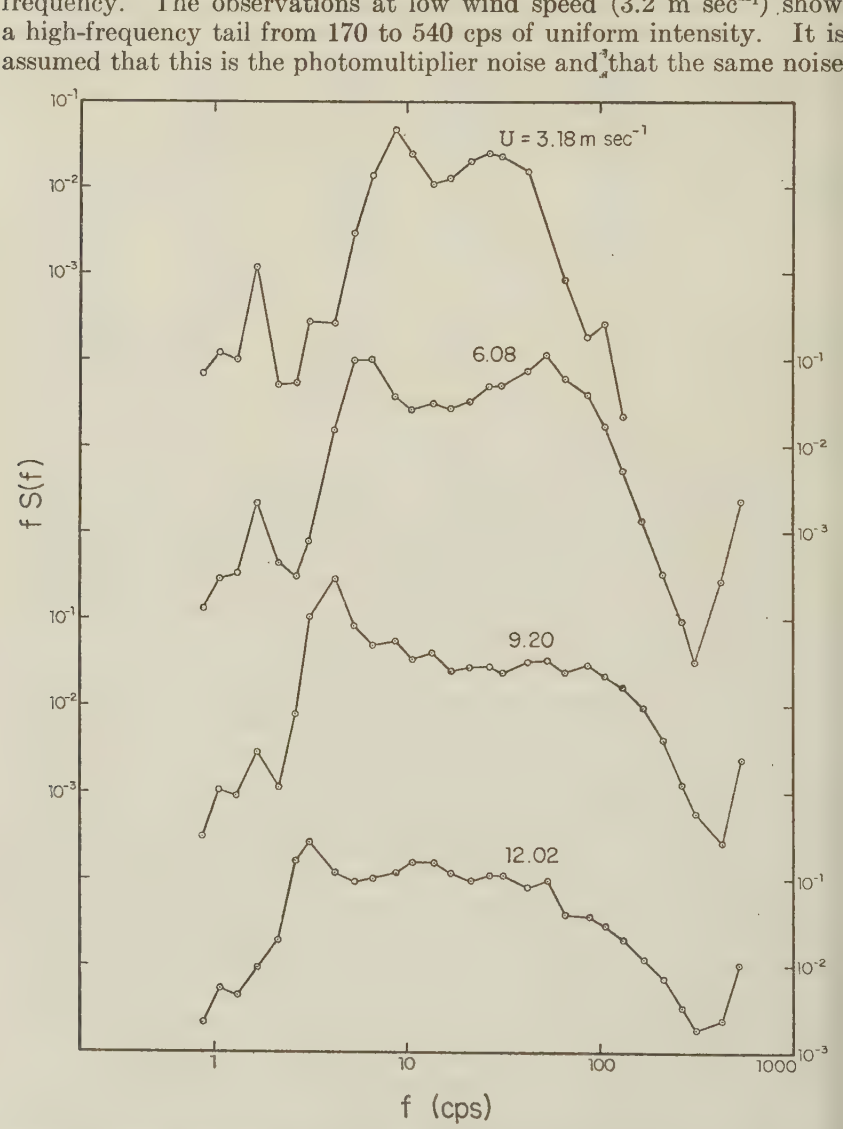

Figure 4. Slope spectrum times frequency, $fS(f)$, of up- and down-wind slopes as a function of frequency, f, for four wind speeds U as shown. The fetch was 2.14 m.

level occurs for each of the spectra at all frequencies; accordingly, this source of noise has been subtracted from all spectra shown in Fig. 4. Some features of doubtful authenticity still remain. The rise of spectral intensity shown by the three lower curves beyond 300 cps is probably not real. It may be caused by imperfect frequency calibration of the magnetic tape at frequencies where large corrections are necessary or by nonlinear recording of slopes larger than tangent 40°.

The spectral intensity, S, is the contribution to mean square slope by waves in a unit frequency band:

$$\langle s_x^2 \rangle = \int_0^\infty S(f)\, df. \tag{1}$$

Since s_x is dimensionless, the dimensions of $S(f)$ are $(\text{cps})^{-1}$.

The observations show that $S(f)$ tends to decrease with increasing frequency. Accordingly, it is clearer to plot $f\,S(f)$, since this quantity gives equal importance to high- and low-frequency waves (Fig. 4). By transforming eq. (1) to the form

$$\langle s_x^2 \rangle = \int_0^\infty f\,S(f)\, d(\ln f),$$

one sees that $f\,S(f)$ is the spectral intensity referred to the *relative* frequency band $\delta(\ln f) = \delta f/f$.

As a check on the spectra, mean square slopes calculated by integrating each spectrum are compared below with those observed directly (Section 3.1):

Wind speed ($m\ sec^{-1}$)	*Mean square slope from spectrum*	*Mean square slope observed directly*
3.2	1.32×10^{-2}	1.36×10^{-2}
6.1	5.18	4.56
9.2	6.21	6.00
12.0	12.6	8.26

The agreement is satisfactory except at the highest wind speed. The causes of the poor agreement here are not entirely clear. Part of the difference can be accounted for by consideration of the poor lens system (Section 2.1) used to measure mean square slope, but this can hardly account for the whole effect.

3.3 Phase Velocity. Phase velocities were measured for three frequencies of waves: 6.6, 37, and 104 cps by the method outlined in Section 2.3. The data are summarized in Table IV. In columns 5–8, f_0 and Q are respectively the center frequencies and quality fac-

tors of the filters. The effective f_0 (column 9) is intermediate between f_0 for each filter and is used together with the corrected wave lengths to compute the phase velocity. Estimations of apparent wave length, λ, and the remaining quantities are described below. Corrections to the apparent wave length (column 11) have to be made for the fact that all wave velocities are not parallel to the axis of the tank. If all wave directions are within a small angular spread of the axis of the tank, it can be shown that the true wave length, λ_0 (column 16), is related to the apparent wave length, λ, by a reduction factor F, (column 15) according to

$$\lambda_0 = \lambda F, \tag{2}$$

where

$$F = 1 - \tfrac{1}{2}(\sigma_y^2/\sigma_x^2). \tag{3}$$

Here σ_x and σ_y are rms filter outputs when the wedge (Fig. 1) is oriented to respond to slopes up-down wind and cross wind, respectively.

If the angular spread of wave directions, $2\theta_0$, is appreciable compared to

$$\left(\frac{10}{\pi^2}\,\frac{\lambda_0^2}{\xi_m^2}\right)^{1/3},$$

where ξ_m is the maximum separation of the photocell telescopes, then the foregoing method is no longer accurate. It is now necessary to know not only the value of σ_y^2/σ_x^2 but also the directional distribution

TABLE IV.

Date 1956	*Temperature* Air °C	Wet °C	Water °C	*Filters* No. 1 f_0 (cps)	No. 1 Q	No. 2 f_0 (cps)	No. 2 Q	*Effective* f_0 (cps)	*Wind speed* (m/sec)	λ (cm)
1	2	3	4	5	6	7	8	9	10	11
Oct. 24–26				36.1	19	36.1	16	36.1	3.69	.853 ±.008
Oct. 29				36.85	22	36.90	19	36.87	9.22	1.007 ±.043
Oct. 29–30				36.9		36.9		36.9	5.48	.838 ±.005
Oct. 30				36.9		36.9		36.9	7.28	.901 ±.037
Oct. 31				37.07	16.5	36.75	19.5	36.95	11.46	.958 ±.064
Nov. 8				6.53	25.5	6.53	36	6.53	5.48	4.971 ±.011
Nov. 8–9				6.53	25.5	6.53	36	6.53	6.55	5.15 ±.15
Nov. 12–13	24.4		20.1	6.57	34	6.62	41	6.60	8.83	5.23 ±.25
Nov. 13	23.9	16.7	18.9	6.57	34	6.62	41	6.60	3.90	5.08 ±.16
Nov. 15	22.6	15.4	16.6	6.87	31	6.88	41	6.88	11.89	
Nov. 21–26	22.8	16.4	18.8	103.63	200	103.63	100	103.63	5.82	.373 ±.006
Nov. 27	25	15.1	20.0	104.3	115	104.0	54	104.2	4.32	.330 ±.013
	26.8	16.5	19.4							
Nov. 28	23.9	15.0	21.1	104.2	130	104.8	50	104.4	7.33	.384 ±.013
Nov. 29	23.9	14.6	21.6	104.2	130	104.3	50	104.2	9.32	.417 ±.009
	26.6	16.8	19.0							
Nov. 29	24.3	16.4	20.6	104.2	130	104.3	50	104.2	11.70	.437 ±.049
			19.2							

of the waves. Since results do not depend critically on this distribution, it has been assumed in the subsequent analysis that the directional spectrum of wave *elevations* is fan-shaped, *i.e.*, the spectral intensity (at the frequency of observation) is uniform for wave directions less than θ_0 (measured with respect to the axis of the tank) and is zero for wave directions larger than θ_0. With this assumption it can be shown that the correlation between two pickups separated by a distance ξ will be proportional to

$$G(\xi)\,[A\,\cos x + B\,\sin x], \tag{4}$$

where

$$x = \frac{2\pi\xi}{\lambda_0};\quad A = \sqrt{\frac{\pi}{x}}\,C\left(\theta_0\sqrt{\frac{x}{\pi}}\right) + \sqrt{\frac{\pi}{x^3}}\,S\left(\theta_0\sqrt{\frac{x}{\pi}}\right) - \frac{\theta_0}{x}\sin\left(\frac{x\theta_0^2}{2}\right);$$

$$B = \sqrt{\frac{\pi}{x}}\,S\left(\theta_0\sqrt{\frac{x}{\pi}}\right) - \sqrt{\frac{\pi}{x^3}}\,C\left(\theta_0\sqrt{\frac{x}{\pi}}\right) + \frac{\theta_0}{x}\cos\left(\frac{x\theta_0^2}{2}\right);$$

C, S are Fresnel's integrals, $C(u) + iS(u) = \int_0^u \exp(\tfrac{1}{2}i\pi t^2)\,dt$; and G is a slowly varying factor which depends on the Q of the filters and on the accuracy with which one can associate a single wave length with waves of one frequency. In deriving the formula, the assumption has been made that $\theta_0^2 \ll 1$.

TABLE IV (cont.)

N	$N_{1/3}$	θ_0 (*radians*)	F	λ_0 (*cm*)	c (*cm sec*$^{-1}$)	c_0 (*cm sec*$^{-1}$)	$c - c_0$ (*cm sec*$^{-1}$)
2	13	14	15	16	17	18	19
8	>4	.26±.15	.989 ±.010	.844±.012	30.5±0.4	26.2±.5	+ 4.3±0.6
4	>2	.17±.04	.9952±.0024	.959±.043	36.4±1.6	25.3±.5	+11.1±1.7
8	3½	.21±.02	.9927±.0014	.832±.005	30.7±0.2	26.4±.5	+ 4.3±0.5
7	3	.19±.03	.9940±.0018	.896±.037	33.2±1.4	25.8±.5	+ 7.4±1.5
5	2½	.21±.04	.9927±.0028	.952±.064	35.2±2.4	25.4±.5	+ 9.8±2.4
3	>3	.52±.05	.958 ±.009	4.76 ±.011	31.0±0.3	28.9±.02	+ 2.1±0.3
5	3	.71±.07	.924 ±.008	4.76 ±.15	31.1±1.0	28.9±.02	+ 2.2±1.0
4	3	1.02±.10	.902 ±.001	4.72 ±.23	31.2±1.5	28.8±.02	+ 2.4±1.5
5	4	1.08±.11	.905 ±.001	4.60 ±.14	30.4±0.9	28.5±.02	+ 1.9±0.9
1	<1	1.29±.13	.88 ±.01				
3	8	.65±.08	.957 ±.006	.357±.006	37.0±0.6	37.0±.24	0.0±0.6
9	>6	.67±.13	.945 ±.013	.312±.013	32.5±1.4	39.5±.24	− 7.0±1.4
4	6	.72±.09	.956 ±.008	.367±.013	38.3±1.4	36.9±.24	+ 1.4±1.4
0	3	1.10±.08	.925 ±.002	.386±.008	40.2±0.8	35.9±.24	+ 4.3±0.8
3	3	1.36±.10	.911 ±.001	.398±.045	41.5±4.7	35.3±.24	± 5.2±4.7

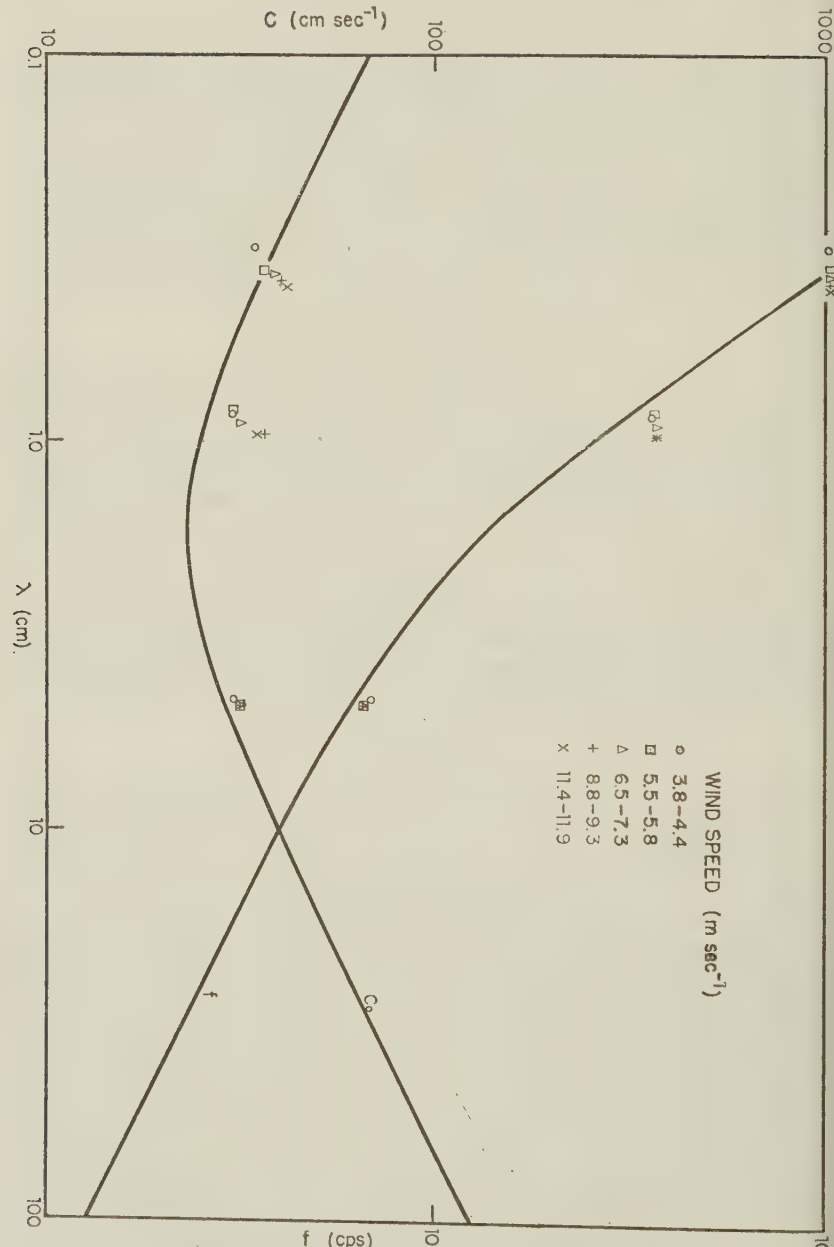

Figure 5. The theoretical phase velocity, c_0, and frequency, f, for waves on still water in the absenc
of wind. The observational data are indicated by points which correspond to the wind speeds shown

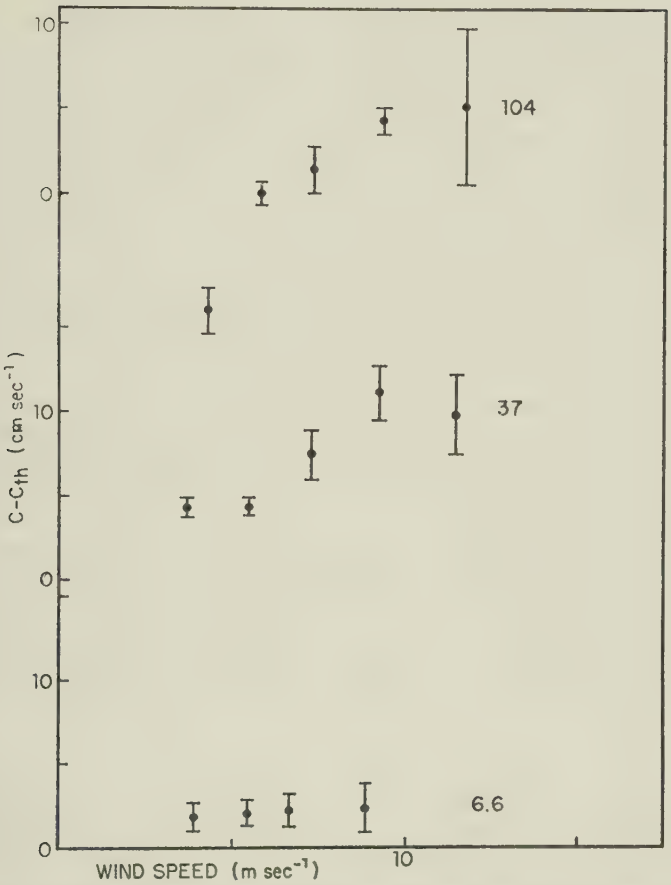

Figure 6. The difference between observed and theoretical phase velocities as a function of wind speed. The three graphs refer to three frequencies (in cps) of waves as noted on the right.

The half-beam width, θ_0, can be found from σ_y/σ_x according to a formula derived by Cox and Munk (1954).

In finding the apparent wave length, λ, the procedure has been to find the successive phototube separations, ξ_n, at which the correlation reverses sign. From a plot of ξ_n vs n, a least square analysis yields λ as well as an estimate of its standard error (see Table IV). Similar plots were made from the theoretical eq. (4) for suitable values of θ_0. From a least square analysis of these plots, one gets a factor F which can be used (eq. 2) to correct the apparent wave length.

Entered in columns 12 and 13 are the total number, N, of changes in

sign of the correlation as well as an estimate of the ordinal number, $N_{1/3}$, of the zero crossing (reckoned from zero separation) at which the *amplitude* of the correlation curve has dropped to one third of its initial value. $N_{1/3}$ permits an estimate of the factor $G(\xi)$, eq. (4), a discussion of which is postponed until Section 4.

The half-beam width, θ_0 (column 14), is estimated together with its standard error from a measurement of σ_y/σ_x (data not shown). Then, from the quantities N and λ, one can estimate ξ_m by $\xi_m \simeq \lambda N/2$ and evaluate the criterion for the applicability of eq. (3). Using eq. (3) or (4), whichever is suitable, one finds F (column 15) together with its standard error. Fortunately the correction factor is always close to unity and its uncertainty is generally of negligible importance for the corrected wave length, λ_0 (column 16). In column 17, c is the phase velocity (and standard error) computed from $c = \lambda_0$ times (effective f_0). In column 18 c_0 is the theoretical phase velocity for free waves on still water without wind (Lamb, 1945: 459, eq. 2). Comparison of theoretical and observed quantities is shown in Fig. 5. In computing c_0 it has been assumed that the surface tension corresponded to the temperature measured by the wet bulb thermometer. Because of the uncertainty of this estimate, there is an uncertainty in c_0. No measurements of wet bulb temperature were made on 24–31 October, and here the temperature is estimated at 16 ± 4°C.

The quantity $c - c_0$ (column 19) shows the difference between the observed phase velocity and c_0. The same quantity is plotted in Fig. 6.

4. DISCUSSION

Measurements of mean square slope may be compared with measurements made in the open sea (Cox and Munk, 1954). Measurements of wind speed in the tank represent average speed throughout the air channel; it may be estimated that the level at which this speed is reached in the boundary layer next to the water is 4 to 8 cm above mean water level. Hence, oceanic measurements of wind speeds made at a height of 12.5 m must be reduced by a large and uncertain correction factor before a useful comparison can be made. I assume the factor is

$$ln\left[\left(\frac{6.0}{0.1}\right) \Big/ \left(\frac{1.25 \times 10^4}{0.1}\right)\right] = 2.2 \ ;$$

this assumes (1) a logarithmic velocity profile near the water in both tank and ocean, (2) an effective height of wind observation in the tank of 6 cm, and (3) a roughness length in both the tank and ocean of 0.1 cm. Ocean measurements reduced in this way show

a linear increase of mean square of the up-down wind component of slope with wind speed from zero at no wind to a value of .044 at a wind speed of 6.3 m sec^{-1}. Tank measurements showed that a mean square slope of .044 was reached at wind speeds of 6.4, 6.1, and 6.0 m sec^{-1} at fetches of 1.5, 2.1, and 3.2 m respectively. With due regard to the uncertainty of comparing wind speeds between tank and ocean, it appears that the mean square slope at 6 m sec^{-1} wind speed will not markedly increase beyond a fetch of 3 m. This is confirmed by the shape of the curves showing mean square slope as a function of fetch (Fig. 3). It appears that, regardless of the mechanism responsible for the explosive growth of waves just beyond the critical fetch, nonlinear effects rapidly set in to limit the slopes at fetches slightly greater than 3 m. On the other hand, it is clear that, for wind speeds lower than 6 m sec^{-1}, oceanic measurements showed appreciable mean square slopes at wind speeds below the critical speed for the tank. This fact indicates that the critical wind speed decreases to a low value for the long fetches encountered in the open sea.[2]

Curves showing the growth of mean square slope with fetch (Fig. 3) may shed some light on the question of the initial generation of waves. According to Jeffreys' (1924–25) "sheltering" theory, the wave amplitude should, in the initial stages, increase exponentially down wind. If this were indeed the case, then observations of very small mean square slope at the critical fetch and rapid growth down-wind imply that waves must be extremely small at the up-wind end of the tank. This was not in fact the case. On viewing objects reflected in the surface, it appeared that there was more wave motion here than at a point just short of the critical fetch (but still so small as to be unmeasurable by the slope apparatus). These small waves at short fetches were probably caused by vibration of the tank and by fluctuating pressures set up by turbulence in the air stream as it flowed around the anemometer at the mouth of the wind channel and over a 1- or 2-cm lip (designed to keep waves from splashing water out at the up-wind end of the water channel). One concludes that there is not an exponential growth of waves at short fetches.

In contrast to Jeffreys' development, in which the air pressure fluctuations are coupled to the already existing waves, Phillips (1957) has developed a theory of wave generation based on a model in which the pressure fluctuations are completely independent of the waves. The theory has been worked out for unlimited fetches and finite duration of winds only. However, Phillips makes the remark that

[2] The waves generated at these low wind speeds are probably gravity waves; Fig. 2 in "Comments on Dr. Phillip's Paper" (J. Mar. Res., *16*(3): 241–245).

waves generated by steady winds at a small fetch are likely to be similar to those described by his theory at a short time after the sudden onset of wind. If this correspondence is valid, Phillips' calculation of the directional distribution of the waves should be comparable to wave measurements in the tank. According to Phillips' result, practically all of the waves of frequency f and wavelength λ will make an angle θ_1 with the wind where

$$|\theta_1| = \cos^{-1}\frac{c(f)}{U_\lambda}, \tag{5}$$

c is the phase velocity of the waves, and U_λ is the "convection velocity" of the turbulent pressure fluctuations: that is, the average speed at which pressure fluctuations of wave length λ are drawn over the water. It seems plausible to assume, with Phillips, that U_λ is the mean wind velocity at a height $\lambda/2\pi$ above mean water level.

This result contrasts with the assumption made in the analysis of phase velocities (Section 3.3) that waves were found at *every* angle to the wind within the fan-shaped beam $|\theta| \leqslant \theta_0$. Measurements of the ratio of mean square filtered slope components, σ_y^2/σ_x^2, cannot distinguish between the two directional patterns of waves; but they do permit a check of eq. (5). In Table V, for waves at $f = 6.6$ cps, estimates of θ_1 from eq. (5) are compared with estimates based on the measurement of σ_y/σ_x according to $\tan\theta_1 = \sigma_y/\sigma_x$.

TABLE V

Mean wind speed ($cm\ sec^{-1}$)	λ_0 (cm)	c ($cm\ sec^{-1}$)	$U\lambda$ ($cm\ sec^{-1}$)	θ_1 (*Eq. 5*)	$\theta_1 = tan^{-1}(\sigma_y/\sigma_x)$
1	2	3	4	5	6
548	4.76	31	402, 120	86°, 75°	17° ± 2°
655	4.76	31	471, 144	86°, 78°	23° ± 2°
893	4.72	31	648, 194	87°, 81°	32° ± 3°
390	4.60	30	286, 86	84°, 69°	39° ± 3°

The first three columns of Table V are taken from Table IV. In column 4, the two values of U_λ have been estimated by calculating the mean wind speed at a height $2\pi/\lambda_0$ above the water, assuming a logarithmic velocity profile near the water, with a roughness length of $\frac{1}{3}$ mm and 3 mm respectively. These are representative limits within which the value of z_0 is likely to lie according to measurements in the open sea (Hay, 1955). The two values of U_λ so derived lead to two values of θ_1 (eq. 5) shown in column 5. The value derived from observation of σ_y/σ_x is shown in column 6.

The uncertainty in U_λ is very large; consequently, one must regard the values of θ_1 calculated by eq. (5) as rough estimates. Nevertheless, it is difficult to see how the observed values of σ_y/σ_x can be reconciled with eq. (5). It is concluded that waves do not run at the angle θ_1 to the wind shown by eq. (5), and this suggests that the hypothesis adopted by Phillips is not correct for the initial generation of waves.

Direct cathode-ray oscillograph recordings of slope at 2.14 m fetch are shown in Figs. 7–9. In Fig. 7, one sees clearly that for each wind speed there are two preferred frequency bands of activity; this

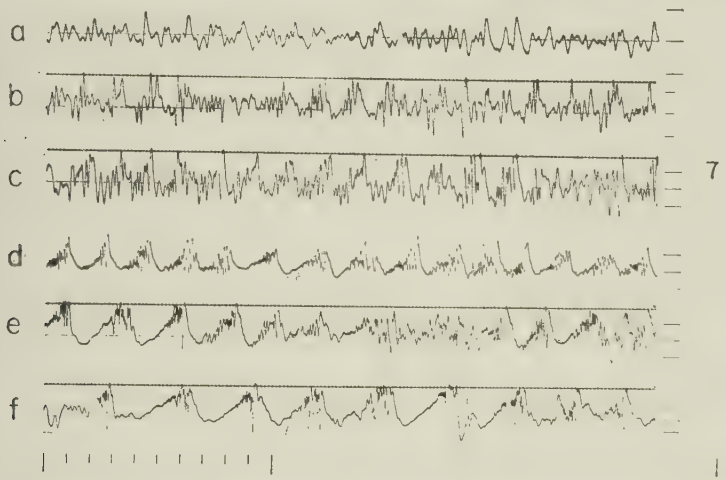

Figure 7. Records of up- and down-wind slope component, s_x, as a function of time for various wind speeds in m sec^{-1} as follows: (a) 3.0; (b) 4.8; (c) 6.1; (d) 8.5; (e) 9.5; and (f) 11.5. (A record at 7.1 m sec^{-1} is shown in Fig. 7b). The slope scale (vertical) is shown by three horizontal dashes to the right of each trace. The separation between dashes is 0.50 in slope. An upward deflection of the trace refers to a water surface element whose up-wind edge is higher than the down-wind edge. The time scale (horizontal) is shown at the bottom of the figure by large marks at one-second intervals and small marks indicating tenths of seconds. Time increases to the right.

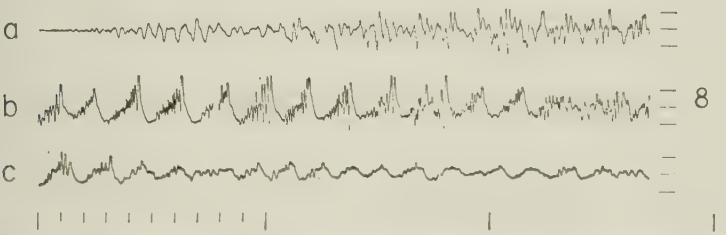

Figure 8. (a) Initial generation of waves; (b) waves in equilibrium with the wind; (c) decay of waves after blower is turned off. These records show up- and down-wind slope (vertical) vs. time (horizontal) as in Fig. 6. The wind speed and fetch are 7.1 m sec^{-1} and 2.14 m, respectively.

is shown also by the frequency spectra (Fig. 4). As the wind speed increases, the low-frequency band tends to low frequencies while the high-frequency band broadens and extends into high frequencies. The dip in the spectrum at low wind speed between the two bands occurs at the frequency of minimum-phase velocity (Figs. 4, 5). Consequently the changes of spectra are such as to keep both bands of activity moving at a speed proportional to the wind.

For winds greater than about 7 m sec^{-1} a new effect becomes important: high-frequency ripples become associated with the *leading slopes* of low-frequency wavelets, *i.e.*, the region down wind of a crest but up wind of the preceding trough (Figs. 7d, e, f; 8b).

Munk (1955) has given two alternative explanations for similar observations in the ocean. According to the first, it is stated that the only stable position for ripples is on the leading slope of a wavelet because the orbital velocity of the wavelet creates a zone of convergence which sweeps ripples onto the leading slope. Some computations of the relative positions of ripples of various length to be expected with this hypothesis are given by Munk. It is thought that these computations are in error because they are based on equating ripple *phase* velocity to the combination of phase and orbital velocity of the underlying wavelet. Since the energy moves with the *group* velocity, it is felt that the correct computation should equate the ripple *group* velocity to the combination of phase and orbital velocity of the wavelet. Qualitatively both computations lead to the same result: that the short ripples should precede the long ones.

Munk's second explanation is based on intermittent generation of ripples by a moving pressure disturbance of short duration. This leads (according to a generalization of the well known solution of the "fish-line" problem) to a dispersive ripple train in front of the moving pressure. Munk associates the pressure disturbance with some (unknown) process located near the crest of wavelets.

From the rather irregular records shown in Figs. 7 and 8, it seems impossible to deduce which of these processes is operative. Accordingly some records were made of wavelets artificially generated by a plunger (Fig. 9). These also show the characteristic ripple trains on the leading slopes of wavelets even though the plunger supplied energy only at the wavelet frequency. It may be that ripples were generated because there was a finite spread of direction of the wavelets; where two crests intersected, there was a momentary nonlinear interaction which gave rise to the ripples.

The rather regular appearance of ripples on the records of Fig. 9 permits not only a rough estimate of the period of individual ripples but comparison with Munk's hypotheses as well. The result is that

plots of position of ripple vs ripple frequency are consistent with Munk's first hypothesis (as modified for equality of ripple group velocity to wavelet phase plus orbital velocity).

It seems likely then that the energy of the ripples is trapped on the leading slope of wavelets by convergence due to the distribution of the orbital velocity in that position. The possibility of trapping in this manner requires that the magnitude of the difference between the phase velocity of the wavelets and the group velocity of the ripples be not greater than the maximum orbital velocity of the wavelets. To a considerable extent this possibility is, therefore, an artifact of the wave tank used in these experiments, because the fetch is sufficient to allow the generation of wavelets with large orbital velocities but is

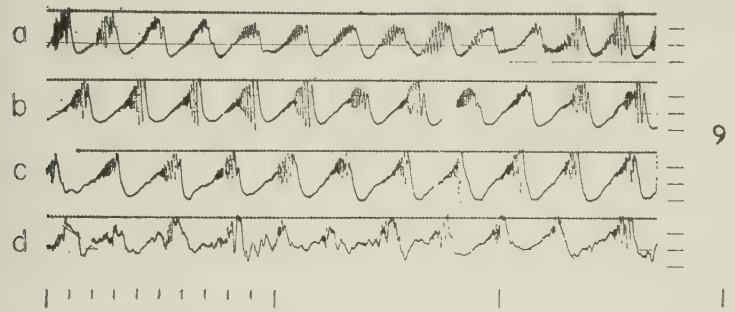

Figure 9. Up- and down-wind slope of plunger-generated waves: (a) without wind; (b) with 2.8 m sec^{-1} wind; (c) with 9.0 m sec^{-1} wind; (d) with 11.6 m sec^{-1} wind. The horizontal and vertical scales are similar to those of Fig. 6. The distance from plunger to recording pickup and the effective fetch was 0.6 m.

not long enough to permit development of wavelets of high phase velocity. In the open sea, where a sharp spectral peak of low-velocity wavelets is not to be expected, one expects that trapping of ripples will not be such a noticeable and persistent phenomenon. Some evidence on this point is shown in Fig. 14; in the left-hand photograph only a few ripples appear to be trapped on the leading (top) slopes of wavelets about 50 cm long; in the right-hand photograph the whole surface appears uniformly covered with ripples.

Also shown in Fig. 9 are records of plunger-generated waves as modified by winds (Fig. 9b, c, d). The effects of wind appear to be an increase in the average energy and frequency of ripples. The increase of energy may be due to generation by wind. The change of frequency suggests that the relation between frequency and group velocity of ripples is altered by the effects of wind in such a way that only high frequency ripples can keep up with the wavelets.

Measurements show pronounced changes of phase velocity (Sec-

tion 3.3) with wind speed. There are four factors which are of the appropriate order of magnitude to be of importance. They are (1) finite amplitude of waves, (2) effects of orbital velocity of low-frequency wavelets, (3) water currents, and (4) dynamic effects of wind.

The theory of finite amplitude capillary-gravity waves has been initiated by Sekerzh-Zenkovich (1956). The velocity, c, of waves of constant form is given in the following form to the third order:

$$c^2 = c_0^2 + \Delta(\lambda, \epsilon^2);$$

here c_0 is the velocity of infinitesimal waves, Δ is a function of wave length λ and ϵ, a parameter (which tends in the limit of infinitesimal amplitude to the maximum slope of the wave). The equation is equivalent to the following expression, correct to the third order in ϵ:

$$c = c_0\left(1 + \tfrac{1}{2}\frac{\Delta}{c_0^2}\right). \tag{6}$$

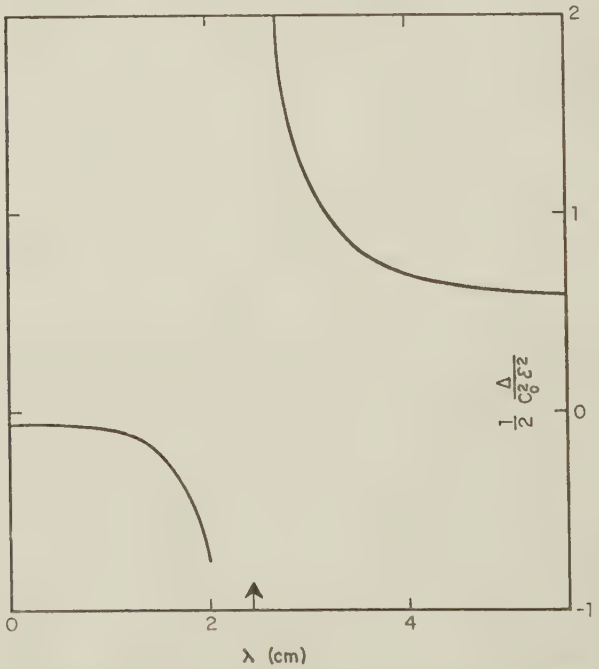

Figure 10. Effects of finite amplitude on wave velocity as a function of wave length, λ. The quantity $\frac{1}{2}\frac{\Delta}{c_0^2\epsilon^2}$ is defined in eq. (5), Section 4. The curve is not valid at the wave length indicated by the arrow.

The quantity $\frac{1}{2}[\Delta/(c_0^2\epsilon^2)]$ is shown in Fig. 10. Certain assumptions in the derivation make the solution invalid when the wave length is such that n capillary waves have the same length as one gravity wave. The wave length where $n = 2$ is indicated in the figure by an arrow.

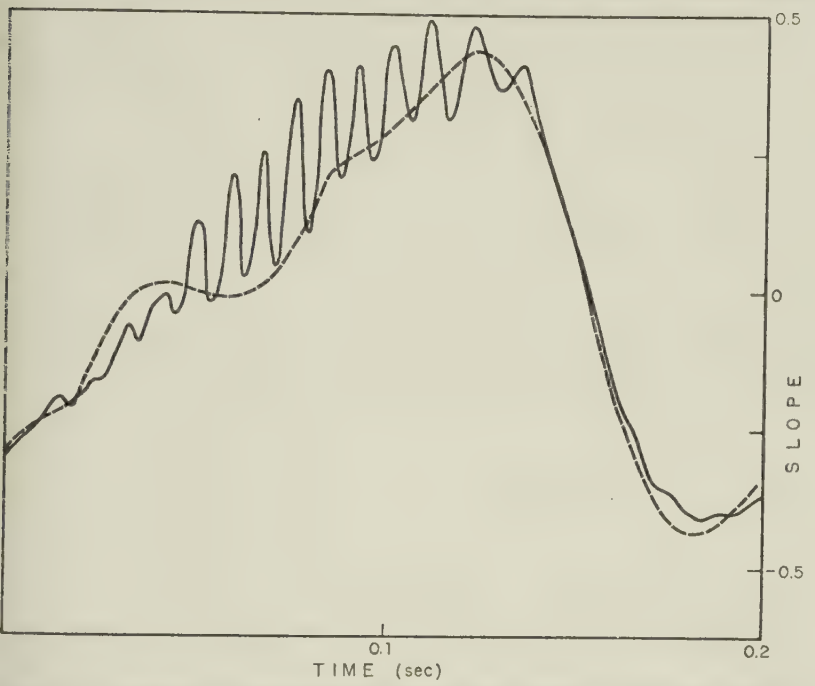

Figure 11. Comparison of plunger-generated wave (solid line) (see Fig. 8a) with slope profile predicted by finite amplitude theory of Sekerzh-Zenkovich (dashed line).

For $\lambda > 3$ cm, the value of $\frac{1}{2}[\Delta/(c_0^2\epsilon^2)]$ is positive and tends to the limit $\frac{1}{2}$ as $\lambda \to \infty$. Hence the phase velocity approaches $c_0(1 + \frac{1}{2}\epsilon^2)$. It is clear that waves of length $\lambda > 3$ cm behave substantially like finite amplitude gravity waves according to Stokes' solution. On the other hand, if $\lambda < 1$ cm, the effect of finite amplitude on the phase velocity is markedly reduced and reversed in sign.

Measurements at 6.6 cps ($\lambda = 4.7$ cm, $c_0 = 28.9$ cm sec^{-1}, wind speeds from 3.9 to 8.8 m sec^{-1}) give $c/c_0 = 1.075 \pm .010$ (Table III). Taking $\frac{1}{2}[\Delta/(c_0^2\epsilon^2)] = 0.62$ from Fig. 10 and $\frac{1}{2}\Delta/c_0^2 = c/c_0 - 1 = .075 \pm .010$, one finds $\epsilon = .35 \pm .05$. To find the value of maximum slope to which this value of ϵ corresponds, it is necessary to fit some wave profiles to the Sekerzh-Zenkovich wave profile formula. One wave from Fig. 9a has been so fitted (Fig. 11). The best fit was for

$\epsilon = 0.33$, $\lambda = 7.0$ cm. (The wiggles on the computed profile are probably the result of pushing the third order theory beyond its limits of validity.) The maximum slope of the observed wave was about 0.42. One estimates then that wavelets with maximum slopes of 0.42 will have a value of ϵ sufficiently large to account for the observed increase of phase velocity. But this is a fairly representative slope for waves near 6.6 cps at the wind speeds where phase velocities were measured. In conclusion, the increase of phase velocity at 6.6 cps for moderate winds is probably the effect of finite amplitude.

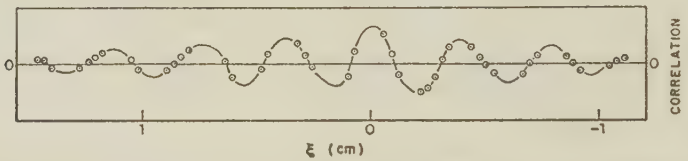

Figure 12. Correlogram of slopes measured at two points a distance ξ apart. Measurements from 28 November; $f_0 = 104$ cps, wind speed = 7.3 m sec^{-1}.

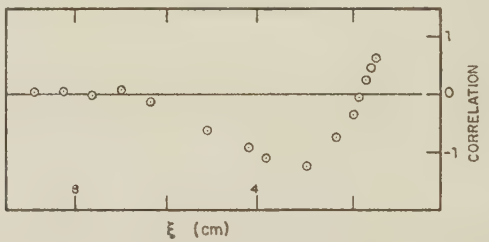

Figure 13. Correlogram of slopes at two points a distance ξ apart. Data from 15 November; $f_0 = 6.9$ cps, wind speed = 11.9 m sec^{-1}.

Phase velocities of 37 and 104 cps waves will scarcely be affected by their finite amplitude according to Sekerzh-Zenkovich's theory, but it can be shown that the other three factors will be effective. Unfortunately it does not now appear possible to disentangle the effects.

Measurements of phase velocity gave as a by-product an estimation of the degree to which one can associate a single wave length with a single frequency of wave. According to the usual theory of infinitesimal waves, those of a single frequency would have an accurately defined wavelength. The effect of waves running in a beam of directions on the correlogram of slopes measured at two points is to reduce, for large ξ, the amplitude of the oscillations of the correlation rather slowly. This reduction is shown by factors A and B of eq. (4), Section 3.3. The effect is rather well illustrated by Fig. 12.

Most correlograms showed a much more rapid decrease of amplitude as ξ was increased, and the effect could *not* have been caused by the

directional beam of waves. An extreme example is shown in Fig. 13 where the decrease of amplitude was so great that it was not possible to measure an apparent wave length at all.

A variation in wave length for waves of a single frequency can be caused by variation of any of the factors which alter phase velocity or by processes of generation and decay. The latter can be illustrated by a simple model. Suppose the slope component due to a narrow range of frequencies of waves can be represented by

$$s(x, t) = \Sigma_i\, g(x - x_i) f\,[x - x_i - v(t - t_i)]\, \cos[k(x - ct)],$$

where $f(x)$ is a slowly varying function compared to $\cos(kx)$ and $g(x)$. The parameters x_i, t_i indicate the general location and epoch of a single train of waves, $f(x - vt)$ represents the motion of the envelope at group velocity, v, and $g(x)$ represents processes of generation and decay. There are two extreme cases to consider: (1) the individual trains are generated completely at random so that x_i, t_i are independent and random variables; (2) the successive trains overlap in a regular fashion so that the sum represents a periodic function of time. In the first case the correlation of slopes at two points a distance ξ apart becomes

$$< s(x, t)\, s(x + \xi, t) > = G(\xi) \cos(k\xi),$$

where

$$G(\xi) = \int_{-\infty}^{\infty} g(x)\, g(x + \xi)\, dx$$

is a measure of the distance traversed by a single wave train; in the second case, the correlation is proportional to $\cos k\xi$.

The first example is representative of random generation of waves while the second represents generation which is locked in phase with the already existing waves. To this extent they represent two theoretical models proposed respectively by Eckart (1953) and Phillips (1957) on the one hand and by Jeffreys (1924, 1925) on the other.

The measurements of $N_{1/3}$ (Table IV; Section 3.3) can therefore yield some estimates of $G(\xi)$ provided variations of phase velocity (see above) are negligible.

In the present data it is not possible to rule out the effects of variations of phase velocity. The values of $N_{1/3}$ must then be regarded as lower limits on the distance (measured in wave lengths) of travel of a single randomly generated wave train. They do not yield any information on nonrandom generation processes.

Measurements showed that $N_{1/3}$ was surprisingly small. In only four out of 15 measurements was $N_{1/3}$ larger than three. The largest values are associated with low winds.

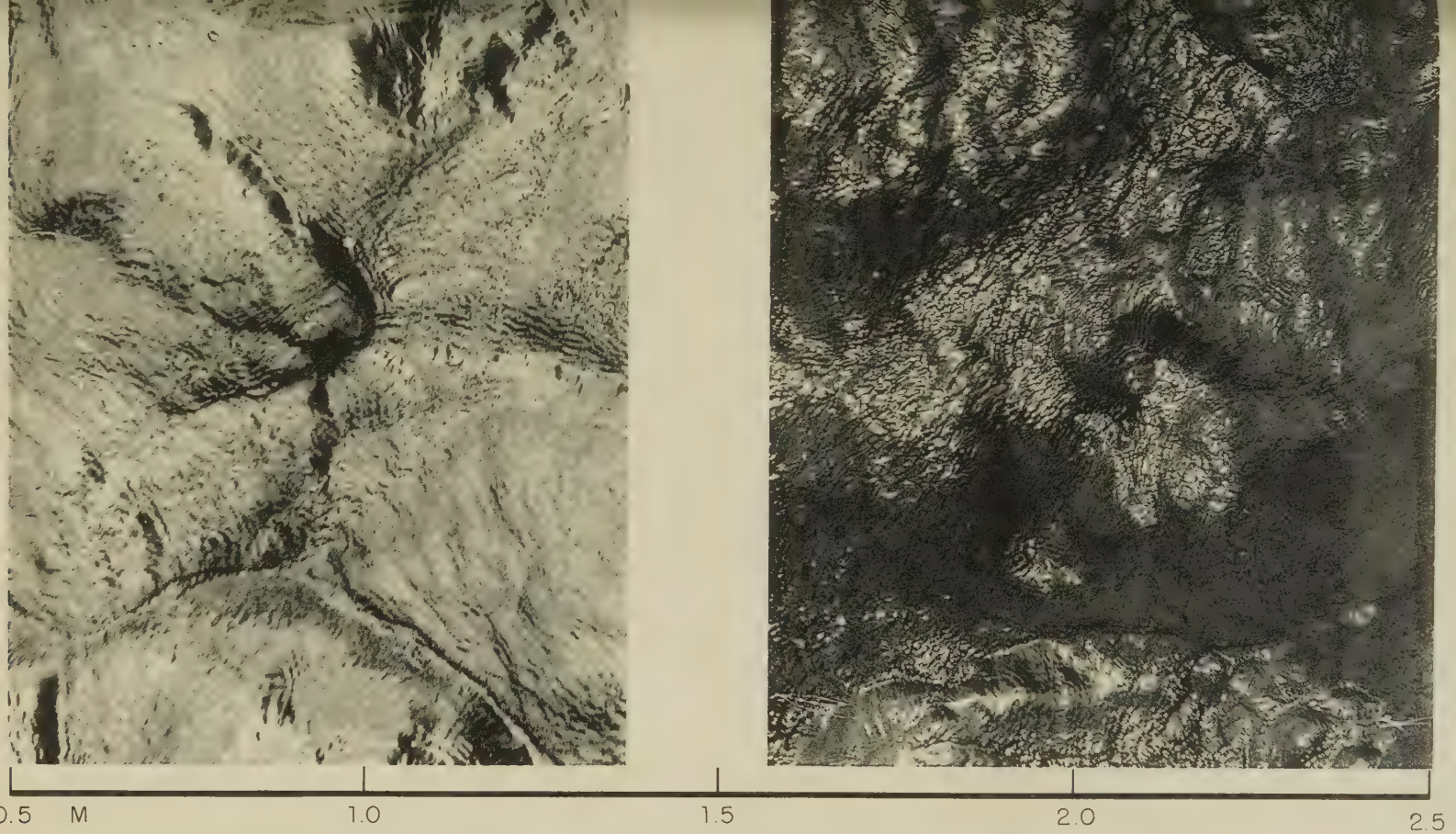

Figure 14. Photographs of the sea surface made from Scripps pier 29 March 1956. Wind speed was 6.5 m sec-1 measured 12 m above sea level. The pronounced white dots on one photograph are reflections of the sun. The other photograph was exposed when the sun was covered with a cloud; the tiny white dots are reflections of a gas-discharge lamp supported 10 m above sea level. The scale indicates distances in meters. In these photographs the wind was blowing from an off-shore direction, hence the fetch was almost unlimited. Some of the larger gravity wave motions shown may be due to reflections from piles supporting the pier, but it was clear to the eye that the ripples were driven by the wind towards the pier.

5. ACKNOWLEDGMENTS

The experimental work reported here has been aided by many people, but particular thanks are due F. Peterson, F. Snodgrass, and P. Teller. J. Zimmerman kindly made the spectrum analyses; G. Groves pointed out Sekerzh-Zenkovich's paper and translated it; and M. DeSelle helped with many computations. W. Munk's advice and encouragement is gratefully acknowledged.

REFERENCES

Cox, Charles and Walter Munk
1954. Statistics of the sea surface derived from sun glitter. J. Mar. Res., *13:* 198–227.

Eckart, Carl
1953. The generation of wind waves on a water surface. J. appl. Phys., *24:* 1485–1494.

Hay, J. S.
1955. Some observations of air flow over the sea. Quart. J. R. met. Soc., *81:* 307–319.

Jeffreys, Harold
1924–25. On the formation of water waves by wind. Proc. roy. Soc., (A) *107:* 189–206; *110,* 341–347.

Kuelegan, G. H.
1951. Wind tides in small closed channels. J. Res. Nat. Bur. Stand., *46:* 358–381.

Lamb, Horace
1945. *Hydrodynamics,* 6th edition. Dover Publications, New York. 738 pp.

Munk, Walter
1955. High frequency spectrum of ocean waves. J. Mar. Res., *14:* 302–314.

Phillips, O. M.
1957. On the generation of waves by turbulent wind. J. fluid Mech., *2:* 417–445.

Schwantes, R. C., H. J. Hannam and A. van der Ziel
1956. Flicker noise in secondary emission tubes and multiplier phototubes. J. app. Phys., *27:* 573–577.

Sekerzh-Zenkovich, Y. I.
1956. On the theory of stationary capillary waves of finite amplitude on the surface of a heavy fluid. Dokl. Akad. Nauk., *109:* 913–918.

Ursell, Fritz
1956. Wave generation by wind, in *Surveys in Mechanics.* Cambridge University Press. 475 pp.

Van Dorn, W. G.
1953. Wind stress on an artificial pond. J. Mar. Res., *12:* 249–276.

COMMENTS ON DR. COX'S PAPER

By

O. M. PHILLIPS

This stimulating paper by Dr. Cox (1958) provides a great deal of information on the inception of high frequency components of wind waves, on which few data of comparable extent have been obtained hitherto under controlled conditions. In these comments I will endeavour to show to what extent Dr. Cox's observations can be interpreted within the present theoretical framework and to what extent they indicate its limitations, so pointing to the need of further investigation.

The Role of Turbulence in Initiating Waves. In the resonance theory (Phillips, 1957, 1958b), pressure fluctuations on a water surface resulting from a turbulent air stream are considered as a means of raising waves. Under conditions of large fetch in all directions and of short duration, it is found that a whole spectrum of waves is generated, with directional maxima for components whose wavenumbers satisfy the resonance condition (Phillips, 1958c: eq. 2). Clearly, an *a priori* condition for the relevance of this theory requires that the air stream should contain pressure fluctuations having a length scale comparable with the wavelength of the waves excited. If this condition is not met (for example, if the air boundary layer is laminar), then any waves that might be observed would necessarily have to be described in terms of some other mechanism, such as that considered by the instability theory of Lock (1954). Even if the boundary layer is turbulent, there is no prior guarantee that the resonance mechanism will be dominant. For example, if the boundary layer thickness is less than, say, one or two centimeters, the pressure fluctuations have a length scale (of the order of half the boundary layer thickness, according to recent work—see Townsend, 1956) corresponding to the wavelength of capillary ripples, which are heavily damped by viscosity. However, there may still be an instability resulting in growth of waves of comparatively long wavelength, as Miles (1957) has shown. Presumably this was the type of wave observed by Jeffreys (1924, 1925) in his original experiments.

Turning to Dr. Cox's paper, one of his most interesting results is the observation of a relation between wind speed and the minimum fetch at which waves begin to grow. In view of the crucial dependence

f wave growth upon wind structure, it seems natural to inquire hether this relation might be associated with some property of the ir boundary layer near the water. One's first supposition is that is critical point might be associated with transition from laminar to rbulent flow in the boundary layer. Forming the Reynolds number $= Ux/\nu$, where U is the free stream speed, x the fetch, and ν the nematic viscosity of the air, the values of R corresponding to the itical fetches shown by Dr. Cox (1958: fig. 3) range from 3.2×10^5 5×10^5. It is known that, in the flow over a flat plate, transition to rbulence occurs at R values between 10^5 and 10^6 (Goldstein, 1938:), the lower values occurring when greater disturbances are present the air stream. The boundary layer over the smooth initial part of e water surface differs in detail from that over a flat plate, but the ansition Reynolds number would be expected to be of the same order f magnitude. The presence of the anemometer and the unavoidable resence of the small step at the leading edge of Dr. Cox's tank (1958: g. 1) would tend to bring about transition at Reynolds numbers low the range 10^5 to 10^6.

It seems plausible therefore to associate this critical fetch observed y Dr. Cox with transition of the air boundary layer from laminar to rbulent flow. Shortly *after* transition occurs, we would expect aves to grow under the influence of the turbulent pressure fluctuaons. The boundary layer thickness at this point is of the order of cm, so that there certainly exist pressure fluctuations of a length ale of several centimetres. An explanation in these terms is also nsistent with Dr. Cox's remark that, for the long fetches encountered the open sea, the critical wind speed decreases to a low value, since nder such conditions the boundary layer Reynolds number is large deed and the air motion invariably turbulent.

This explanation also enables us to make some quantitative predicons based on the ideas of the resonance theory. Comparison of ese predictions with Dr. Cox's observations is encouraging but not cisive. It has been shown (Phillips, 1958b) that, according to the sonance theory, the mean square slope should initially increase nearly with fetch from the point of inception. This is not incontent with Dr. Cox's fig. 3, where the broken lines represent extralations. This linear relation would be expected to fail as soon as nlinear interactions between the wave components become signifint. The slope of this line cannot be estimated because of our lack the right detailed information on the structure of the turbulent undary layer, but the theory predicts that it should be approxiately proportional to U^3. The circled points in his figure indicate a riation as $U^{7.4}$, with a fairly high uncertainty in the exponent—

again close but not decisive. The variation of mean square slope with wind speed at constant fetch (Cox, 1958: fig. 2) is more difficult to express simply, and no definite prediction has been made.

The Occurrence of Resonance Waves. The resonance theory does predict, as Dr. Cox mentions in his §4, that there will be directional maxima in the wave field at angles θ to the wind (see Cox, 1958: eq. 5), *provided* the fetch is large in all directions. However, in a long narrow tank such as the one used in these experiments, when the wind velocity is large compared to the wave velocity, these waves travel almost across the tank. The fetch appropriate for these waves is only a little more than the tank width at most (or half the width if observations are made at the center), which is much less than that for waves travelling along the tank. Thus there is a strong weighting in favour of the latter, and it would be rather surprising if, under these conditions, true resonance waves made a significant contribution at all to the wave field. Apparently the waves observed here are still associated with turbulence but are not the true resonance waves for which this interaction is (for unlimited fetch) most efficient. Such wave components are also considered in the paper to which Dr. Cox here refers.

It seems, then, that the correspondence is not close and that any agreement between columns 5 and 6 of Table V in Dr. Cox's paper would have been surprising.

The Frequency Spectrum of Slope. It is of interest to examine the possibility of making predictions concerning the shape of the frequency spectrum $s(f)$ of the surface slope under the saturation conditions of the equilibrium range (Phillips, 1958a). For gravity waves, the arguments I gave in that paper lead us to expect that, in the equilibrium range, $s(f)$ should be a function of f and g, the gravitational acceleration alone, and independent of U and fetch x in particular. The slope frequency spectrum $s(f)$ has the dimension (time). On dimensional grounds, the only possibility is

$$\begin{aligned} s(f) &\propto f^{-1} \\ f\,s(f) &= \alpha_1, \text{ a constant} \end{aligned} \tag{1}$$

provided f is much less than the frequency associated with waves of minimum phase velocity or for water $f \ll 10$ c.p.s. This represents an upper limit on the function $s(f)$; the slope spectrum would be expected to fall below this limit if the energy supply is insufficient or if the dissipation is too large.

In the capillary range we are on less certain grounds, since viscosity may well be an important parameter as well as surface tension T. However, if the energy supply to the capillary ripples by nonlinear interaction or by direct action of the wind is sufficient to overcome the viscous dissipation, then an upper limit might be sought by neglecting viscosity and by seeking a saturation spectrum determined by f and T/ρ alone, where ρ is the water density. On dimensional grounds, we find again that

$$f\,s(f) = \alpha_2, \text{ constant}, \tag{2}$$

but in this instance it is for frequencies where $f \gg 10$ c.p.s. for water. For extremely large values of f, (2) will inevitably fail, since the energy supply is limited and since the rate of viscous dissipation increases sharply for increasing f. The limit of validity of (2), then, is near a high frequency "cut off" $f_{\max}$, which is higher when the energy transfer processes are more vigorous.

This idea of an equilibrium range for capillary ripples was advanced to me by Dr. Bruce Hicks at the University of Illinois, who pointed out in conversation that the surface displacement spectrum is of the form

$$\Phi(f) \propto \left(\frac{T}{\rho}\right)^{2/3} f^{-7/3},$$

subject to the same conditions as (2).

This type of dimensional argument cannot predict anything definite about the form of $s(f)$ in the range where both gravity and capillary effects are important, since we have an additional dimensionless ratio $Tf^4/\rho g^3$. A full investigation of the nonlinear interaction process would be required before the behaviour of $s(f)$ in this range could be predicted. Nor can such an argument say anything on the interesting details of the capillary patterns on the forward slope of larger waves described in Dr. Cox's paper.

Turning now to the results shown in Dr. Cox's fig. 4, we see many of the features described above. The function $f\,s(f)$ is approximately constant, even near $f = 10$ c.p.s. from the unsaturated low frequency end of the spectrum to the high frequency cut off. The magnitude of $s(f)$ in this range seems independent of wind speed, as predicted by (1) and (2), and the high frequency cut off $f_{\max}$ decreases at the lower wind speeds. At the lowest wind speed shown in Dr. Cox's fig. 4, the saturated range is quite short, and as he points out, it has a fairly definite dip near $f = 10$ c.p.s. If this is a real effect, it would bear some investigation.

It has been a privilege to comment on Dr. Cox's paper, and I hope that these remarks may encourage efforts to obtain a better understanding of these complex phenomena.

REFERENCES

Cox, C. M.
1958. Measurements of slopes of high-frequency wind waves. J. Mar. Res., *16*(3) 199–225.

Goldstein, Sidney (Ed.)
1938. Modern developments in fluid mechanics. Oxford University Press. 702 pp.

Jeffreys, Harold
1924; 1925. On the formation of water waves by wind. Proc. roy. Soc., (A) *107:* 189–206; *110:* 341–347.

Lock, R. C.
1954. Hydrodynamic stability in the laminar boundary layer between parallel streams. Proc. Camb. phil. Soc., *50:* 108–124.

Miles, J. W.
1957. On the generation of surface waves by shear flows. J. fluid Mech., *3* 185–204.

Phillips, O. M.
1957. On the generation of waves by turbulent wind. J. fluid Mech., *2:* 417–445
1958a. The equilibrium range in the spectrum of wind-generated waves. J. fluid Mech., *4:* 426–434.
1958b. Wave generation by turbulent wind over a finite fetch. Proc. 3rd Natl Cong. Appl. Mech., pp. 785–790.
1958c. On some properties of the spectrum of wind-generated ocean waves. J Mar. Res., *16*(3): 231–240.

Townsend, A. A.
1956. The structure of turbulent shear flow. Cambridge University Press. 315 pp.

ON SOME PROPERTIES OF THE SPECTRUM OF WIND-GENERATED OCEAN WAVES[1]

By

O. M. PHILLIPS

Department of Mechanical Engineering
The Johns Hopkins University

ABSTRACT

The resonance theory of wave generation predicts that, for a given scalar wavenumber κ in the two-dimensional instantaneous wave spectrum $\Phi(\kappa)$, resonance maxima should occur at angles α_c such that $\kappa U \cos \alpha_c = (g\kappa)^{\frac{1}{2}}$, where U is the wind speed at a height of approximately κ^{-1} above the surface. Measurements made in the Stereo Wave Observation Project confirm the existence of these resonance maxima near the critical angles predicted by the theory. Other measurements obtained in this project confirm the existence of equilibrium ranges in both the wavenumber and frequency spectra. These comparisons suggest a composite description of the wave spectrum in terms of an equilibrium range at high frequencies ω or wave-numbers κ, a range of low values of ω or κ which is described by a linear theory, and an intermediate transition range.

1. INTRODUCTION

Recently two different mechanisms have been proposed for the generation of waves by wind. One of these theories (Miles, 1957) considers the waves that are produced as a result of instability of the air-water interface when the velocity profile is assumed to have the logarithmic form associated with a turbulent wind. In the other approach (Phillips, 1957; 1958b), turbulence in the air is regarded as imposing on the water surface a random convected distribution of fluctuating pressure. It has been found that waves grow most rapidly by means of a selective resonance between the Fourier components of the fluctuating pressure distribution convected across the water surface by

[1] This work was supported by the Office of Naval Research under Contract Nonr 248 (38).

This article by Dr. Phillips and the one by Dr. Cox which precedes it, both pertinent to the same area of interest, were submitted at approximately the same time, and since it is the policy of this Journal to encourage discussion, I asked each author if he would be willing to prepare a constructive comment on the other's article. Both authors gladly agreed to my proposal, and the Comments which appear after each article resulted. To each author, many thanks.

Y. H. Olsen

the mean wind and those components of the wave field having both the same wave number and the same velocity as the convected pressure fluctuations. Each theory appears to be capable of explaining a number of observed phenomena and each leads to a rate of energy transfer from wind to waves that is of the correct order of magnitude.

It is likely that the two theories are complementary in the sense that waves may be raised by either mechanism or by both operating together according to the particular conditions prevailing, or, more specifically, according to the intensity and scale of the turbulence present in the air stream. It is clear, therefore, that experimental conditions should be carefully controlled; if one mechanism is found to be important in generating ocean waves, it will not necessarily be dominant in a laboratory experiment, and vice versa. Few laboratory studies in the past have included measurements of turbulence in the air stream, and this omission has probably contributed to the frequent conflict in results of different observers and of observations in the laboratory and in the field. This point has been emphasized clearly by Ursell (1956) in his well known review of the subject.

However, the primary interest of oceanographers is in natural conditions that prevail at sea, and an evaluation of the relative roles played by the two processes under these circumstances is a matter of some importance. One objective of this paper is to show how certain detailed properties of the low wave-number or of the low frequency part of the sea spectrum, as observed in the Stereo Wave Observation Project (1957), can be explained simply by the resonance theory. In the higher wave-number and frequency ranges, effects of nonlinear interactions between the wave components become increasingly important and the linear wave generation theories become invalid. It might be expected that a statistical equilibrium can be attained over these ranges of large wave-number and frequency (Phillips 1958a); deductions based on this expectation are compared with the S.W.O.P. data in Section 3.

2. THE OCCURRENCE OF RESONANCE WAVES

The fundamental expression given by the resonance theory for the asymptotic form at large wind durations, t, of the two-dimensional instantaneous spectrum, $\Phi(\boldsymbol{\kappa})$, of the sea-surface displacement is

$$\Phi(\boldsymbol{\kappa}) \sim \frac{\kappa^2 t}{4\sqrt{2\rho^2 n_2^2}} \int_{-\infty}^{\infty} \Pi(\boldsymbol{\kappa}, \tau) \exp\{-i(n_1 - n_2)\tau\} d\tau \qquad (1)$$

(Phillips, 1957: eqs. 4.3 and 4.9), where $\boldsymbol{\kappa}$ is the two-dimensional wave-number vector, ρ the water density, and $n_2 = (g\kappa)^{\frac{1}{2}}$ the angular fre-

quency of gravity waves of wave-number $\kappa = |\boldsymbol{\kappa}|$. The frequency $n_1 = \boldsymbol{\kappa} \cdot \boldsymbol{U} = \kappa U \cos \alpha$ say, where U is the convection velocity of the pressure fluctuations or the wind velocity at a height of approximately κ^{-1} above the surface. Thus the angle α is the angle between the direction of the wind and the direction of propagation of the waves of wave-number κ. The function $\Pi(\kappa, \tau)$ is the spatial Fourier transform of the covariance between the fluctuating pressures, p, at points on the sea surface separated by a distance $\mathbf{r}$ and by a time interval τ, measured in a frame of reference moving with velocity U:

$$\Pi(\boldsymbol{k}, \tau) = (2\pi)^{-2} \int \overline{p(\mathbf{x}, t)\, p(\mathbf{x} + \mathbf{r}, t + \tau)}\, e^{i\boldsymbol{k}\cdot\mathbf{r}}\, d\mathbf{r} \ .$$

The expression for the wave spectrum in the fetch-limited case is similar to (1) (Phillips, 1958b), and the following arguments apply equally to this case also.

The integral in (1) is a maximum for a given value of the scalar wave-number κ when the oscillatory behaviour of the integrand vanishes; that is, when $n_1 = n_2$ or at angles α_c such that

$$\kappa U \cos \alpha_c = (g\kappa)^{\frac{1}{2}} \ , \tag{2}$$

$$\cos \alpha_c = \frac{g^{\frac{1}{2}}}{\kappa^{\frac{1}{2}} U} \ . \tag{3}$$

Condition (2) will be known as the resonance condition, and waves whose wave numbers and directions of propagation under a given wind field satisfy (2) will be called resonance waves. The resonance theory then makes the simple prediction that, for a given scalar wave-number of the spectrum, there will be resonance peaks in the directional distribution at angles $\pm\alpha_c$ given by (3).

This result can also be obtained by more intuitive physical arguments. The integral in (1), as was shown by Phillips (1957: section 4.1), can be represented as

$$I = 2\Pi(\kappa)\, \theta(\kappa, V) \ , \tag{4}$$

where $\Pi(\kappa) = \Pi(\kappa, o)$ is the usual *instantaneous* spatial pressure spectrum and where $\theta(\kappa, V)$ represents the integral time scale of the pressure fluctuations when observed in a frame of reference moving with speed $V = c(\kappa)/\cos \alpha$ in the wind direction where $c(\kappa) = (g/\kappa)^{\frac{1}{2}}$ is the speed of free surface waves of wave-number κ. $\theta(\kappa, V)$ is therefore the time scale of pressure fluctuations acting upon such components of the wave field; the slower the pressure fluctuations experienced by the wave, the larger the time scale, θ, and the faster the wave growth. The function $\theta(\kappa, V)$ is largest for values of κ asso-

ciated with components of the wave field propagating at such a speed that they just keep up with the convected pressure distribution; that is, the time variations in pressure fluctuations result only from the relatively slow time evolution of the turbulence as it is carried along with the wave and not from its spatial pattern being swept past the wave. The time scale, hence the rate of growth, is therefore a maximum for values of κ such that

$$U = c(\kappa)/\cos\alpha \ , \tag{5}$$

which is exactly equivalent to the resonance condition (2).

This prediction can be tested directly by examination of the S.W.O.P. data, which were obtained by taking stereo-photographs of a part of the surface of the North Atlantic under fairly well defined meteorological conditions. A contour map of the instantaneous surface configuration was constructed, and a Fourier analysis of this gave the two-dimensional wave-number spectrum. The frequency spectrum was measured at the same time by using a wave pole. The observational difficulties encountered and the computational labour involved were immense, but the results, whatever their shortcomings, are probably the most complete to date. Fig. 1 represents a number of sections of the observed wave spectrum for constant values of the scalar wave-number κ, plotted as functions of the angle α between the direction of propagation of the wave and the direction of the wind. These data are taken from table 11.6 of the S.W.O.P. report (1957); the ordinates represent the function $\kappa\Phi(\kappa, \alpha)$ in the units m^3 to provide some comparison of the relative contributions of each wave-number range to the mean square surface displacement

$$\bar{\xi}^2 = \int_0^\infty \int_{-\pi/2}^{\pi/2} \kappa\Phi(\kappa, \alpha)\, d\alpha d\kappa \ .$$

The black arrows indicate the angles at which resonance waves would be expected for the various wave-numbers. It is evident that maxima do occur near positions predicted by the theory, though some scatter is apparent. This is probably the result of both sampling errors and lack of steadiness in the wind field, the asymmetries in the observed distributions presumably being a measure of these uncertainties. It is difficult to see how these maxima could occur as a result of any other mechanism; for example, the instability theory would predict maxima at $\alpha = 0$. The characteristic double peaked form of these distributions for wave-numbers $\kappa > 0.1\ m^{-1}$ offers good evidence that the resonance mechanism plays a considerable part in the generation of these ocean waves.

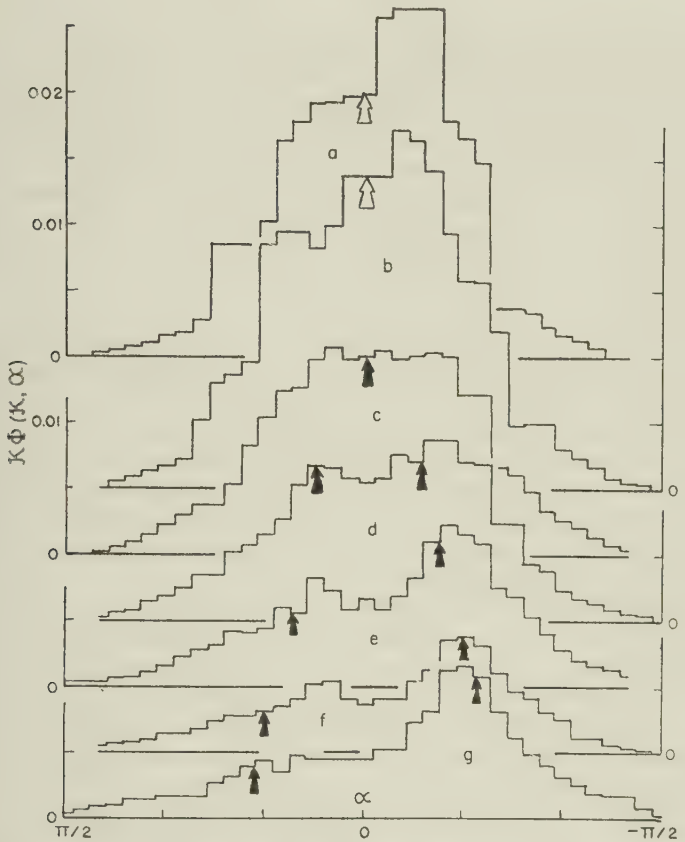

Figure 1. Sections of the weighted instantaneous wave spectrum $\kappa\Phi(\kappa, \alpha)$ for fixed wave-numbers observed in the Stereo Wave Observation Project. The wave-numbers and wavelengths associated with each section are:

Distribution			
	(a)	$\kappa = 0.053m^{-1}$	$\lambda = 118m$
	(b)	$\kappa = 0.063m^{-1}$	$\lambda = 100m$
	(c)	$\kappa = 0.086m^{-1}$	$\lambda = 73m$
	(d)	$\kappa = 0.099m^{-1}$	$\lambda = 64m$
	(e)	$\kappa = 0.112m^{-1}$	$\lambda = 56m$
	(f)	$\kappa = 0.128m^{-1}$	$\lambda = 49m$
	(g)	$\kappa = 0.143m^{-1}$	$\lambda = 44m$

The curve (*c*) corresponds to a wave-number of 0.086 m^{-1}, and the resonance angle for this wave-number under the observational wind speed is zero. For wave-numbers smaller than this, $g^{\frac{1}{2}}/\kappa^{\frac{1}{2}} U > 1$, so that from eq. (3) there are no real resonance angles, since the propagation velocity of these waves is greater than the wind velocity at a height

of κ^{-1} above the surface. Eq. (1) shows that maximum values of the time scale θ for a given U and for each scalar wave-number κ smaller than the critical value g/U^2 would then occur when $| n_1 - n_2 |$ is a minimum; that is, in the direction $\alpha = 0$. In the directional distribution of these smaller wave-number components (or larger wavelength components) we should expect a single maximum at $\alpha = 0$ rather than the two maxima at $\alpha = \pm\alpha_c$ which are characteristic of true resonance waves. This property is indicated by the open arrows in Fig. 1 at $\alpha = 0$; the measured distributions confirm our inference reasonably well, and the contrast between (a) and (e), say, is striking.

These predictions have been made without detailed information about the shape of the spectrum $\Pi(\kappa)$ of the atmospheric turbulent-pressure fluctuations. If such information were available, the detailed shape of these distributions could be calculated readily from eq. (1) and would provide a further basis for comparison. No relevant measurements have been made, however, and it is difficult to make a reasonable inference concerning the form that this function should take. We must await further information before this more detailed comparison is possible.

The observations shown in Fig. 1 have one implication that was unforeseen previously. A simple expression (Phillips, 1957: eq. 4.13) was derived for the mean square surface displacement $\bar{\xi}^2$ in terms of the mean square fluctuating surface pressure $\bar{p}^2$, with the assumption that resonance waves and waves moving faster than the wind contributed only a small part to $\bar{\xi}^2$. Fig. 1 shows that this is not so, such contributions appearing to be very significant, at least in this situation. This earlier expression then gives a serious underestimate of wave heights, and the value of $\bar{p}^2$ inferred by Phillips (1957) from some meagre atmospheric turbulence data is probably larger than the values actually present.

3. THE EQUILIBRIUM RANGES

If the fetch and duration of the wind are both sufficiently large, the wave field develops to such an extent that nonlinear interactions among the components over certain ranges begin to play an important role. The sea surface is then characterized by the appearance of sharp wave crests which may be unable to maintain their attachment and so degenerate into whitecaps. Consideration of this process suggests the existence of equilibrium ranges (Phillips, 1958a) in the wave-number and frequency spectra of high values of κ and ω, over which the form of the spectrum is determined by the gravitational acceleration g alone. On dimensional grounds, therefore, we have

$$\Phi(\omega) \sim \beta g^2 \omega^{-5}, \tag{6}$$

$$\Phi(\kappa) \sim f(\alpha)\, \kappa^{-4} \tag{7}$$

for large values of the arguments, where β is a dimensionless constant and $f(\alpha)$ is a dimensionless function specifying the directional distribution of the large wave-number components. It has been shown that (6) agrees very well with observations made by Burling (1955)

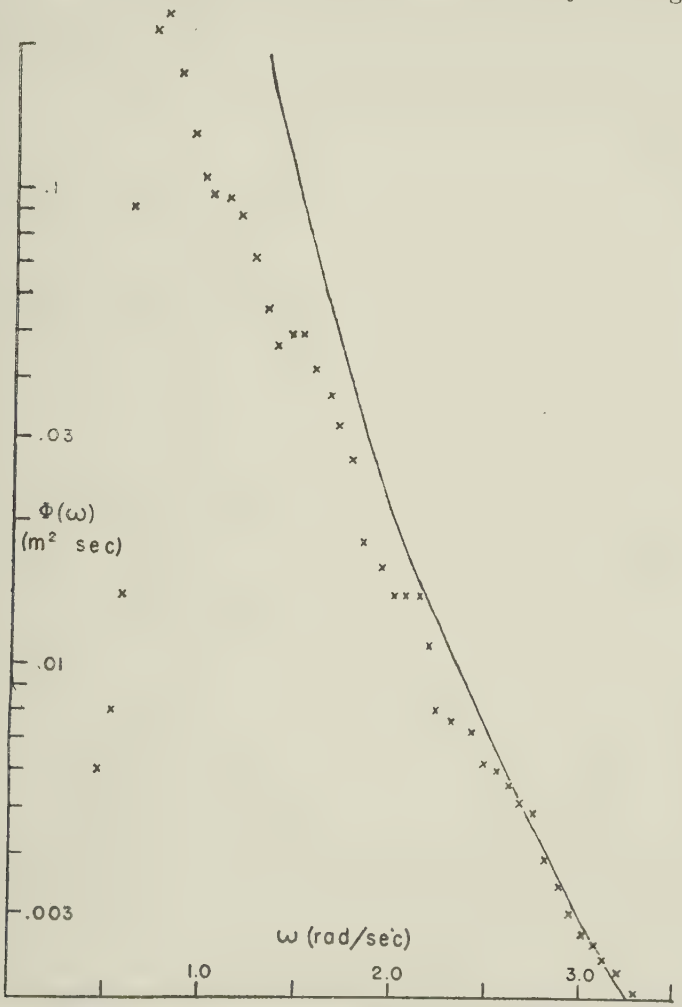

Figure 2. The frequency spectrum $\Phi(\omega)$ from the S. W. O. P. wave-pole data. The solid curve presents the equilibrium range spectrum $\Phi(\omega) \sim 7.4 \times 10^{-3}\, g^2 \omega^{-5}$.

on Staines Reservoir in Middlesex over a frequency range of about 4 to 12 radians per second; the dimensionless constant β was found to be 7.4×10^{-3}.

The S.W.O.P. data enable us to compare (6) with observation over a range of frequencies that extends to much smaller values than those in Burling's measurements. We are interested in discovering not only the lower limit to the range of ω over which the asymptotic law (6) is valid but also an approximate upper limit to the part of the spectrum described by the linearised resonance theory of wave generation. For the first time, measurements of the instantaneous wave-number spectrum $\Phi(\kappa)$ also make possible a comparison with the prediction (7).

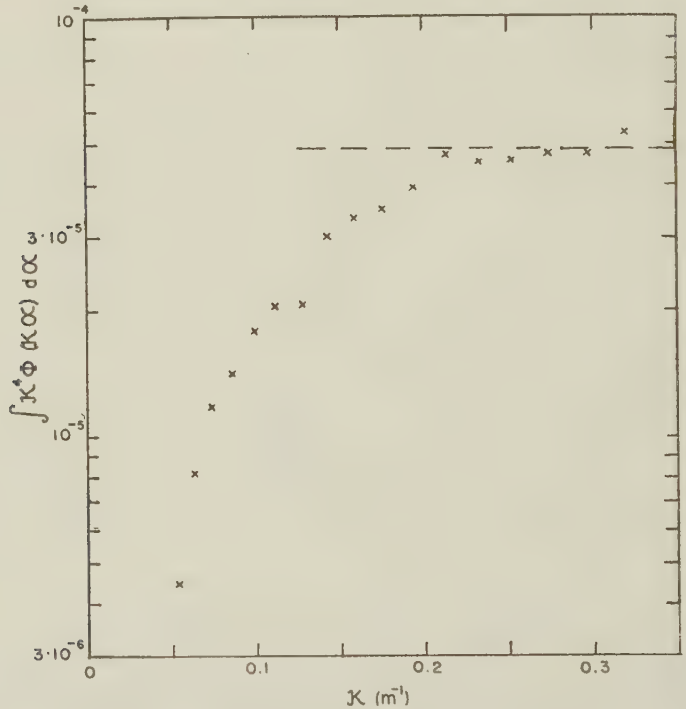

Figure 3. The approach to an equilibrium range $\Phi(\kappa) \sim \kappa^{-4}$ at high wave-numbers of the two-dimensional instantaneous spectrum.

Fig. 2 shows the frequency spectrum, as obtained from wave-pole measurements, together with the asymptotic law $\Phi(\omega) \sim 7.4 \times 10^{-3} g^2\omega^{-5}$. Agreement is seen to be best for the larger values of ω, with the departure of the measured spectrum from the relation (6) becoming serious for frequencies below about 1.5 radians per second.

Fig. 3, derived from data given in table 11–6 of the S.W.O.P. report, epresents, as a function of wave-number, values of the spatial spec-rum $\Phi(\kappa, \alpha)$ at a fixed κ, integrated over angles α from $-\pi/2$ to $\pi/2$ nd then multiplied by κ^4. According to eq. (7), this function should end asymptotically to a constant for large κ. Fig. 3 gives a strong ndication that this is so, the constant being approximately 5×10^{-5}. The asymptotic value appears to be attained in these measurements y a wave-number of about 0.2 m^{-1}, which corresponds to a wave-ngth of about 30 m and a frequency of approximately 1.4 radians er second; this is very close to the lower limit of the range of validity

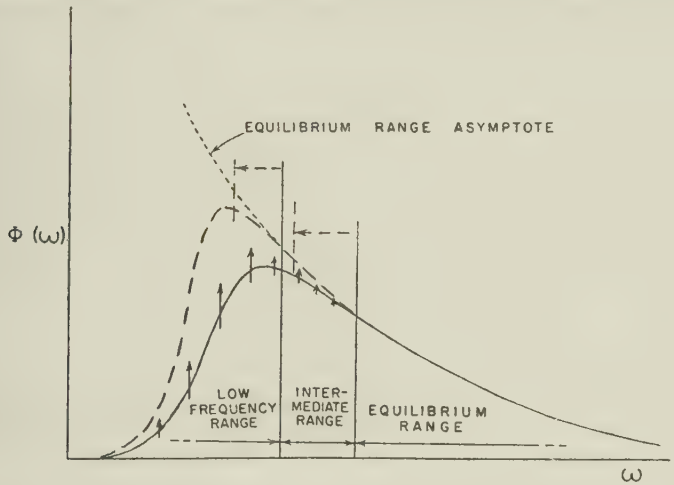

Figure 4. The low frequency, intermediate and equilibrium ranges of the spectrum $\Phi(\omega)$. Arrows ndicate the direction of further development; the broken curve indicates the shape of the spectrum a later time in a duration-limited situation.

f the relation (6). On the other hand, Fig. 1 shows that predictions f the linear resonance theory are verified under present observational onditions for wave-numbers up to about 0.12 m^{-1} corresponding to a requency of about 1.1 radians per second; presumably, then, the re-trictions of nonlinearity which are dominant over the equilibrium ange are not too severe in this case for wave-numbers and frequencies ss than these particular values.

These comparisons enable us to construct a composite description f the wave spectrum in terms of the physical processes that determine arious ranges. This is shown diagrammatically in Fig. 4 for the asily illustrable case of the frequency spectrum; corresponding re-arks can be made about the wave-number spectrum. At large fre-uencies, the spectrum has an equilibrium range described by (6), in hich nonlinear wave interactions prevent further development;

any added energy is lost by wave breaking. Contributions from these frequencies to the mean square surface displacement ξ^2 (or to the wave height) are small. At lower frequencies there is an intermediate range in which wave interactions are appreciable but not dominant. This is difficult to describe analytically, since the wave growth cannot be specified by a linear theory and since the spectrum does not possess the simple properties of the equilibrium range. However, this range does make a significant contribution to $\overline{\xi^2}$, as Fig. 2 shows. Finally, at low frequencies the spectrum can be described by a linear generation theory such as the resonance theory, since interactions among these components are apparently of minor importance. Frequencies in this range also appear to make a significant contribution to $\overline{\xi^2}$.

As the duration of the wind, or its fetch, increases, the spectral components in this last range grow linearly until the wave slopes are such that interactions begin to be significant and the intermediate transition range moves to lower frequencies. At the same time, the values of the spectrum that lay originally in the intermediate range may have attained their saturation values, so that the equilibrium range also extends to lower frequencies as time goes on. As a result, the peak of the spectrum becomes sharper and moves to lower frequencies as the fetch or duration of the wind increases, which is in qualitative accord with many observations.

The need for further careful observation and interpretation is clear. A number of experimental programmes are now being undertaken and these should help to clarify or indicate the shortcomings of the concepts described here.

REFERENCES

Burling, R. W.

1955. Wind generation of waves on water. Ph.D. dissertation, Imperial College, University of London.

Miles, J. W.

1957. On the generation of surface waves by shear flows. J. fluid. Mech., *3:* 185–204.

Phillips, O. M.

1957. On the generation of waves by turbulent wind. J. fluid Mech., *2:* 417–445.

1958a. The equilibrium range in the spectrum of wind-generated waves. J. fluid Mech., *4:* 426–434.

1958b. Wave generation by turbulent wind over a finite fetch. Proc. 3rd. U. S. Nat. Cong. Appl. Mech.: 758–790.

Stereo Wave Observation Project

1957. The directional spectrum of a wind generated sea. Research Division, College of Engineering, New York University. 267 pp.

Ursell, Fritz

1956. Wave generation by wind. Surveys in Mechanics, pp. 216–250. Cambridge University Press.

COMMENTS ON DR. PHILLIP'S PAPER[1]

By

CHARLES S. COX

Dr. Phillips (1958) has found evidence to support his "resonance" theory of wave generation in the wave directionality measurements computed from the Stereo Wave Observation Project data (S.W.O.P., 1957). On the other hand, my observation of 5 cm wavelength waves in a wind and water tunnel (Cox, 1958) showed that the waves did not have the directionality predicted by Phillips. These observations are not necessarily contradictory since different processes may control the growth of 5 cm waves in the tank and of waves 40 m and longer considered by Phillips in the ocean. The inability to settle this point is due to a serious lack of knowledge of the pressure fluctuations in the air stream—a lack which Dr. Phillips has rightfully emphasized to experimentalists.

Phillips (1958: fig. 1) has interpreted the peaks in the directional spectra deduced from S.W.O.P. data in terms of his resonance mechanism; however, another possibility needs examination: that waves are generated predominantly in the direction of the wind but that the wind direction fluctuates. This possibility gains some weight when one examines the original sections from which Phillips' fig. 1 is abstracted. Phillips has omitted one section, $\kappa = .074$ m^{-1}, $\lambda = 85$ m, and this is shown here as Fig. 1 and may be labeled b' because it belongs in the sequence between b and c of Phillips' fig. 1. There are two features on this section which call for attention.

First, a peak centered at an azimuth of $-45°$ is not explained by the resonance mechanism since these waves are traveling faster than the wind. One gets the impression, on comparing a, b, b', and c, that this peak is connected with the left-hand peak in d, e, f, and g. If so, there is no definite trend to the azimuth of this peak since the peak tends to move to the right in the sequence a, b, and b', while it moves to the left in c, d, e, f, and g.

Second, note in Fig. 1 the peak centered at an azimuth of 60°. A similar feature exists on all of the original sections corresponding to a–f, but Phillips does not indicate this peak, presumably because one of the authors of S.W.O.P. considered that it was due to swell from a distant source. On the other hand, another author states "For the

[1] Contribution from Scripps Institution of Oceanography, New Series.

entire period [of five days preceeding the stereo-photographs] there appears to have been little or no possibility of a contribution to the waves at the ship by wind fields in other parts of the North Atlantic. Therefore, the ship was essentially in the generating area at all times and no swell should be recorded." This statement and the observations that the spectral peak has a rather broad azimuth and frequency range suggest that the generation is local.

Weather maps from S.W.O.P. (fig. 10.3) show: 1) that wind directions were highly variable for a period of 12 to 42 hours before stereo-photographs were taken; 2) that wind observations to the west of the

Figure 1. The angular variation of ocean waves of wavelength 85 m according to measurements by S.W.O.P. The ordinate is proportional to the estimated spectral density, the abscissa is the azimuth of the direction of the waves measured in degrees eastward of true north. The estimated wind direction is indicated by arrow and establishes the origin $\alpha = 0$ of Phillips' fig. 1.

stereo observation point showed strong westerly winds from 42 to 36 hours before the stereo-photo time; 3) that lack of information prevents determining whether these winds persisted until 28 hours before stereo-photographs were exposed. If they did, then waves of 85 m wavelength, traveling at their group velocity, would reach the photograph area in time. These waves would arrive from an azimuth of about $-90°$; owing to an indeterminacy of 180°, these waves would appear on the directionality sections at an azimuth of $+90°$. One can therefore identify the observed peak in this way, although identification is not certain. What then of the peaks discussed by Phillips? I believe there is a possibility that they can be interpreted in a similar way and that the wind observations are certainly not sufficient to rule out this possibility.

The considerations above suggest that definitive experiments must be designed to measure not only the parameters of the turbulence in the wind stream but also the large-scale meteorological effects of variable wind direction.

In the second part of his paper Phillips has found new data (also from S.W.O.P.) which support his dimensional arguments for an "equilibrium" range in the wave spectrum where the frequency spectrum has the form

$$\Phi(\omega) \sim \beta g^2 \omega^{-5} ,$$

with $\beta = 7.4 \times 10^{-3}$, independent of wind speed. The notation follows Phillips' usage. The dimensional argument is independent of any theory of wave generation. It is gratifying to find that experimental data now supply information down to much lower frequencies than those available earlier (due to Burling).

Wind and wave tank observations (Cox, 1958: fig. 4) suggest that the equilibrium range is limited at the high-frequency end by a sharp cut-off at an angular frequency of $\omega_1 = 85$ sec^{-1}, independent of wind speed, followed by a capillary spectral peak for still higher frequency waves.

The contribution of capillary waves to the mean square slope in the open sea can be estimated with the help of the expression for the equilibrium spectral density. Let σ^2, σ_1^2 be the contributions of all waves and of gravity waves respectively to the mean square slope. By a known formula

$$\sigma_1^2 = \int_0^{\omega_1} \kappa^2 \Phi(\omega)\, d\omega .$$

Because of the factor κ^2, the contribution by long waves to the integrand is minor. Consequently it should be possible to replace the spectrum function by its equilibrium expression, provided one starts the integration at a suitable lower limit ω_0. From many studies it seems plausible that the lower limit should be taken such that the longest waves run at a speed nearly equal to U, the wind speed measured at "anemometer level." This gives

$$\omega_0 = cg/U,$$

where $c \doteq 1$. Taking the appropriate gravity wave formula for κ, one finds

$$\sigma_1^2 = \int_{\omega_2}^{\omega_1} \beta \omega^{-1}\, d\omega = \beta \ln \left(\frac{\omega_1 U}{cg} \right).$$

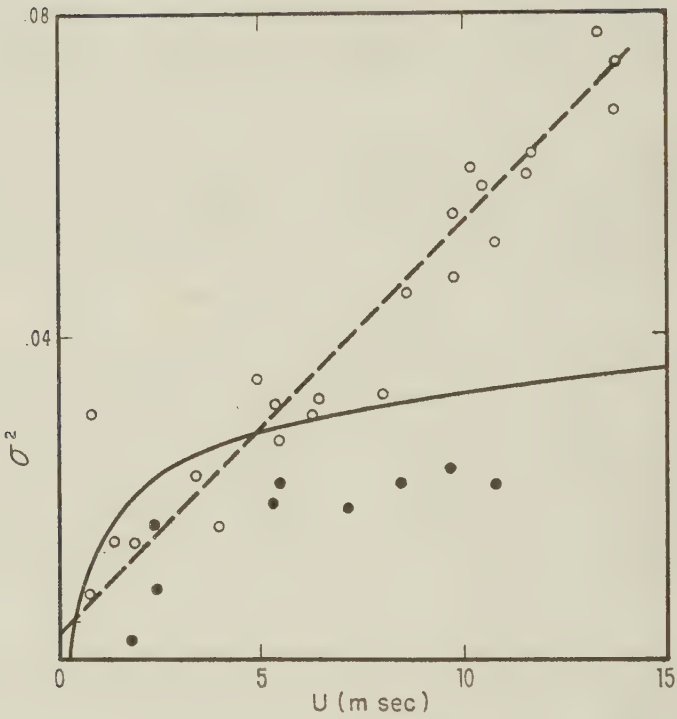

Figure 2. Mean square slope, σ^2, vs. wind speed U measured 41 feet above sea level according to Cox and Munk (1954). The open circles represent measurements over clean water surfaces; the solid circles, measurements over water covered with an oil slick. The dashed curve is a least square fit to the open circles; the solid curve represents σ_1^2, the contribution to mean square slopes by gravity waves according to Phillips' form of the equilibrium spectrum. The difference $\sigma^2 - \sigma_1^2$ must represent the contribution by capillary waves.

Fig. 2 compares σ_1^2 (computed with $c = 1$) with σ^2 as measured in the open sea (Cox and Munk, 1954). If $c = \frac{1}{2}$ or 2, the computed curve would be moved up or down by only .005. For winds below 4 m sec^{-1}, the computed value of σ_1^2 lies above σ^2. Since this is an impossibility, one concludes that the equilibrium waves are not fully developed at such low winds. It is only for winds above 6 m sec^{-1} that the curve for σ_1^2 falls significantly below the one for σ^2 and that an appreciable contribution from capillaries can occur. Observations of mean square slope where the ocean was covered by an oil slick fit into this picture well because detailed estimates (Cox and Munk, 1954) indicate that all capillaries and some of the gravity waves should be removed by such a slick; therefore the mean square slope in a slick

hould be slightly less than σ_1^2, as is indeed found. Observations in he wind and wave tank are also consistent with a rapid growth of apillaries for winds above a critical windspeed. (The speed measured n the tank was 2.5 m sec^{-1}; see Cox, 1958: table II; the windspeed neasured at an anemometer level of 40 feet would have been approxiately 5.5 m sec^{-1}.)

Conclusions of this commentary are:

irst, additional experiments are necessary before directional proper-es of ocean waves become known. In this work it will be necessary pay particular attention to large-scale fluctuations of wind direction ver the generating area.

econd, the form of the equilibrium spectrum proposed and verified by r. Phillips is at harmony with measurements of water slopes both ith and without oil slicks. An indirect calculation based on com-arison of the analytical form of the equilibrium spectrum with ob-rvations of slopes in the open sea suggests that capillary waves be-ome important only for winds above 6 m sec^{-1}.

REFERENCES

ox, Charles and Walter Munk
1954. Statistics of the sea surface derived from sun glitter. J. Mar. Res., *13:* 198–227.

ox, Charles
1958. Measurements of slopes of high frequency wind waves. J. Mar. Res., *16:* 199–225.

illips, O. M.
1958. On some properties of the spectrum of wind-generated ocean waves. J. Mar. Res., *16:* 231–240.

tereo Wave Observation Project
1957. The directional spectrum of a wind generated sea. Research Division, College of Engineering, New York University. 267 pp.

TRACE ELEMENTS IN THE PELAGIC COELENTERATE, *VELELLA LATA*

By

ROBERT BIERI

Antioch College, Yellow Springs, Ohio

AND

DAVID H. KRINSLEY

Queens College, New York

ABSTRACT

Twelve elements (Cu, Ni, Mn, Ti, Si, Cr, Sr, V, Ba, Ag, Pb, and Mo), not previously reported from the genus *Velella*, were found in the ash of *V. lata*; zirconium was also searched for but was not found. Cu, Ni, Mn, Ti, Mg, Ca, and Al were determined quantitatively. The concentration of trace elements in the whole animal and in five different tissues of *V. lata* was determined in specimens ranging from 14.4 to 84.6 mm in length. The Mg:Ca ratio in *Velella* is lower than that in sea water but higher than that in Scyphozoa. Presumably this is due to concentration of magnesium in the chlorophyll of commensal zooxanthellae.

INTRODUCTION

Although the distribution and function of trace elements in plants and animals has received widespread attention in the past 50 years, especially with regard to agriculture, the influence of trace elements on marine plankton is still relatively unknown. One of the many difficulties that has delayed advances in this field is the extreme variability of trace element concentration, not only among species but also among individuals of the same species (Vinogradov, 1953). When a study of the trace element content of plankton from different water masses was thwarted because of the great variation in results between different parts of the same plankton sample, the present study of variability in a single species, *Velella lata*, was undertaken. An attempt has been made to eliminate the following variables: collection time, collection locality, individual variation, and variation due to undigested food.

METHODS

The animals used in this study were dip-netted at Lat. 32°41′N, Long. 121°04′W on 10 May 1950. Immediately after capture they were preserved in a 5% buffered formalin solution. The body parts

were dissected and all particles identifiable as food were removed from the gastrozooids and gonozooids.

Wet weights of the body parts were determined volumetrically or gravimetrically, depending on the amount of material. After drying at 100°C, the body parts were ashed in a muffle furnace that was raised slowly to 800°C. Dry and ash weights of the parts were determined before the samples cooled to room temperature.

The ash residue of each kind of body part was mixed with a pure graphite powder matrix in a ratio of 1:1, after which the mixture was ground to a fine homogeneous powder in a silica mortar. The graphite matrix was prepared by adding potassium sulfate to graphite in a ratio of 1:9 and then by adding cobalt oxide to this mixture in the ratio of 0.001:1. The K_2SO_4 was used to promote uniform volatilization of the ash. The cobalt served as an internal standard of known concentration for correction of such variables as the amount of sample packed in each electrode or length of burning time, local variation in plate sensitivity, and amperage variation during burning. Preliminary analysis of ash from whole animals revealed less than 20 ppm cobalt.

Standards for calcium and magnesium were prepared by mixing appropriate amounts of dolomite (analyzed by U. S. National Bureau of Standards) with NaCl and combining this with the cobalt-graphite matrix. Standards for heavy metals were made up from their salts mixed in suitable concentrations with dolomite and the matrix. Duplicate quantitative analyses were run in all cases, and only those that agreed within $\pm 12\%$ were averaged and are reported here.

Details of equipment and technique used are as follows: Spectrograph—Jarrel-Ash, 3.4 m plane grating. Excitation—17 amp, D.C. Exposure—complete burning time of sample averaged about one minute. Rotating sector—seven steps with 1:2 step sector. Gap—4μ. Slit—10μ. Electrodes—$\frac{1}{8}$ inch (3 mm) diameter graphite drilled to 10 mm depth with a $\frac{3}{32}$ inch drill; counter electrode $\frac{1}{8}$ inch graphite, pointed. Film—spectrum analysis No. 1, Eastman. Development—D-19 developer, three minutes at 20°C, stop bath one minute, fixer three minutes, wash 10 minutes, air dried. CO_2 blower —O. Joensuu modification of the Stallwood (1954) carbon dioxide blower used to provide uniform burning and to reduce drift of working curves; pressure controlled with the aid of a mercury manometer. Emission lines (Å)—Ca 3181, Mg 3336, Al 3082, Cu 3274, Ti 3088, Ni 3050, Mn 2576, Fe 3021, Si 2882, Cr 2843, Sr 3464, V 3102, Ba 4554, Ag 3383, Pb 2833, Mo 3170, Zr 3391.

RESULTS

In the sun-dried remains of 100 kg of wet *Velella*, Haurowitz and Waelsch (1926) found nine elements: Na, K, Mg, Ca, Al, Fe, Cl, S, and P. In addition to these, the present study shows the following to be present in *V. lata*: Cu, Ni, Mn, Ti, Si, Cr, Sr, V, Ba, Ag, Pb, and Mo. Elements measured qualitatively in this study were present in concentrations greater than the following limiting sensitivities: Fe 10 ppm, Si 10 ppm, Cr 100 ppm, Sr 200 ppm, V 70 ppm, Ba 100 ppm, Ag 3 ppm, Pb 10 ppm, and Mo 10 ppm. One element, zirconium, was below the limit of detectability (150 ppm).

Table I lists the concentrations of Mg, Ca, Al, Cu, Mn, Ni, and Ti which were determined quantitatively in the ash of *V. lata* at five sizes. In order to facilitate conversion of the data in Table I to percent of dry or wet weight, the ratios of wet weight to dry weight and of dry weight to ash weight are given in Table II; also given are total wet weights. At a length of 85 mm, 61% of the wet weight of

TABLE I. Trace elements in *Velella lata*, percent of ash (mean of 2 analyses)

	$\bar{X}$ length (mm) and number of specimens					
	14.4	24.4	34.9	53.8	84.6	*Wtd. Mean*
	39	31	15	8	6	
Tissue	Magnesium					
P	2.6	4.8	7.8	5.5	12.0	7.7
SL	—	—	—	—	—	5.2
G	5.4	7.0	8.8	4.0	7.4	6.9
M	—	1.9	2.5	5.0	6.0	4.7
D	(2.9)		6.7	—	3.1	4.3
W	5.1	5.7	7.1	5.0	7.1	—
	Calcium					
P	7.5	—	4.6	9.0	9.8	6.0
SL	—	—	—	—	—	4.8
G	0.54	0.64	0.78	0.76	1.4	0.71
M	—	0.30	0.32	0.99	1.7	1.1
D	(0.53)		2.2	6.4	6.5	5.2
W	1.5	0.56	2.4	5.2	5.6	—
	Aluminum					
P	—	—	—	—	—	—
SL	—	—	—	—	—	—
G	0.37	0.25	0.32	0.17	0.26	0.29
M	—	0.31	0.20	0.32	0.28	0.28
D	(0.29)		0.12	—	0.018	0.17
W	0.36	0.29	0.23	0.28	0.16	—

TABLE I.—*Continued*

Tissue						
	Copper					
P	0.078	0.060	0.26	0.27	0.52	0.28
SL	—	—	—	—	—	0.36
G	0.070	0.16	0.15	0.04	0.16	0.13
M	—	0.09	0.13	0.12	0.10	0.11
D	(0.024)		0.02	0.057	0.049	0.042
W	0.071	0.12	0.16	0.13	0.22	—
	Manganese					
P	0.0031	0.0019	0.0010	0.0034	0.0055	0.0029
SL	—	—	—	—	—	0.0026
G	0.0004	0.0004	0.0008	0.0010	0.0027	0.0007
M	—	0.0004	0.0004	0.0027	0.0030	0.0023
D	(0.0006)		0.0004	0.0047	trace	0.0016
W	0.0010	0.0009	0.0007	0.0036	0.0041	—
	Nickel					
P	0.0084	—	0.0085	0.026	0.025	0.018
SL	—	—	—	—	—	0.011
G	0.0054	0.0026	0.011	0.019	0.0052	0.0060
M	—	0.0026	0.0038	0.019	0.0093	0.013
D	(0.0085)		0.0050	—	—	0.0019
W	0.0059	0.0033	0.0079	0.022	0.016	—
	Titanium					
P	0.14	—	0.034	0.061	0.032	0.044
SL	—	—	—	—	—	—
G	0.046	0.017	0.062	0.014	0.014	0.034
M	—	0.070	0.10	0.14	0.082	0.11
D	(0.058)		0.015	—	trace	0.027
W	0.059	0.14	0.046	0.088	0.051	—

P = Tissues covering the skeleton, SL = Skeleton, G = Gonozooids, M = Medusae, D = Dactyls, W = Whole Organism.

Samples in parentheses were combined because of insufficient ash. Size group analyses were not made on skeletons due to insufficient ash.

Dashes indicate analysis not available.

$$\text{Weighted mean} = \frac{\Sigma \text{ weights of the element in each size group}}{\Sigma \text{ ash weight of each size group}}$$

TABLE II.

Mean length mm	14.4	24.4	34.9	53.8	84.6
Wet weight / Dry weight	22.4	19.0	20.0	20.5	23.5
Dry weight / Ash weight	3.0	4.1	4.5	6.5	10.1
Total wet weight per specimen (mg).	128	370	1050	2670	8310

whole *V. lata* was tissue covering the skeleton, 15% dactyls, 12% skeleton; the gonozoids and medusae each made up 6%.

Magnesium and Calcium. These occur in sea water at concentrations of 0.13 and 0.04% respectively. Strictly speaking they are not trace elements. In *V. lata* magnesium made up 6.0% of the total ash and calcium 3.4%. Thus the Mg:Ca ratio is 1.8:1 in *Velella* compared to 3.7:1 in sea water, indicating that calcium is concentrated over magnesium in *Velella*. The Mg:Ca ratio in *Aurelia* has been reported as 0.92:1 and in *Cyanea* and *Aequorea* as 1:1 (Prosser, 1950), but since these are ratios of ions in the body fluids, they are not strictly comparable to the present data on the whole animal. However, it seems reasonable to expect *V. lata* to have a higher Mg:Ca ratio than these medusae, because *V. lata* contains large amounts of commensal zooxanthellae. Presumably these organisms would add to the concentration of magnesium since they contain chlorophyll.

Calcium is important in the control of permeability and hence of osmoregulation in estuarine animals. It is also essential for normal neuromuscular activity, for amoeboid and ciliary movement and for stabilization of intercellular matrices and mucus coverings. Thus it has widespread and vital physiological functions. Magnesium, on the other hand, though an essential constituent of chlorophyll, is not as important to animals as calcium and generally is not taken up as readily by marine animals. The Mg:Ca ratio varies widely in different tissues of *V. lata*. It is highest in the gonozooids and medusae, 9.7 and 4.3 respectively, is intermediate in the skeleton and in the tissue covering the skeleton, 1.1 and 1.2, and is lowest in the dactyls, 0.83. This distribution agrees well with the occurrence of the zooxanthellae, which are most abundant in the medusae and gonozooids and less common in the dactyls and tissue covering the skeleton. The ratio decreases in the gonozooids, medusae and dactyls as the size of *V. lata* increases, but it remains relatively constant or perhaps increases slightly in the tissue covering the skeleton. The relative concentration of calcium in the ash of the gonozooids, medusae, and dactyls appears to increase with size of *V. lata*. In the whole animal, from 14 to 85 mm total length, calcium concentration increases by a factor of about 5.

Aluminum. Although this is an essential element in terrestrial plant nutrition and is widespread in its occurrence in the animal kingdom, its function or functions are not known. It appears to be an essential constituent of the succinic oxidase system (Prosser, 1950). That Haurowitz and Waelsch (1926) found aluminum in *Velella* in a

preliminary qualitative analysis of its ash indicates that it is unusually common there. In the present study it was concentrated by a factor of 2000 over its average concentration in sea water and appears to remain relatively constant in the gonozooids and medusae as *V. lata* becomes larger. Aluminum appears to decrease in concentration in the dactyls with increase in size of *V. lata*. In the whole animal its concentration appears to decrease by a factor of about 2. Its concentration varies rather widely in the sea, Sverdrup, *et al.* (1946) reporting a range of 0.16 to 1.8 ppm. If aluminum should prove to be vital to the metabolism of *V. lata*, variations in the concentration of this element in the sea could be important in the ecology of the species.

Copper. This element is generally considered to be an essential constituent of protoplasm. It is necessary in the synthesis of haemocyanin, haemoglobin, and cytochrome a, and it occurs (like molybdenum, iron, and manganese) in certain metalloflavoproteins (Mahler, 1956).

The skeleton and the tissue covering the skeleton had relatively more copper than the gonozooids and medusae, which contained about three times more than the dactyls. The percent of copper in the ash of all tissues remained fairly constant as *V. lata* increased in size, excepting the tissue that covers the skeleton, where it increased by a factor of about seven. The only other comparable increase in concentration with increase in age of *V. lata* is manganese in the gonozooids and medusae. In the whole animal the copper concentration increases by a factor of about three.

Using the value of 0.003 ppm of copper in sea water (Goldberg, 1957), it appears that its concentration in *V. lata* tissues is about 5000 times greater than its abundance in sea water. This agrees well with its approximate concentration factor by soft marine invertebrates (Krumholz, *et al.*, 1957).

Manganese. This element was found in small amounts, making up from 0.0016 to 0.0029% of the total ash in all tissues except the gastrozooids, where it averaged about 0.0007%. In general the proportion of manganese in the ash increased in all tissues as *V. lata* increased in size. In the gonozooids and medusae the concentration of manganese increased by a factor of about seven, and in the whole animal by a factor of four.

It seems possible that manganese in *V. lata* is primarily tied up with the chlorophyll of the zooxanthellae, because it is essential for the synthesis of chlorophyll. However, there is a less pronounced correlation of manganese with the occurrence of the zooxanthellae

than there is in the case of magnesium. On the average, *V. lata* appears to concentrate manganese by a factor of about 100 over its concentration in sea water.

Nickel. Nickel makes up between 0.01 and 0.02% of the total ash except in the gonozooids and dactyls, where it is 0.006 and 0.002% respectively. In the largest specimens nickel is about three times more concentrated than in the smallest *Velella* examined. On the average, *V. lata* concentrates nickel about 2000 times over its concentration in the sea. This is considerably greater than the nickel concentration factors of 170–970:1 reported by Laevastu and Thompson (1956) for fresh plankton. They reported a greater concentration of nickel by plankton at the surface than by plankton in deeper water.

Titanium. This element, found in all tissues except the skeleton, forms 0.02 to 0.04% of the ash in the skin, gonozooids, and dactyls, and 0.1% in the medusae. In the whole animal the concentration may vary by a factor of 4; however there is no trend with increase in size. Goldberg (1957) has recently reported titanium in sea water at a concentration of 0.001 ppm. Thus it appears that titanium is concentrated in *Velella* by a factor of about 5000, which is about five times the approximate concentration in most other soft marine invertebrates studied so far (Goldberg, 1957).

Griel and Robinson (1952) have reported that ash of marine diatoms is between 0.003 and 0.2% titanium, and that this is about $^1/_{20}$ of the range reported by Webb and Fearon (1937) for living organisms in general. The titanium content of *V. lata* falls within the range reported by Griel and Robinson. Some recent workers, Goldberg and Arrhenius (1958) for example, have suggested that titanium in the marine environment is primarily of terrigenous origin. Note that these *Velella* as well as the diatoms analysed by Griel and Robinson were collected relatively near shore, in water that could well be characterized as neritic. Thus organisms collected in truly oceanic water might show considerably lower titanium concentrations than these.

CONCLUSION

This study has demonstrated the presence of 12 elements not previously reported from *Velella*. Those analysed quantitatively are concentrated from 100 to 5000 times over their concentrations in the sea. The problem of uptake, distribution, and utilization of these elements in *V. lata* is complicated by the fact that each individual

contains large quantities of commensal zooxanthellae, hence both plant and animal have been analyzed simultaneously. The plant factor could possibly be eliminated by keeping *Velella* in darkness long enough to bleach or kill the zooxanthellae. It seems reasonable to postulate that the higher Mg:Ca ratio in *V. lata* compared to that reported in scyphozoans is due to the presence of the zooxanthellae.

Between the lengths of 14 and 85 mm, manganese and calcium increase by factors of 4 and 5 respectively in whole *V. lata*. Nickel and copper increase by a factor of about 3, while aluminum and magnesium increase by factors of 2 and 1.5. Titanium showed no consistent change in concentration with change in size of *Velella*. The greatest changes noted in any tissues were those of copper in the skin covering the skeleton, a 7-fold increase, and of manganese in the gonozooids and medusae, a 7- and 7.5-fold increase.

ACKNOWLEDGEMENTS

Preliminary analyses were carried out at the University of Chicago with the assistance of Mr. O. Joensuu. Final determinations, made in the geochemistry section of the Lamont Geological Observatory, were partially supported by a grant from the Rockefeller Foundation. The material was collected by the Scripps Institution of Oceanography in connection with the Cooperative Oceanic Fisheries Investigations. Miss Marla Bottesch assisted with part of the dissection of *V. lata*. The assistance of these persons and organizations is gratefully acknowledged.

REFERENCES

GOLDBERG, E. D.
1957. Biogeochemistry of trace metals, in: Treatise on marine ecology and paleoecology. Chap. 12. Mem. Geochem. Soc. Amer., 67, *1:* 345–357.

GOLDBERG, E. D. AND G. O. S. ARRHENIUS
1958. Chemistry of Pacific pelagic sediments. Geochim. Cosmochim. Acta, *13:* 153–212.

GRIEL, J. V. AND R. J. ROBINSON
1952. Titanium in sea water. J. Mar. Res., *11*(2): 173–179.

LAUROWITZ, F. AND H. WAELSCH
1926. Ueber die chemische Zusammensetzung der Qualle *Velella spirans*. Hoppe-Seyl Z., *161*(6): 300–317.

RUMHOLZ, L. A., E. D. GOLDBERG AND H. BOROUGHS
1957. Ecological factors involved in the uptake, accumulation, and loss of radionuclides by aquatic organisms, in: Effects of atomic radiation on oceanography and fisheries. Chap. 7. Publ. nat. Res. Coun. Wash., No. 551: 69–79.

Laevastu, Taivo and T. G. Thompson
1956. The determination and occurrence of nickel in sea water, marine organisms, and sediments. J. Cons. int. Explor. Mer, *21*(2): 125–143.
Mahler, H. R.
1956. Nature and abundance of metalloflavoproteins, in: Advances in enzymology and related subjects of biochemistry, by F. F. Nord, *17*, Interscience Publishers, N. Y. 556 pp.
Prosser, C. L. (Edit.)
1950. Comparative animal physiology. Saunders Co., Philadelphia. 888 pp.
Stallwood, B. J.
1954. Air cooled electrodes for spectrochemical analysis of powders. J. opt. Soc. Amer., *44*(2): 171–176.
Sverdrup, H. U., M. W. Johnson and R. H. Fleming
1946. The Oceans. Prentice Hall, Inc., New York. 1087 pp.
Vinogradov, A. P.
1953. The elementary chemical composition of marine organisms. Mem. Sears Found. Mar. Res., II; 647 pp.
Webb, D. A. and W. R. Fearon
1937. Studies on the ultimate composition of biological material I. Sci. Proc. R. Dublin Soc., *21:* 484–504.

ELLIPTICAL POLARIZATION OF SUBMARINE ILLUMINATION[1]

By

ALEXANDRE IVANOFF

École Supérieure de Physique et de Chimie Industrielles, Paris

AND

TALBOT H. WATERMAN

Department of Zoology, Yale University, New Haven, Conn.

ABSTRACT

Field and laboratory measurements have been made to extend our understanding of ubmarine elliptically polarized light, which occurs in lines of sight just beyond the ritical angle. It is not detectable in bearings of the sun or anti-sun, is strongest ithin a few centimeters of the surface, is more easily observed with large solar zenith stances, and is not affected by light entering the water at the surface in the line of ght. The most likely origin of this elliptical light is by total reflection at the water rface of linearly polarized light arising from the scattering of directional light in the ater. Aquarium observations of total reflection of linear light fulfill in all basic ays the expectations of the hypothesis. The latter is developed quantitatively by lculating the relations between elliptical polarization and the bearing and elevation the line of sight as well as the sun's zenith distance. These figures show that when e line of sight is 58° from the vertical and between 70 and 160° from the sun's bear-g, maximal ellipticity ratios of about 0.3 may be present for solar zenith distances reater than 50 to 70°. The orientation of the ellipse's major axis does not differ gnificantly from the plane of linear light which gives rise to it. Under the best con-tions, elliptical light reaches more than 10% of the total light and its ratio to linear olarized light may be 0.5 or more. The theoretical section, while limited by certain mplifying assumptions, is nevertheless in general accord with field and laboratory easurements and provides directives for future quantitative work on this henomenon.

INTRODUCTION

The polarization pattern of natural underwater illumination consists mainly of linearly polarized light. This arises through the attering of penetrating sunlight by particles in the medium (Waterman and Westell, 1956; Ivanoff, 1957). However, elliptically polarized ght is also present as a definite but less prominent component of atural submarine light (Waterman, 1954, 1958). Until now its tailed occurrence and its origin have not been studied; the present

[1] Contribution No. 244 from the Bermuda Biological Station.

report describes field and laboratory measurements of this phenomenon supplemented by a theoretical analysis.

METHODS

Previous observations demonstrated merely that at shallow depths and in lines of sight near the critical angle, significant amounts of subsurface polarized light are neither linearly nor circularly polarized and consequently must be elliptical (Waterman, 1954). This information was obtained while using SCUBA and employing a hand-held interference analyzer which indicates directly the absence or presence and type of polarization in any light source examined (Waterman, 1955). The observations reported here were made with a similar device which consists of a calcite plate cut perpendicular to its optic axis and followed by a circular polarization analyzer.

When convergent elliptically polarized light is observed through this optical system (Waterman, 1955), the concentric series of isochromatic rings produced with circularly polarized light become distorted (Figs. 3D, F; 4D, F) into ellipsoidal figures (Bertin, 1859). At the same time the central spot in the pattern is altered to a bilobed form whose brightness or darkness depends, as in the case of circular light, on the direction of rotation of the vibrations concerned.

In use this device was either hand-held by an observer using an aqualung or set on an adjustable tripod so that its line of sight could be more accurately controlled. In addition, visual observations were supplemented by photographs of the interference figures produced under various circumstances. While such crystallographic information is not ideal for quantitative analysis because of the complex relations between input parameters and the resulting interference pattern, it does provide an adequate basis for describing the underlying phenomenon and for testing the theory here proposed to account for the origin of the ellipticity.

Field data were obtained in Bermuda at depths ranging from 1 to 5 m below the sea surface. Most of the observations were made in shallow water over a bottom of light sand or weathered aeolean limestone 1 to 2 m below the point of view. The water was moderately turbid, and maximum linear polarization was about 20%. On one occasion a few observations were made near the surface at a station where the water's depth was more than 200 m. Lines of sight were taken through 360° of azimuth relative to the sun's bearing and at various elevation angles from horizontal to vertical. Present data were obtained at times when the sun's zenith distance was between 45 and 90° because elliptical light seems to be observed more easily

at such times than when the sun is higher in the sky; however, no systematic field study has been made of the effects of this parameter, although its influence has been calculated in the theoretical section below. Photographic records were made by holding the interference analyzer close against the underwater case of a Zeiss Contaflex camera focussed on the interference figure (Fig. 3).

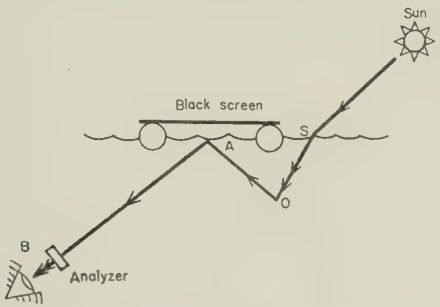

Figure 1. Method of using a floating black screen to reduce effects of sun and sky light on water between observer and sea surface. Totally reflected light was observed in the direction *BA* and, as without the screen, it was linear in azimuths of sun and anti-sun and more or less elliptically polarized at intermediate angles (see Fig. 3).

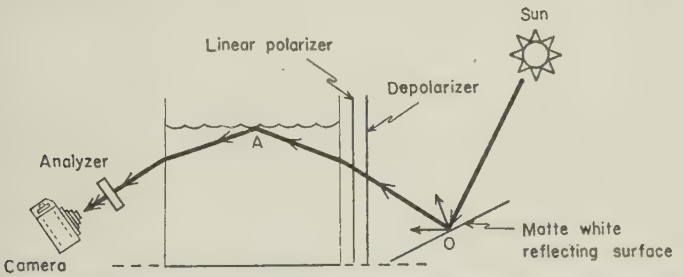

Figure 2. Method of photographing the polarization pattern in totally reflected linear light from the water surface in an aquarium. The linear polarizer's predominant e-vector could be rotated and the relative position of the depolarizer and polarizer interchanged as a control. Typical results, closely resembling those observed in the field (see Fig. 3), are shown in Fig. 4.

From the first field measurements, a tentative hypothesis was devised to explain the observed elliptical polarization, which presumes that total reflection of underwater linearly polarized light by the sea surface viewed beyond the critical angle is responsible. To test this, both field and laboratory observations were made. In the field, a dark horizontal screen about 2 m square, held above the water on floats, was used to determine whether elliptical polarization depends on effects such as scattering of light by the water between the surface and the observer (Fig. 1). In the laboratory, total reflection of

linearly polarized light by the air-water interface was observed and photographed in aquaria arranged so that the plane of vibration of incident light could be adjusted (Fig. 2). To do this a large sheet of linearly polarizing film was placed outside the wall of the aquarium opposite the observer. Beyond this polaroid filter a sheet of waxed paper eliminated any stray polarization which may have been present in the light source; this was an oblique white matte surface illuminated by direct sunlight which was screened from the rest of the set-up. Under such conditions the surface-reflected image of the lighted side of the tank can be viewed or photographed from outside at any angle where complete reflection occurs.

RESULTS

Field Observations. The present results confirmed the original observation (Waterman, 1954) that underwater illumination in shallow water is in part elliptically polarized near the critical angle. In lines of sight differing from the vertical by less than the critical angle, the polarization pattern near the surface is mainly established by that of the sky which is observed directly even though distorted by surface refraction. In lines of sight differing from the vertical by much more than the critical angle (48°16′ if n for sea water is taken as 1.34), light is linearly polarized by scattering (Fig. 3A, C, E). But within an area close beyond the critical angle there is a significant amount of ellipticity under certain conditions (Fig. 3D, F). Observations with a black screen shielding the point observed from overhead (Fig. 1) showed that this does not affect the occurrence and pattern of elliptical light. Such data are important in supporting our hypothesis for the origin of elliptical polarization.

In lines of sight of about 35 to 40° above the horizontal, the presence and orientation of the ellipticity depend on the relative position of the sun. In the sun's bearing and in that of the anti-sun, the light observed is linearly polarized with the e-vector horizontal, just as it is in these azimuths for all elevation angles of the line of sight. But in directions between those of the sun and anti-sun the polarization is not merely linear; it then has an elliptical component, unless the sun is in the zenith.

Visibility of the elliptical interference figures and *pari passu* the amount of elliptical light diminish with the observer's distance from the surface and with the degree to which the zenith angle of the line of sight exceeds the critical angle. Thus the greatest amount of elliptical polarization occurs within a few centimeters of the surface. Here, too, ellipticity is apparent at angles which may considerably

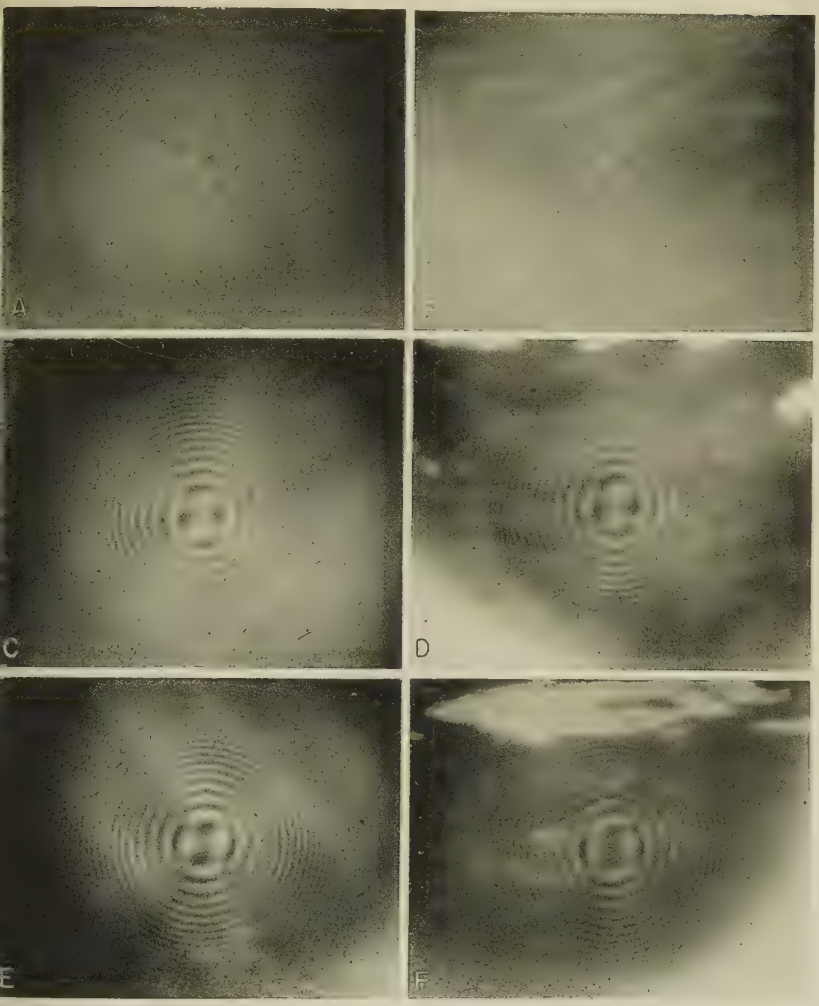

Figure 3. Polarization patterns in underwater illumination observed in various directions in shallow water with solar zenith distances between 60 and 70°. **A.** Line of sight horizontal in sun's bearing. **B.** Looking upward at 40° from horizontal in sun's bearing. **C.** Horizontal, 90° to left of sun's bearing. **D.** Upward 40°, 90° to left of sun's bearing. **E.** Horizontal, 90° to right of sun. **F.** Upward 40°, 90° to right of sun. In **A** and **B**, polarization is linear and the E-vector tilt corresponds to the angle of refraction of the sunlight (40 to 45°), as is clearly seen from rays visible in the water; in **D** and **F**, polarization is elliptical, rotation being counter-clockwise in **D** and clockwise in **F**. Similar patterns also occur when the floating black screen is used as diagrammed in Fig. 1.

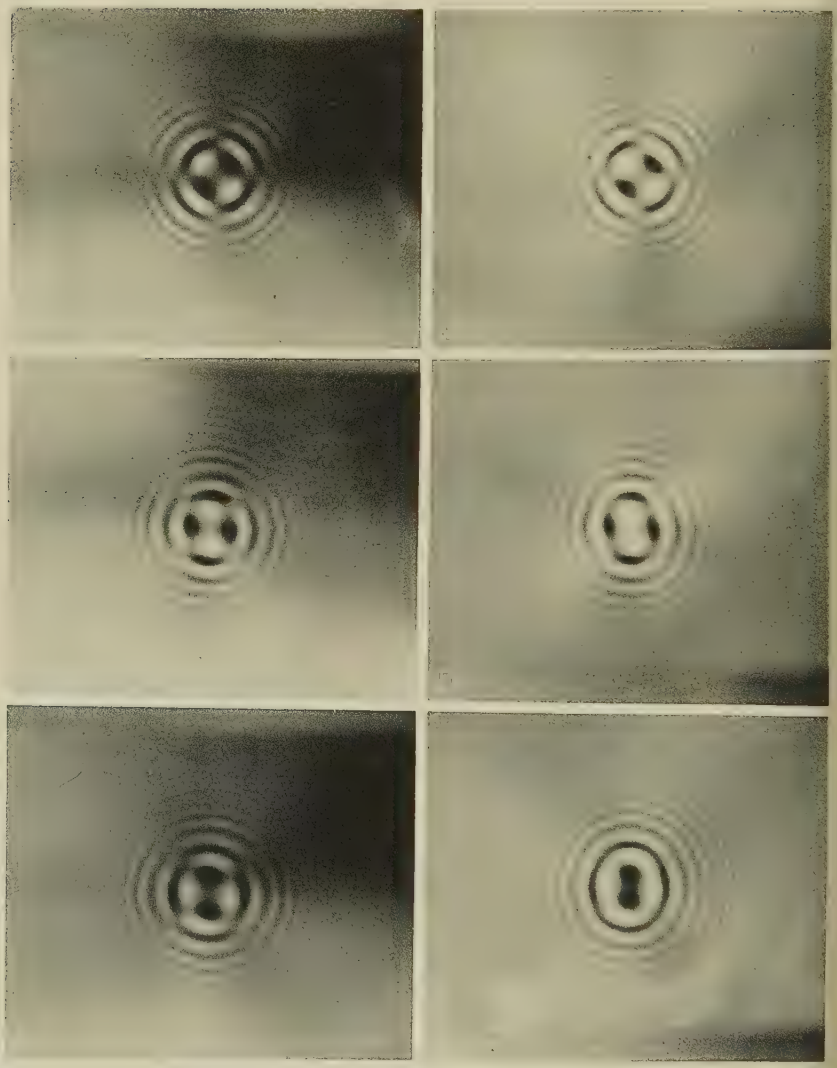

Figure 4. Polarization patterns observed in aquarium set-up as diagrammed in Fig. 2. In **A** and **B** the linear polarizer had its predominant e-vector horizontal; in **C** and **D** this was tilted 45° clockwise from horizontal; in **E** and **F** it was tilted 45° counter-clockwise from horizontal. In **A**, **C**, and **E** the line of sight was horizontal; the edge of the water surface at the far side of the tank is just seen near the upper edge of each frame. The light observed in the direction of the interference figure therefore came directly through the side wall and is linearly polarized. In **B**, **D** and **F** the line of sight was elevated 40° from horizontal; the junction between water surface and tank side is visible near the lower edge of each frame. The light observed in the interference figure thus is linearly polarized light totally reflected from the surface. Where the e-vector was not perpendicular or parallel to the plane of incidence, reflected light was elliptically polarized (**D** and **F**) with different directions of rotation depending on the angle between the e-vector and the horizontal. Note the basic correspondence to the polarization pattern of natural light observed in the field (Fig. 3).

exceed 48°16′. But at greater depths, even at 2 to 3 m, the amount of elliptical light seems appreciably reduced, as is the angle over which it is detectable; the latter becomes more closely restricted to lines of sight just beyond the smallest angle of total reflection. These two facts together suggest that the amount of elliptical light in total submarine illumination diminishes with an increase in the length of the underwater path from the observer's eye to the totally reflecting sea surface.

The actual interference pattern produced by submarine elliptically polarized light is strongly dependent on the sun's relative bearing. When the line of sight is to the left of the sun the figure's center is light and the most central isochromatic ellipse has two dark swellings in it (Fig. 3D). When it is to the right of the sun the pattern has a dark somewhat dumbbell-shaped center (Fig. 3F). Because of the optics of the analyzer, this means that the rotation of the elliptical light is counterclockwise to the left of the sun and clockwise to the right of it.

In general the major axis of the elliptical interference patterns recorded is nearly vertical and differs considerably from the plane of linear polarization observed horizontally in the same azimuth. For example, one pair of photographs made at 90° to the right of the sun's bearing shows that the major axis of the elliptical figure in a line of sight having a 40° elevation made an angle of 86° clockwise from horizontal (Fig. 3F) while the plane of linear light in a line of sight with a 0° elevation made an angle of 38° counterclockwise from horizontal (Fig. 3E).

In a complex way the orientation of the interference ellipse is apparently related also to the azimuth of the line of sight. For instance, looking upward at 40°, and at 90° to the left of the sun, the major axis of the figure was inclined at 82° counterclockwise from horizontal (Fig. 3D); at the same elevation, and at 135° to the left of the sun, it was inclined clockwise by 84°. Further data are required to establish these relations systematically and to demonstrate in addition the relation between the elliptical figure observed and the actual orientation of the elliptical vibrations. From present qualitative results one may predict that both azimuth and elevation of the lines of sight as well as the zenith distance of the sun and the state of the sea surface will influence the resulting pattern.

Aquarium Observations. If our hypothesis is correct that elliptical light present in the sea results from total reflection of linearly polarized light by the surface, similar patterns should be reproducible in an aquarium under appropriate conditions. This expectation has been

fulfilled in a series of visual and photographic observations (Fig. 4) made as described above. The kind of light totally reflected from the air-water interface of an aquarium was found to depend on orientation of the **e**-vector of incident linear light. Thus, when this vector is horizontal or vertical (*i.e.*, parallel or normal to the reflecting surface), reflected light is also linear, and its polarization plane remains unchanged (Fig. 4B). But when the polarization plane of incident light is oblique relative to the surface, then the interference figure of reflected light is ellipsoidal (Fig. 4D, F).

The direction of the light's rotation and the orientation of the figure's major axis depend on the angle between the **e**-vector and the plane of incidence. **E**-vectors tilted clockwise from the horizontal produce interference patterns with bright centers, indicating a counterclockwise rotation (see p. 261 and Fig. 4D); those tilted counterclockwise from the horizontal produce dark-centered patterns, indicating clockwise rotation of the light (Fig. 4F). Of course, when the line of sight is horizontal and normal to the polarizing filter, the light observed is linearly polarized in the transmitting plane of the filter (Fig. 4A, C, E).

From comparison of the nearly identical figures photographed in the field and in the laboratory (Figs. 3, 4) it seems quite probable that in both cases the same mechanism is at work producing elliptically polarized light. In view of this and the obvious correlation of laboratory studies with the hypothesis proposed to explain the field observations, a more detailed development of the theory seems desirable. This may serve not only to organize the facts already known but to provide also some useful cues for future fruitful work.

THEORY AND PREDICTIONS

To develop a satisfactory theory for the elliptical component of submarine polarization it is essential to select conditions which are less complex than those observed in the field, particularly at low sun elevations. Consequently detailed comparison of field measurements and curves predicted from the theory is not possible, although good basic agreement nevertheless will be found between them. Consider first (Fig. 5) a ray of light travelling underwater in the direction AB which intercepts the vertical at an angle V which is greater than the angle of total reflection and smaller than 90°. The light in this ray consists of a portion scattered by the water in the direction AB as well as a portion scattered by the water along OA and then totally reflected along AB by the sea surface. The first portion is partially linearly polarized by scattering; let P_d (Fig. 6A) be the angle between its electric vector and the horizontal. The second portion is also partially linearly polarized by scattering along OA; let P_r (Fig. 6B) be

the angle between its **e**-vector and the horizontal. When total reflection occurs at A, the component of the **e**-vector parallel to the plane of incidence (having an amplitude proportional to sin P_r) undergoes a change of phase different from that of the perpendicular component (having an amplitude proportional to cos P_r). Let the difference between these phase changes be ϕ (Fig. 6B). As a result of this total reflection, an elliptical oscillation travels in the direction AB and is added to the light scattered in this direction by the water. Let a and b be axial lengths of this elliptical oscillation and ψ the angle between its major axis and the horizontal.

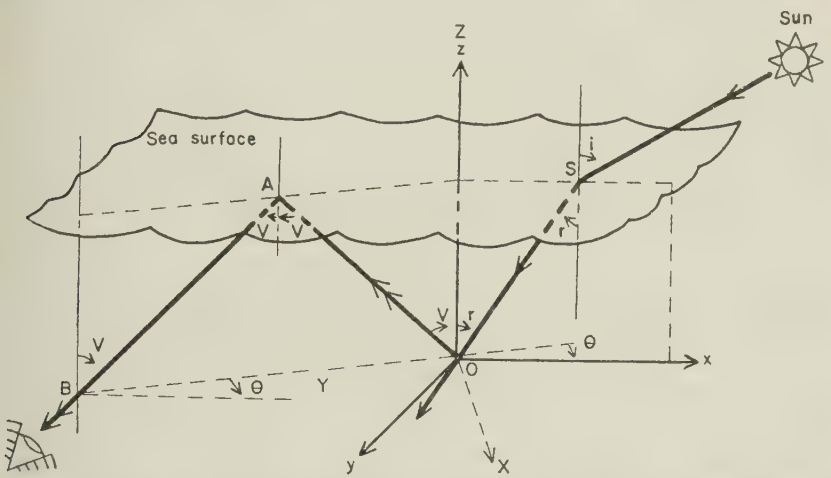

Figure 5. Diagram to illustrate origins of polarized light seen by an observer at B looking in direction BA. One component originates in light directly scattered along AB, the second from total reflection at A of light scattered along OA. The former is linearly polarized while the latter may be elliptically polarized. i, solar zenith angle; r, refracted angle of sun's rays; xz, vertical plane of sunlight incidence parallel to the plane through observer and sun; YZ, vertical plane passing through the line of sight BA; xyz, perpendicular coordinate system relative to the plane of incidence; XYZ, coordinate system relative to the plane of the line of sight; θ, difference angle between xz and YZ planes; V, angular deviation of the line of sight from the vertical.

1. *General Equations.* If the angle P_r is known and if the sea surface is assumed to be a plane, the theory of specular electromagnetic reflection permits not only the ratio b/a but the angle ψ to be calculated. For this only the classic equations (1), (2), (3) are required:

$$\tan \frac{\phi}{2} = \frac{\cos V \cdot \sqrt{\sin^2 V - \sin^2 L}}{\sin^2 V}; \tag{1}$$

$$| \sin 2\beta | = | \sin 2 P_r \cdot \sin \phi |, \quad \text{where } | \tan \beta | = | b/a | ; \tag{2}$$

$$\tan 2\psi = \tan 2 P_r \cdot \cos \phi . \tag{3}$$

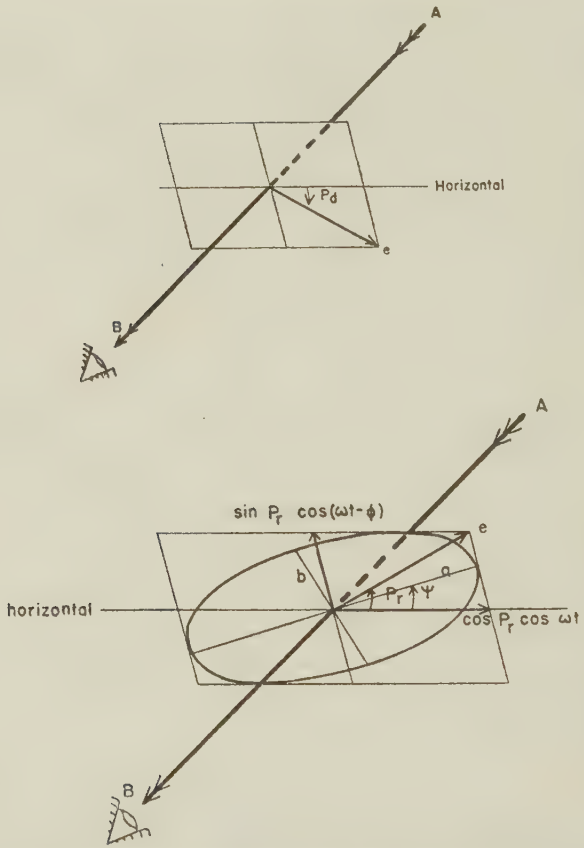

Figure 6. The two components of polarized light propagated along AB (see Fig. 5). **Top**. Portion scattered by superficial water layers in direction AB. The characteristics of this light are labelled with the subscript d to emphasize light scattered *directly* along AB. The vector **e** shows the direction of vibration and P_d its angle with the horizontal. **Bottom**. Component scattered along OA and then totally reflected in direction AB by the sea surface. The characteristics of this light are labelled with the subscript r to emphasize light *reflected* or to be *reflected* from the sea surface. The vector **e** is the predominant electric field before reflection. Its projections on the vertical and horizontal are labelled appropriately; a and b are the major and minor axes of the reflected elliptical light. P_r and ψ are the angles made by the e-vector and by the major axis respectively with the horizontal.

In (1), L is the angle of total reflection; this is related to refractive indices of air (n') and sea water (n) so that $\sin L = n'/n$. In the following calculations n/n' is assumed to be 1.34 and L 48°16′. For a given ϕ (equivalent to a given inclination of the line of sight V), the ratio b/a is maximal when $P_r = \pm 45°$, in which case $|\beta| = |\phi/2|$ and $\psi = P_r$. Fig. 7 shows the relations between V and ϕ calculated

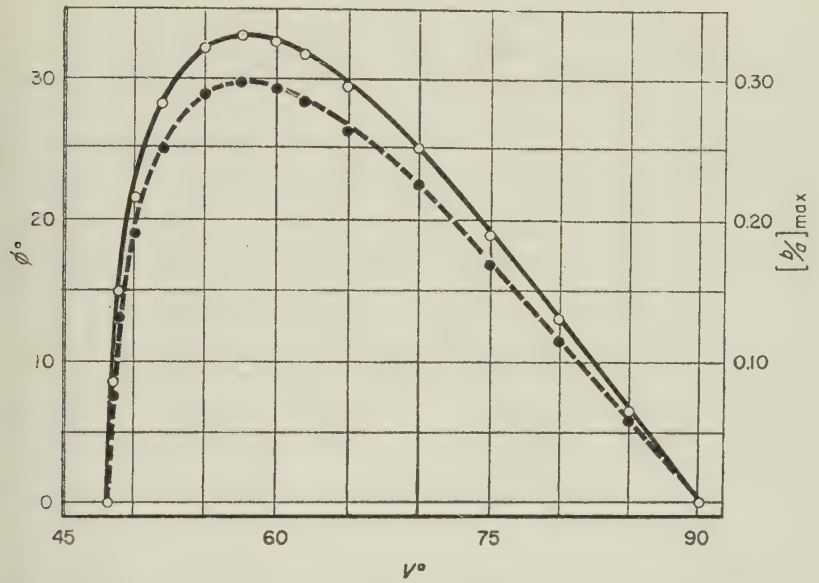

Figure 7. Difference in phase shifts (ϕ, solid line) effected by total reflection at A (Fig. 5) between components perpendicular and parallel to the plane of incidence; also the corresponding axial ratios (b/a, broken line) of the elliptical vibration reflected along AB. Both are a function of the angle between the line of sight and the vertical (V).

from eq. (1) as well as corresponding values of $[b/a]_{max}$ found when $P_r = \pm 45°$. Under the best conditions, when $P_r = \pm 45°$ and $V \cong 58°$ (or more accurately 57°44′, since ϕ is maximum when $\sin^2 V = 2 \sin^2 L/1 + \sin^2 L$), the ratio b/a may reach a value of 0.297.

Note that, according to eq. (2), b/a approaches zero at the same time as the angle P_r which occurs when the **e**-vector of light scattered in the direction OA approaches the horizontal. This implies that the amount of elliptical oscillation decreases in cloudy weather since at such times the **e**-vector approaches the horizontal in all lines of sight (Waterman, 1954; Ivanoff, 1957). On the other hand, the presence of elliptical polarization at sunset would seem to indicate that the angle P_r does not decrease when the sea surface is illuminated by the clear blue sky, an effect probably due to sky polarization. Apparently a cloudy sky and a clear sky without the sun have quite different effects on orientation of the plane of submarine light polarization.

However this may be, P_r must be known to solve (2) and (3). To make the calculation of P_r easy, the simple case is used below where illumination coming from the sky is quite weak compared with direct sunlight. Consequently the ensuing data are restricted to sun's

altitudes greater than 20 or even 30°; hence they cannot be directly compared with the previously mentioned field results obtained at sunset. It is hoped that further observations will be made at greater sun's altitudes.

According to the classic theory of light scattering, the **e**-vector of scattered light is a projection of the **e**-vector of incident light on a plane normal to the direction of scattering. Consequently if this theory is valid in sea water and if the incident light is unpolarized, the polarization plane of scattered underwater light is obtained by projecting, on a plane normal to the direction of scattering, the circle whose center is traversed perpendicularly by the incident light's direction. In general this projection is an ellipse whose major axis is oriented in the same direction as the polarization plane in question. Furthermore, the ellipse's major axis is parallel to the line of intersection of the two planes, one normal to the direction of scattered light and the other normal to the direction of incident light.

This line of intersection, which is the orientation of the predominant **e**-vector, may be derived as follows. Let i and r (Fig. 5) be the angles of incidence and refraction of the sun's rays. Through some point in the water O let z be the vertical axis and x the bearing of the sun. The plane xz is thus a vertical plane parallel to the vertical plane passing through the sun as well as the observer who is at B. Then let θ represent the angle between the plane OAB with the plane xz; θ is therefore the angle between the azimuth of the line of sight BA and the sun's bearing; this angle will be measured from the sun's bearing to the azimuth of the line of sight, being considered positive for clockwise rotation; thus for lines of sight to the right of the sun, or to the left of the anti-sun, θ will be between 0 and $+180°$. In contrast the angles i, r and V will always be used in the positive sense and will always be less than 90°, since changing i and r to $-i$ and $-r$, or V to $-V$, is equivalent to altering θ to $\theta + 180°$.

The axial components of the direction of the incident light SO are: $x = -\sin r; y = 0; z = -\cos r$; those for the direction OA of scattered light are: $x = -\sin V \cdot \cos\theta; y = -\sin V \cdot \sin\theta; z = \cos V$.
The equation for the plane normal to SO and passing through O is therefore

$$x \sin r + z \sin r = 0$$

while that for the plane normal to OA and passing through 0 is

$$-x \sin V \cdot \cos\theta - y \sin V \cdot \sin\theta + z \cos V = 0 \ .$$

From these equations we derive:

$$\frac{x}{\sin V \cdot \sin\theta} = -\frac{y}{\sin V \cdot \cos\theta \tan r \cdot \cos V} = -\frac{z}{\tan r \cdot \sin V \cdot \sin\theta}$$

whence the components of the intersection of the two planes in question and hence of the predominant **e**-vector of the light scattered along the line OA can be obtained: $x = \sin V \cdot \sin\theta$; $y = -\sin V \cdot \cos\theta - \tan r \cdot \cos V$; $z = -\tan r \cdot \sin V \cdot \sin\theta$.

To determine the components of the **e**-vector parallel and normal to the plane of incidence OAB, take X as the axis normal to this plane, Y as the projection of OAB on the xy plane, with Z the same as axis z. In these terms the normal component of the **e**-vector is

$$X = -x\sin\theta + y\cos\theta = -\sin V - \tan r \cdot \cos V \cdot \cos\theta$$

while the component parallel to the plane of incidence (with the positive direction assumed towards the sea surface) is

$$Z\sin V - Y\cos V = z\sin V + x\cos V\cos\theta + y\cos V \cdot \sin\theta = -\tan r \cdot \sin\theta .$$

The angle P_r between the **e**-vector and the horizontal is therefore such that

$$\tan P_r = \frac{Z\sin V - Y\cos V}{X} = \frac{\tan r \cdot \sin\theta}{\sin V + \tan r \cdot \cos V \cdot \cos\theta} \qquad (4)^2$$

with P_r being measured from the horizontal with the positive rotation being clockwise for an observer at A looking towards O or at B looking towards A.[3]

Equation (4) together with (1), (2) and (3) allows the ellipticity ratio b/a and the orientation ψ of the major axis of elliptical polarization to be calculated for any line of sight AB. It is of interest to compare the orientation of the ellipse (ψ), not only with the P_r (Fig. 6B) of the linearly polarized light which gave rise to it but also with the P_d (Fig. 6A) of linearly polarized light scattered by the water in the direction AB, to which the elliptical light is added. Since a change from the direction OA to the direction AB merely alters $V = \angle AOZ$

[2] In the theoretical curves plotted by Waterman and Westell (1956: fig. 12), the cross products factor in the denominator of this equation was omitted.

[3] When $V = 90°$, $\tan P_r = \tan r$ when $\theta = +90°$ and $\tan P_r = -\tan r$ when $\theta = -90°$. This results from our sign conventions that r is always positive whereas P_r changes sign above and below the horizontal.

to $180° - V = <BAZ$, appropriate substitution in equation (4) yields

$$\tan P_d = \frac{\tan r \cdot \sin \theta}{\sin V - \tan r \cdot \cos V \cdot \cos \theta} \quad . \tag{5}$$

The same result could be obtained by changing θ to $180° - \theta$; in other words, the value of P_d corresponding to θ is the same as that of P_r corresponding to $180° - \theta$ for a given r and V:

$$[P_d]_\theta = [P_r]_{180°-\theta} \tag{6}$$

and when $\theta = \pm 90°$,

$$\tan P_d = \tan P_r = \pm \frac{\tan r}{\sin V} \quad .$$

2. *Direction of Rotation of the Elliptical Oscillation.* In the azimuths of the sun ($\theta = 0$) and the anti-sun ($\theta = 180°$), $\tan P_r = 0$. Since the angles r and V are positive and less than 90°, $\tan P_r$ is positive if $\sin \theta$ is also positive and if at the same time

$$\sin V + \tan r \cdot \cos V \cdot \cos \theta > 0 \ ,$$

which is equivalent to

$$\cos \theta > - \frac{\tan V}{\tan r} \quad .$$

This is always the case since V is greater than the angle of total reflection. The fact that angle P_r is positive for lines of sight to the right of the sun and negative for those to the left agrees with field observations (Waterman, 1954). Since the component advanced by total reflection is that parallel to the plane of incidence, the resulting elliptical polarization produced at A as seen by an observer at B looking towards A is clockwise when $0 < \theta < +180°$ and is counterclockwise when $0 > \theta > -180°$.

3. *Axial Ratio of Elliptical Polarization in the Totally Reflected Light.* Absolute values of the axial ratio b/a, when $\theta = \pm 90°$, are given in Fig. 8 as a function of V for nine different zenith distances of the sun (i) ranging from 10 to 90°. Since the method used above to determine P_r is not valid for low solar altitudes, the curves for $i = 80$ and 90° are shown only as broken lines. The graph shows that b/a is maximal when $V = 58°$ (already shown as the maximal V for $\sin \phi$) and that b/a decreases rapidly as i decreases from 50 to 0°. Similar results have been obtained for $\theta = \pm 45°$ and $\pm 135°$,

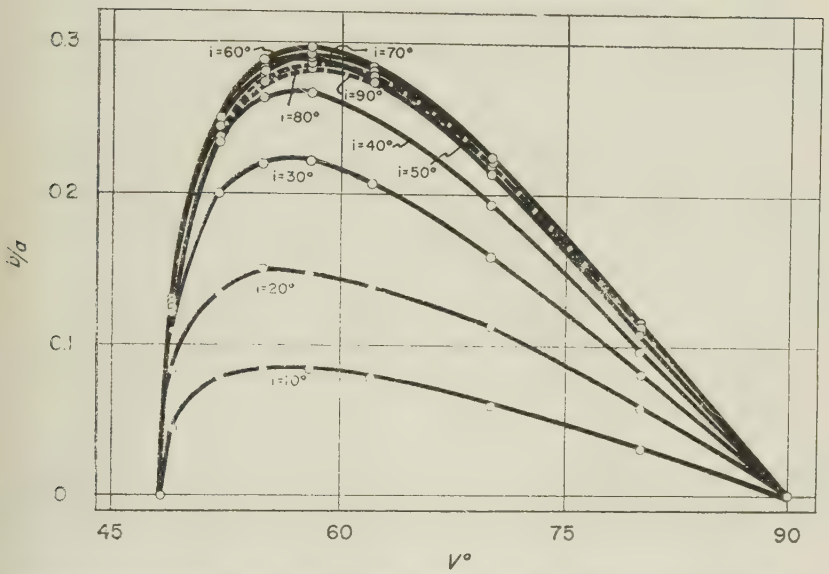

Figure 8. Ellipticity ratios (b/a) for $\theta = \pm 90°$ at various zenith distances of the sun (i) plotted as functions of the angle between the line of sight and the vertical (V). The broken lines for $i = 80°$, $i = 90°$ indicate the speculative nature of the calculations near sunrise and sunset.

with b/a being maximal for $55° < V < 61°$ and decreasing rapidly as i is less than 50 to 70°.

Absolute values of b/a are shown in Fig. 9 as a function of θ for cases where $V = 58°$ (maximum value of $b/a = 0.297$) and for four values of i between 30 and 90°, the latter again being drawn in broken lines. Note that ellipticity decreases steeply when the azimuth of the line of sight approaches that of the anti-sun and then decreases less rapidly towards the sun's bearing. If i is less than 50°, b/a has two maxima, one at $|\theta| \cong 70°$ and the other at $|\theta| \cong 160$ to 165°. Between these points the ellipticity varies relatively little. (The same results may be derived from the second order equation of $\cos\theta$ obtained by setting $\tan^2 P_r = 1$).

Similar relations have been obtained for $V = 49$, 52 and 70°; maximal values for b/a are 0.131, 0.251, 0.224 respectively; the functions decrease rapidly towards the anti-sun and less abruptly towards the sun; when i is 30° a single maximum occurs, but when $i = 70$ and 90° there are two maxima. In general, then, for $i \geq 50°$ and $40° < |\theta| < 165°$, the ratio b/a varies mainly with the angle between the line of sight and the vertical (V); when the latter is about 52 to 65° the ratio is greater than 0.2. The axial ratio decreases: 1) when the

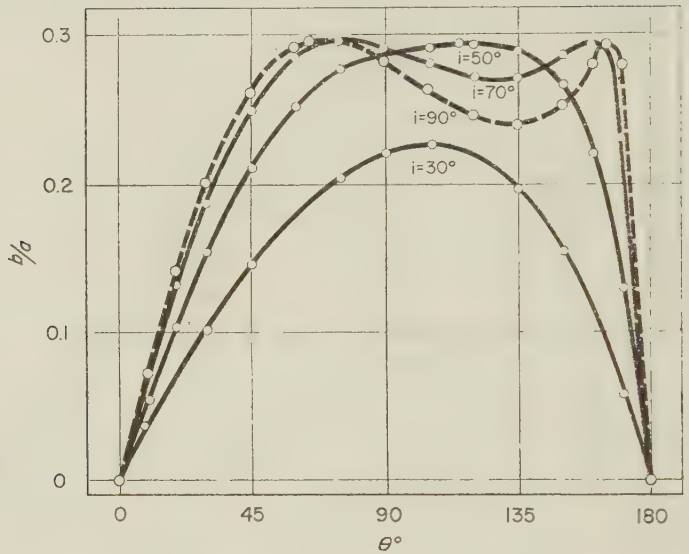

Figure 9. Ellipticity ratios (b/a) for $V = 58°$ at various zenith distances of the sun plotted as functions of the angle between the line of sight and the sun's bearing (θ). The broken line for $i = 90°$ indicates the speculative nature of the function.

sun's zenith distance decreases from 50 to 0°; 2) when the azimuth of the line of sight approaches that of the sun or the anti-sun; and 3) when V is less than 52° or greater than 65°.

4. *Influence of Surface Roughness.* The angles r, θ and OAB will vary about their means if the sea surface is rough, but from what has just been said, variations in the value of OAB would seem especially important for the relation b/a. Since the curve relating ϕ and V (Fig. 7) is concave downward, any oscillations of V will decrease the maximal value of b/a. This effect should be particularly marked when the average V is about 58°. Then a ± 10 to 15° slope of the sea surface would prevent b/a from exceeding 0.2 under the best conditions. Note that these considerations are independent of P_r so that they hold also around sunrise and sunset.

5. *Orientation of the Major Axis of Ellipticity.* The difference $|\psi| - |P_r|$ is shown in Fig. 10 as a function of V for $\theta = \pm 90°$ and for nine values of i from 10 to 90°; as before, the curves for 80 and 90° are merely speculative. The graph shows that $|\psi| - |P_r|$ scarcely exceeds 2°, which means that the major axis of the elliptical

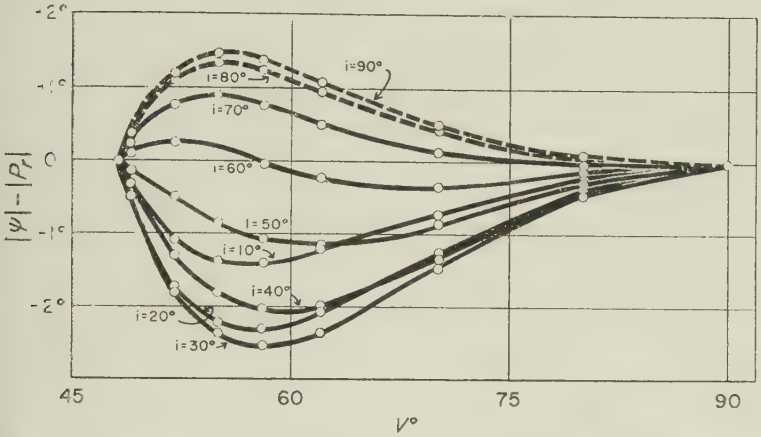

Figure 10. Difference between the tilt of the reflected elliptical light's major axis (ψ) and the tilt of the e-vector of incident linear light (P_r) which gives rise to it by reflection at A (Fig. 5) plotted as a function of the angle between the line of sight and the vertical (V) for $\theta = \pm 90°$ at various solar zenith distances including the speculative cases where $i = 80$ and 90° (broken lines).

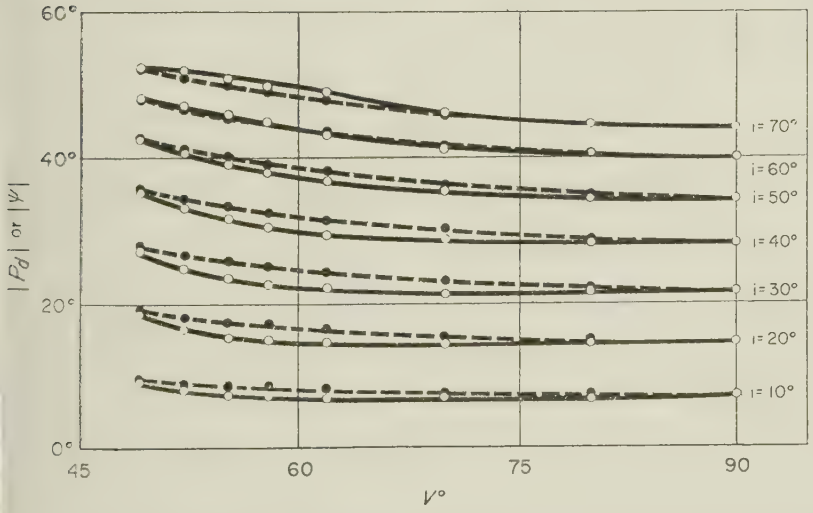

Figure 11. Tilt of the reflected elliptical light's major axis (ψ, solid lines) and the tilt of the e-vector of the linear light (P_d, broken lines) directly scattered along AB (Fig. 5) plotted as functions of the angle between the line of sight and the vertical (V) when $\theta = \pm 90°$ (therefore $| P_d | = | P_r |$) for various solar zenith distances (i).

polarization makes an angle with the horizontal which is nearly equal to that made with the same reference by the linear polarization which gives rise to it. In Fig. 11, $|\psi|$ and $|P_d|$ are plotted as functions of V when $\theta = \pm 90°$ and when i varies from 10 to 70°. As stated above, when $\theta = \pm 90°$ P_d and P_r are the same so that $|\psi| - |P_r|$ and $|\psi| - |P_d|$ would also be the same. In other words, for lines of sight at right angles to the sun's bearing, reflected elliptically polarized light in the direction AB has nearly the same orientation as linearly polarized light scattered in that direction by the water. Only their elliptical and linear qualities distinguish these two kinds of light provided the axial ratio b/a is not too small.

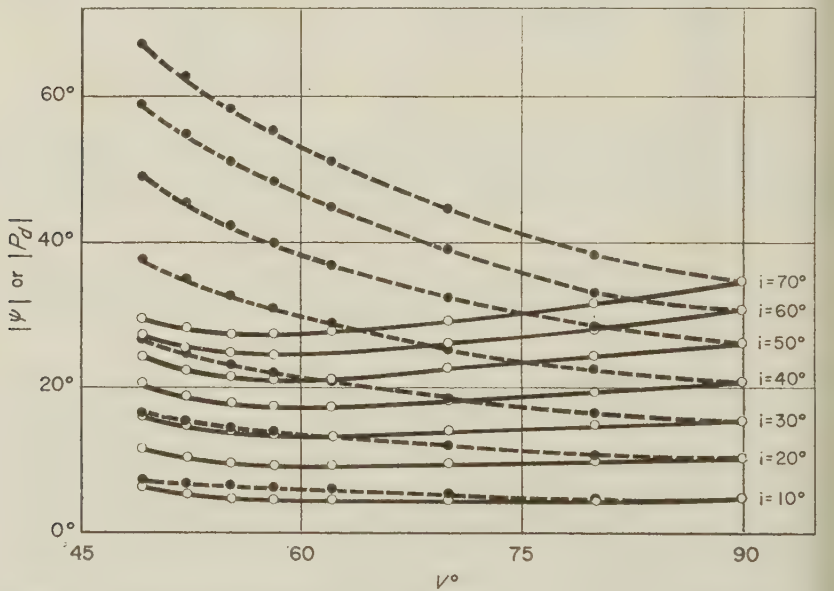

Figure 12. Same as Fig. 11 except that $\theta = 45°$ (therefore $|P_d| \neq |P_r|$). As before, solid lines represent ψ, broken lines P_d.

For $\theta = \pm 45°$ and $\pm 135°$, the differences between $|\psi|$ and $|P_r|$ are similar to those for $\theta = 90°$ and never exceed 2°. In contrast, $|\psi|$ and $|P_d|$ may differ appreciably when θ is not $\pm 90°$. This is shown in Fig. 12 where $|\psi|$ and $|P_d|$ are plotted as a function of V when $\theta = \pm 45°$ and where i varies in seven steps from 10 to 70°. This shows that the difference between ψ and P_d is greater with diminishing V and increasing i, reaching 30° when V is about 58° and i about 70°. The same holds for $\theta = 135°$, but in that case $|\psi| > |P_d|$. Under such conditions elliptical polarization may be distinguishable

rom linear polarization scattered in the same direction even if the atio b/a is very small.

The difference $|P_r - P_d|$, which is within 2° of being the same as $\psi - P_d|$, is plotted in Fig. 13 as a function of θ with $V = 58°$ and at four values from 30 to 90° (again 90° is speculative). This difference increases with i, and for $i \geq 50°$ its maximum lies between = 25 and 35° and between 145 and 155°, since eq. (6) shows that

$$[P_r - P_d]_{180°-\theta} = [P_d - P_r]_\theta .$$

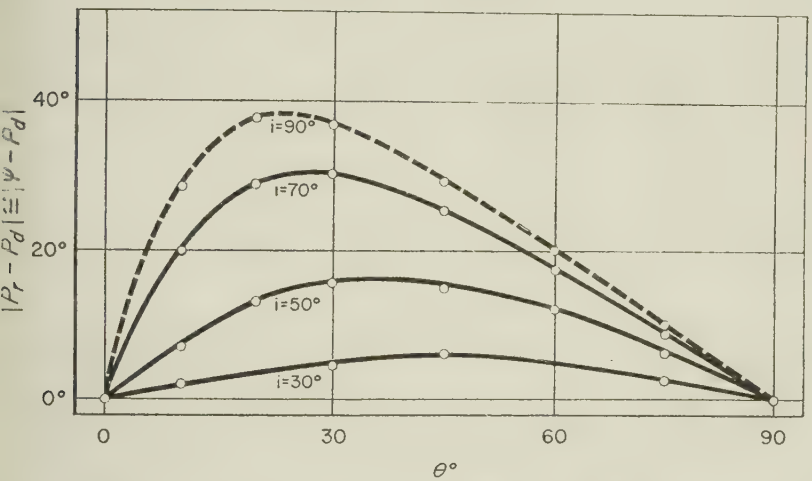

Figure 13. Difference between the e-vector orientation of linear light (P_r) reflected at A (Fig. 5) nd that of linear light scattered directly along AB (P_d) plotted as a function of the angle between the ne of sight and the solar bearing (θ) for $V = 58°$ at various solar zenith distances (i) including the peculative case where $i = 90°$. Note that $P_r - P_d$ is approximately the same as $\psi - P_d$ (Fig. 10).

Similar relations hold when $V = 49$ and 52°, but on the one hand $P_r - P_d|$ increases as V decreases (as already noted for Fig. 12) nd on the other hand the maximum difference at the same time moves oward values of θ nearer 0 and 180°. For example, when $V = 52°$ nd $i = 70°$, $|P_r - P_d|$ reaches 43° for $\theta = \pm 22°$ and $\pm 158°$. On his basis one would expect that the best conditions for detecting the ifference between ψ and P_d would be found near the critical angle, ith the sun low on the horizon and with θ about 20 or 160°.

6. *Amount of Elliptical Polarization.* Possibly a comparison of ne amounts of linear and elliptical polarization propagated in the irection AB is even more interesting than their orientation, particularly in terms of their importance relative to each other and to

total radiance. These relations require a knowledge of the angular distributions of radiance and of its polarization at various depths, but unfortunately these factors are poorly known and vary markedly with the water mass and with different conditions of overcast and solar altitude. Consequently the following relations are perforce quite crude approximations which must be interpreted carefully.

Let I_d[3a] be the radiance at B which has been directly scattered along AB, and p_d the corresponding degree of polarization. Let I_r be the radiance at A (sea surface) which has been scattered along OA and which will be reflected in the direction AB by the surface; p_r is the corresponding degree of polarization. Finally call h the depth of point B and c the extinction coefficient of the sea water. Then the radiance at point B for linear light[3b] transmitted in the direction AB is $I_d \cdot p_d$ while that for elliptical light is

$$I_r \cdot p_r \cdot e^{-c\frac{h}{\cos V}}$$

and the total radiance at B in the direction BA is

$$I_t = I_d + I_r e^{-c\frac{h}{\cos V}} \cdot$$

The lack of symmetry in these equations arises because I_d refers to point B whereas I_r refers to point A which nevertheless seems to have advantages.

The absolute importance of elliptical polarization at B in the direction BA (defined as the ratio of elliptical light to total light) is therefore

$$\frac{I_r \cdot p_r \cdot e^{-c\frac{h}{\cos V}}}{I_t} = \frac{I_r \cdot p_r \cdot e^{-c\frac{h}{\cos V}}}{I_d + I_r \cdot e^{-c\frac{h}{\cos V}}} \cdot \tag{7}$$

This decreases with depth since I_t certainly diminishes less quickly than $e^{-c\frac{h}{\cos V}}$.[4] Similarly, the relative importance of elliptical polarization (defined as the ratio of elliptical to linear light) is given by

[3a] According to the International Lighting Vocabulary (Ed. 2, 1957, Comm. int de l'Éclaraige), the symbol for radiance is L_e, but since several subscripts are required here, I is used for this parameter.

[3b] Strictly in this and in subsequent uses of the word "*light*," "*radiance*," as defined in the International Lighting Vocabulary, is more precise because wavelengths beyond the visible are included.

[4] The way in which I_t varies with depth is a function of V and is complex at shallow depths. When $45° < V < 90°$ probably I_t even begins to increase somewhat with depth because of the increasing importance of scattered light. At greater depths I decreases exponentially with an exponent less than c and thus certainly less than $c/\cos V$.

$$\frac{I_r \cdot p_r \cdot e^{-c\frac{h}{\cos V}}}{I_d \cdot p_d}. \tag{8}$$

Here the effect of depth is less certain, since p_d also becomes smaller with depth. Nevertheless for values of V which are of interest here, $e^{-c\frac{h}{\cos V}}$ probably decreases more rapidly than $I_d \cdot p_d$.

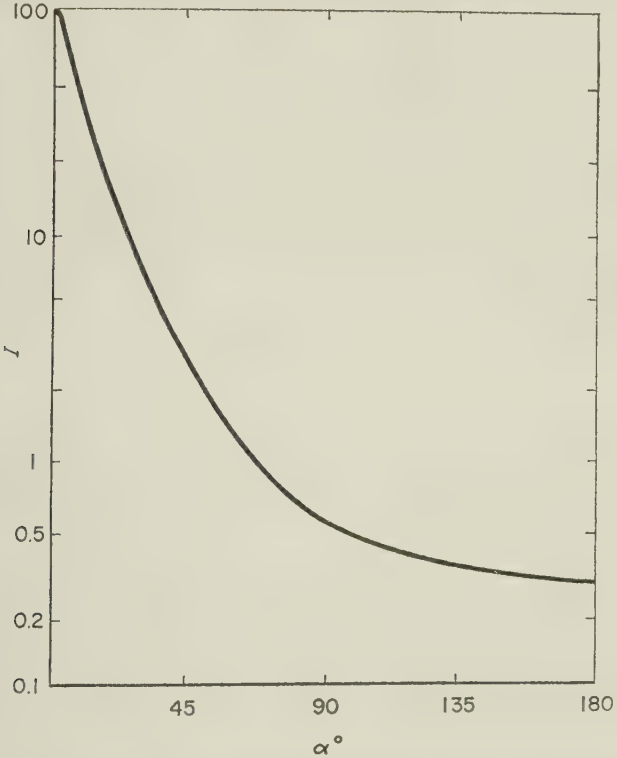

Figure 14. Angular distribution of submarine radiance at shallow depths in clear water with a cloudless sky and the sun well above the horizon as averaged from data obtained by Jerlov (1951) at 5 m in the Mediterranean Sea and by Sasaki, *et al.* (1957) at 10 m in the northwestern Pacific. α is the angle between a given line of sight and the direction of maximal radiance underwater (*SO* in Fig. 5) where it has been taken as 100. The distribution has been assumed radially symmetrical around *SO*, although this is only a rough approximation.

First consider the limiting case of negligible depth for which (7) and (8) reduce respectively to $I_r \cdot p_r/I_t$ and $I_r \cdot p_r/I_d \cdot p_d$. To solve these expressions the angular distributions of radiance and of its degree of polarization must be known immediately below the surface. A particular angular distribution of radiance (Fig. 14) has been assumed

for the following analysis. This is valid only at depths of about 5 to 10 m in clear water when the sun's zenith distances are not too great. In using this approximation, I_r is obtained by taking[5] $\alpha = \alpha_r$ (the angle between OA and the prolongation of SO) and $I_t = I_d + I_r$ by taking $\alpha = \alpha_d$ (the angle between AB and the prolongation of SO).

From the axial projections of SO, OA and AB it can be shown that

$$\cos \alpha_r = \sin r \sin V \cos \theta - \cos r \cos V \ ,$$

$$\cos \alpha_d = \sin r \sin V \cos \theta + \cos r \cos V \ .$$

These equations and Fig. 14 permit calculation of I_r, I_t and I_d as functions of r, V, and θ.

The angular distribution of the degree of polarization has been assumed to follow the eq. $\sin^2 \alpha / 1 + \cos^2 \alpha$. This is probably only a rough approximation (Ivanoff and Waterman, 1958), even for directions beyond the critical angle which is the region of present interest.[6] From this one obtains

$$p_r = p_{\max} \frac{\sin^2 \alpha_r}{1 + \cos^2 \alpha_r} \ ,$$

$$p_d = p_{\max} \frac{\sin^2 \alpha_d}{1 + \cos^2 \alpha_d} \ ,$$

where $p_{\max}$ is the maximum amount of submarine polarization which occurs when $| \alpha | \cong 90°$.[7]

The relations $I_r p_r / I_t p_{\max}$ and $I_r p_r / I_d p_d$ are plotted in Fig. 15 as a function of θ for cases where $V = 58°$ and i is varied in three steps from 30 to 70°. This shows that elliptical light may be more than 10% of total radiance under the conditions assumed in deriving the equations, provided $V = 58°$, $i \geq 50°$ and $70° < | \theta | < 120°$. Such absolute importance decreases rapidly in azimuths towards the sun and the anti-sun. The ratio of elliptical to linear polarized light is about 0.5 for θ's between 30 and 120°. This relative importance decreases towards the anti-sun's azimuth and increases towards the sun's bearing where the degree of linear polarization is even weaker than the elliptical.

Quite comparable relations have been calculated for $V = 49$ and 70°. At 49° elliptical polarization shows roughly half the relative and absolute values found at 58°, and at 70° these are about twice as great

[5] For definition, see Fig. 5.

[6] Within the critical angle, sky polarization complicates matters considerably.

[7] $p_{\max}$ is about 0.4 to 0.6 in clear water in the immediate neighborhood of the sea surface.

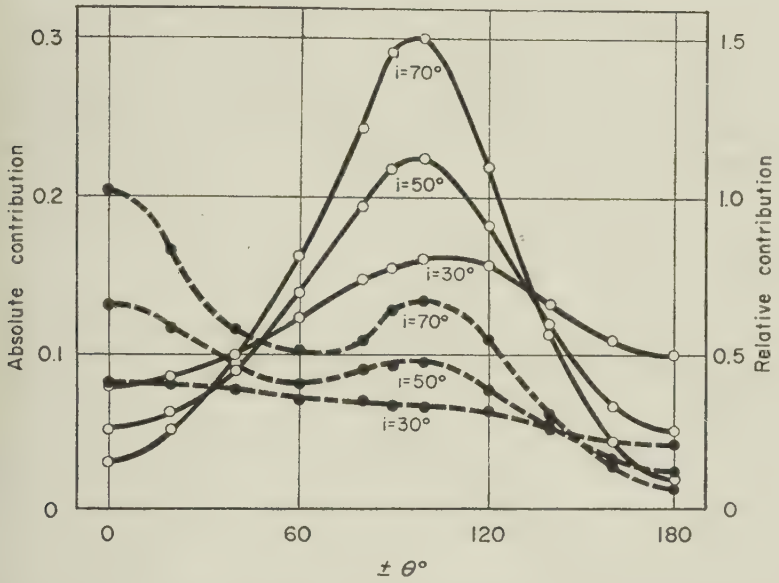

Figure 15. Absolute importance (*i.e.*, ratio of elliptical light to total luminous flux) and relative importance (*i.e.*, ratio of elliptical to linear components) of elliptically polarized light plotted as functions of the angle between the line of sight and the solar bearing (θ) for $V = 58°$ at various solar zenith distances. Computed for clear water and infinitely shallow depth. Absolute contributions shown as solid lines, relative contributions as broken lines.

s at 58°. Apparently then, at an infinitely shallow depth, elliptical polarization increases steadily with V although this is not so for the real case of a finite depth. The absolute importance is maximal for $= \pm 90°$, and the relative importance varies less than the absolute with azimuth although it always decreases towards the anti-sun's azimuth. Note finally that if p_{max} decreases because of either more turbid water or the proximity of a light bottom (Waterman, 1954, 958; Ivanoff and Waterman, 1958), the absolute importance of elliptical light decreases proportionately (as do p_r and p_d) although the relative value is constant. However, since turbidity and bottom reflection also affect the angular distribution of radiance underwater, it is difficult to predict their over-all influence on the situation. It is hoped that further observations will be made on these relations.

Now the real case of a finite depth h will be considered. The amount of elliptical polarization then becomes $I_r p_r e^{-c\frac{h}{\cos V}}$, where I_r and p_r are as above because they are functions of zero depth. The amount of linear polarization becomes $I_d p_d$, where $I_d = I_t - I_r e^{-c\frac{h}{\cos V}}$

and $$p_d = p_{\max} \frac{\sin^2 \alpha_d}{1 + \cos^2 \alpha_d}.$$

Here I_t and $p_{\max}$ are no longer the same as those immediately unde the sea surface since the angular distribution of both radiance an polarization vary with depth. As already stated, these are difficu to study quantitatively. But the gross effects of angle V can b

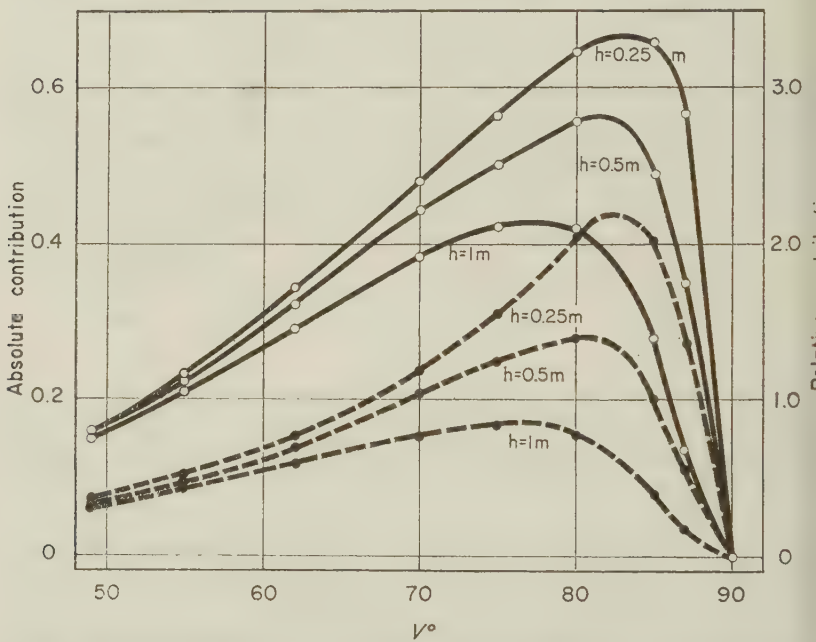

Figure 16. Absolute and relative importance of elliptical polarization plotted as functions of t angle between the line of sight and the vertical (V) when $\theta = \pm 90°$, $i = 70°$, $c = 0.1$/m, and when is varied.

computed as a function of depth if I_t and $p_{\max}$ are assumed constan at shallow depths. This relation is plotted in Fig. 16 for cases whe $i = 70°$, $\theta = \pm 90°$, $c = 0.1$/m (which is reasonable for moderatel clear water) and where h varies from 0.25 to 1.0 m. Obviously th importance of elliptical polarization passes through a maximum f an angle V which decreases with depth and turbidity. Such a resu is easy to predict, but elliptical polarization would appear to b maximal at angles V greater than 75° in clear water of less than 1 depth. Note finally that in Fig. 16 the importance of elliptical pola ization is shown decreasing with depth to a degree dependent on th

onstancy of I_t and p_{max}. However, as already suggested, I_t prob-bly increases at shallow depths for the pertinent lines of sight; con-equently the relation $I_r p_r e^{-c\frac{h}{\cos V}}$ decreases with h more rapidly than ppears in Fig. 16. But it is hard to say what happens to the relative nportance (eq. 8).

DISCUSSION

The results of the above theoretical analysis of the axial ratio of liptical light, the orientation (ψ) of its major axis and its amount ay now be reviewed with particular emphasis on general relations nce the calculations are not rigorous for details.

The ratio b/a of the axes of elliptical polarization: 1) increases with e zenith distance of the sun; 2) varies little with θ between 40 and 5° and $i \geq 50°$; 3) diminishes towards the azimuth of the sun and e anti-sun; 4) is maximal for V's between 52 and 65°, when it is reater than 0.2 under the best conditions; and 5) decreases with in-reasing roughness of the sea surface.

In the orientation of elliptical polarization: 1) the major axis makes n angle ψ with the horizontal within 2° of P_r which represents the lane of linear light that produces the elliptical component; 2) angle $_r - P_d$ is nearly equal to $\psi - P_d$, the angle between the major axis the elliptical component and the plane of the linear component avelling in the same direction, and it increases as i increases and as decreases; as i increases or V decreases it becomes maximal for s which move toward 0 or 180°, but it is 0 when $\theta = 0$ and 180° as ell as ±90°.

The amount of elliptical polarization: 1) increases with i; 2) is aximum when V is 70 to 85° in clear waters within 1 to 2 m of the rface; 3) shows an absolute maximum (10% under the best con-tions) when $\theta = \pm 90°$ and decreases towards 0 and 180°; and 4) aries little relative to linear polarized light scattered in the same rection when θ is 30 to 120°, decreases towards 180°, increases wards 0°, and probably decreases with depth; under the best con-tions the ratio scarcely exceeds one. Recall however that these lculations are limited by the fact that they become less valid as the n approaches the horizon.

Thus the importance of elliptical polarization seems to increase th three predominant factors: 1) the calmness of the sea; 2) the imuth distance of the sun; and 3) nearness of the observation point the surface. The effects of the azimuth and elevation of the line of ght are more subtle because conclusions differ depending on whether e is interested in b/a or in $P_r - P_d$, that is, in the relative or in the solute importance of elliptical polarization. Only one example

will be considered here. This relates to b/a and the ratio of elliptical to linear polarization, both of which affect the interference analyzer used in making field observations. When traversed by elliptical light, this device produces an interference pattern deformed from that produced by linear polarization. This deformation will be seen if the ratio b/a is not too small and if the intensity of elliptical oscillation is large enough in relation to linear polarization.

The calculations have shown that, when $i \geqslant 50°$, the ratio b/a varies little between $\theta = 40°$ and 165° and is maximum when V = 52 to 65° while the relative importance of elliptical polarization varies little between $30° < |\theta| < 120°$ and is maximum when V is about 70 to 85°. Consequently, for the analyzer in question, the influence of θ probably would be weak when this angle is between about ±40 to 130°, and the optimum V would be about 65° if the water is clear. Now, according to calculations for $V \cong 65°$, the relative importance of elliptical polarization reaches a maximum of about 1 (Fig. 16), which means that it is the same order of magnitude as linear polarization. Such a ratio seems inadequate to explain the clearly deformed interference figures observed in the field.

This suggests that, around sunrise or sunset, conditions beyond those assumed for the calculations may occur so that the importance of the elliptical polarization becomes greater, probably because the underwater illumination becomes more diffuse. As a result the ratios I_r/I and I_r/I_d increase, which means, in agreement with actual measurements (Jerlov, 1951), that the amount of light scattered upward in the direction OA increases relative to that scattered downward along AB. Possibly, under conditions assumed in the calculations, elliptical polarization is so weak that it could be observed only under a floating screen which suppressed all scattering along AB.

However, this suggestion that elliptical polarization may become stronger around times of sunrise and sunset is not unequivocally acceptable and is in fact false under certain conditions. Thus, close to sunset the **e**-vector has been observed to be vertical in some azimuths, which is probably an effect of sky polarization (Waterman, 1955, 1958). In such a case there is no elliptical polarization because b/a is obviously zero or infinite if the **e**-vector of the linear light which is totally reflected is normal or parallel to the plane of incidence. Such may be the explanation of the occasion when the sun was within a few degrees of the horizon and elliptical polarization was so weak that it was detectable only within a few centimeters of the surface. This was a single observation period and was the only one made in deep water far from the bottom. Certainly it seems quite unlikely that the small amount of elliptical light present is explainable by the

remoteness of the bottom. The absence of bottom reflection and scattering would be expected to increase the directionality of the light and probably both its linear and elliptical polarization; instead the reverse changes actually occurred. Clearly this observation re-emphasizes the fact that complex and poorly understood polarization patterns occur at sunrise and sunset when the direct rays of the sun are not the predominant element that produces submarine illumination (Waterman, 1954, 1958). Further field work is obviously needed here, particularly to check the specific contribution of the sky at such times.

When the predictions here calculated from theory are compared with results obtained in the laboratory and in the sea, good agreement is found on basic points, but quantitative field data are required to test some of the comparisons critically. Thus elliptical light is more detectable at shallow depths, at large zenith angles of the sun, in directions just outside the critical angle, and in azimuths excluding the bearings of the sun and the anti-sun. The elliptical light rotates clockwise to the right of the sun, anticlockwise to its left and is not affected by light entering the water near the point of surface reflection. In the aquarium records, basic similarities are present too; again elliptical light is observed obliquely just beyond the critical angle, but not horizontally. The consequent rotation of the e-vector has the same sign changes relative to the linear polarization pattern in all three cases.

On the basis of these facts the hypothesis that elliptical light in the sea originates by total reflection of linearly polarized light produced by scattering of directional underwater illumination seems clearly consonant with the facts. Further work is needed to test the quantitative correlations between the functions here computed and those actually present in the sea. It will be of interest also to determine whether or not elliptically polarized natural light is of any biological significance.

ACKNOWLEDGMENT

Dr. R. F. Nunnemacher provided helpful assistance during some of the field measurements and Dr. W. H. Sutcliffe, JR., Director of the Bermuda Biological Station, gave invaluable cooperation.

REFERENCES

BERTIN, A.
1859. Sur les franges que présente, dans la pince à tourmalines, un spath perpendiculaire placé entre deux micas d'un quart d'onde. Ann. Chim. (Phys.), *57*(3): 257–290.

Ivanoff, Alexandre

1957. Contribution à l'étude des propriétés optiques de l'eau de mer en Bretagne et en Corse, et à la théorie de la polarisation sous-marine. Ann. Géophys., *13:* 22–53.

Ivanoff, Alexandre and T. H. Waterman

1958. Factors, mainly depth and wavelength, affecting the degree of underwater light polarization. J. Mar. Res., *16*(3): 283–307.

Jerlov, N. G.

1951. Optical studies of ocean waters. Rep. Swedish Deep Sea Exped. 1947–8, *3*(1): 1–59.

Sasaki, T., N. Okami, S. Watanabe and G. Oshiba

1957. Measurements of the angular distribution of daylight in the sea. Rec. oceanogr. Works Japan, Spec. No.: 42–45. March.

Waterman, T. H.

1954. Polarization patterns in submarine illumination. Science, *120:* 927–932.

1955. Polarization of scattered sunlight in deep water. Deep-Sea Res., Suppl. *3:* 426–434. Bigelow Festschrift.

1958. Polarized light and plankton navigation. *In:* "Perspectives in Marine Biology". (Ed.: A. A. Buzzati-Traverso) University of California Press, Berkeley, pp. 429–450.

Waterman, T. H. and W. E. Westell

1956. Quantitative effects of the sun's position on submarine light polarization. J. mar. Res., *15:* 149–169.

FACTORS, MAINLY DEPTH AND WAVELENGTH, AFFECTING THE DEGREE OF UNDERWATER LIGHT POLARIZATION[1]

By

ALEXANDRE IVANOFF

École Supérieure de Physique et de Chimie Industrielles, Paris

AND

TALBOT H. WATERMAN

Department of Zoology, Yale University, New Haven, Conn.

ABSTRACT

Field and laboratory comparisons of visual, photographic and photoelectric methods of measuring linear polarization of underwater light demonstrate that satisfactory agreement may be obtained between their results. While laboratory data match closely, several uncontrollable factors, especially changes in cloudiness, increase the variance of field measurements. Of the three, the photoelectric polarimeter lends itself best to the study of degree of polarization in the horizontal plane at various depths. The present report briefly describes the principle of this device and summarizes the results of a series of measurements correlating principally the effects of wavelength (λ) and depth (h) down to 115 m with the degree of linear polarization in submarine illumination (p) of water masses having a wide range of turbidities. Although the data so obtained are continuous through 360° in azimuth, most of the analyses have been made for $\theta = 0$, ± 90 and 180° with a few for $\pm 45°$, where θ is azimuth measured from the sun's bearing, positive to the right, negative to the left. In general, p is maximal near the surface, diminishes rapidly in the first 10–40 m, and then decreases more slowly to some equilibrium level. The maximal p, the extent of its rapid decrease, and the equilibrium value all depend strongly on the turbidity of the water, on the cloud cover, and on the proximity and albedo of the bottom. Polarization increases rapidly with transparency in turbid and moderately clear waters but more slowly in extremely clear water. Thus, in quite clear water far from the bottom p may reach 60% or more near the surface, decrease rapidly at greater depths to about 40 m, and then level off slowly to 30% in deep water. Under such conditions, with the solar zenith angle (i) not too small, p is maximum for $\theta = \pm 90°$, less for $\theta = 180°$ and least for $\theta = 0°$. With i smaller or with greater turbidity, p at $\theta = 180°$ may equal p at $\pm 90°$; under extreme conditions of this sort p may not vary with θ. The influence of λ on p is small but definite, with p_{min} occurring at blue or blue-green wavelengths; both ends of the spectrum, particularly the longer wavelengths, polarize more strongly. The amplitude

[1] Contribution No. 245 from the Bermuda Biological Station.

of the effect of λ on p (Δp) is small when p is small, but $\Delta p/p$ appears relatively constant.

Most of these facts are consistent with the origin of submarine linear polarization by scattering. The degree of polarization decreases when the diffuseness of underwater light increases; that is, it decreases mainly with cloudiness, with depth, with turbidity, and with the λ of greatest penetration.

INTRODUCTION

The pattern of linearly polarized light in the sea was first demonstrated in shallow water (Waterman, 1954) and then at greater depths down to 200 m (Waterman, 1955). Later, quantitative measurements were initiated using photographic (Ivanoff, 1955, 1956a, 1956b) and visual (Waterman and Westell, 1956; Waterman, 1958) techniques. A theoretical analysis correlating the degree of polarization (p) with the angular distribution of submarine illumination showed that p should decrease both with depth (h) and for the most penetrating wavelength (λ) (Ivanoff, 1957a). However, at that time the available field data were limited to shallow water and were not suitable for studying the effect of λ. To help remedy these deficiencies, a remote control polarimeter capable of operating down to 120 m and of selecting any of six spectral regions was built (Ivanoff, 1957b). Preliminary measurements with this device showed that polarization does in fact decrease with h, but they still did not demonstrate the effect of λ (Ivanoff, 1957b).

The present paper reports results of a systematic application of this instrument in Bermuda, where the influence of various factors, mainly h and λ, on the degree of polarization of submarine light were measured. Also included are comparisons of the two other methods previously used independently by the authors. At the same time, the occurrence and origin of elliptical polarization in the sea was studied, but this work is reported elsewhere (Ivanoff and Waterman, 1958).

INSTRUMENTATION

The Photoelectric Polarimeter. Since the three methods we have used to measure underwater light polarization have already been described (Waterman, 1955; Ivanoff, 1956b, 1957b; Waterman, 1958) they need not be considered in detail. However, the principle of the photoelectric polarimeter must be understood because it provided most of the data presented here; consequently it is diagrammed (Fig. 1) and briefly described. Essentially the photocell, with the aid of the revolving mirror (M), scans the horizontal lines of sight underwater through 360° at a rate determined by the mirror's rota-

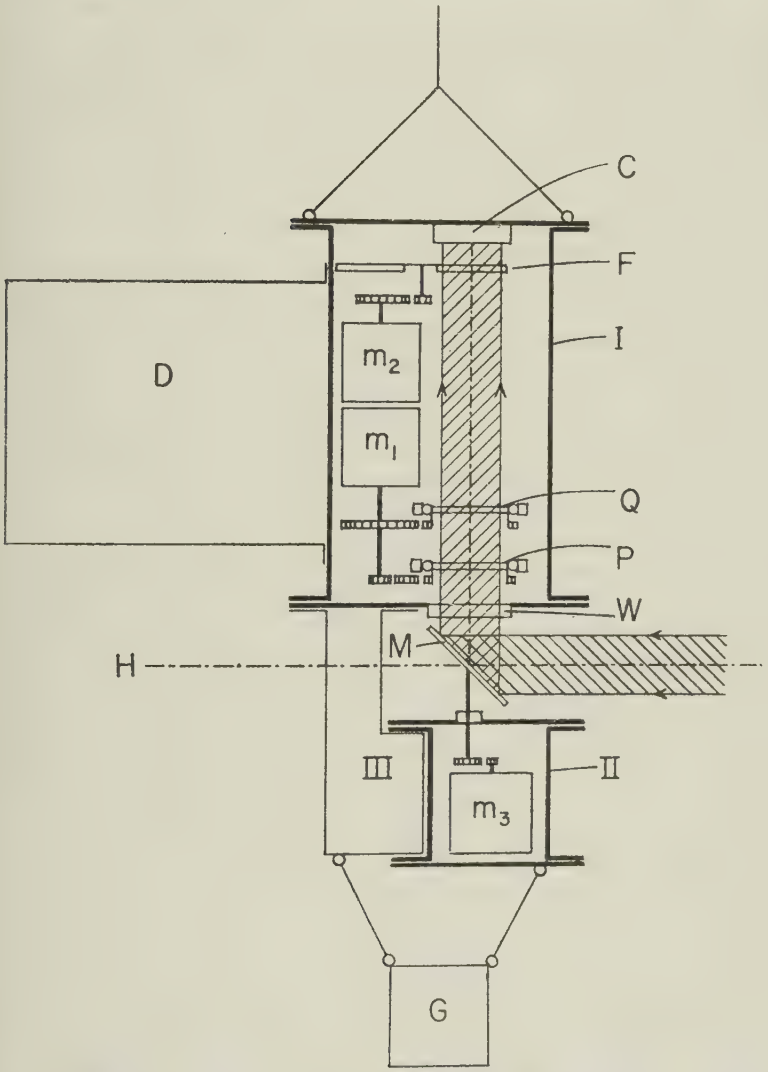

Figure 1. Photoelectric polarimeter. I, II, water-tight compartments suspended by cable and solidly connected by stiff metal plate, III; C, Westaphot photocell; D, azimuth stabilizing fin; F, changeable interference filters; G, weight to maintain vertical; H, horizontal plane; M, 45° front surface mirror to reflect horizontal light rays into window, W, of chamber I; m_1, motor to rotate Polaroid P filter (P) at about 2 RPM and a half-wave mosaic (Q) at about 500 RPM; m_2, motor to change or remove filters in light path; m_3, motor to rotate mirror at 0.22 RPM.

tions. The revolving Polaroid filter (P) acts as an analyzer for any linear polarization present in the incoming light, and the rapidly rotating half wave (for λ = ca. 550 mμ) mosaic (Q) depolarizes the light from the Polaroid to eliminate the possibility of an artifact arising from variations of photocell sensitivity with plane of polarization. The fact that the Polaroid filter is not a perfect analyzer will result in measured degrees of polarization somewhat smaller than the actual ones, an effect which will be increased to some extent by the finite angular field of the instrument.

The further possibility of artifacts due to pressure birefringence originating in the window (W) of chamber I is minimized or excluded by using a special type of plexiglass. This shows but little birefringence under pressure, and even this small amount would be appreciable only for rays deviating considerably from the optical axis. The photocell is connected by an insulated cable (not shown in Fig. 1) to a shock mounted galvanometer on the ship's deck. Because of the rotation rate of the Polaroid, a fast indicating instrument is required with a time constant shorter than 2 sec.

The dimensions of the optical system are such that the beam being measured illuminates nearly the whole photocell surface (about 61 mm in diameter). The sensitivity of the latter, which is maximal for a horizontal pencil of parallel light, decreases to 75% for a ray inclined to the horizontal by 7°. It is well known that the current produced by a barrier photocell is proportional to the irradiance so long as the latter is low and the cell feeds into a low resistance. In the case of the Westaphot cell and galvanometer (internal resistance = 680Ω) used here, the response is linear within 1% so long as the illuminance does not exceed 12 lux and the loading current is less than 2μA. This was generally the case in our measurements, made either with colored filters or without filters at considerable depths. On the other hand, without filters at shallow depths the conditions necessary for a linear response were not present. However, the error so introduced for I_{max} and I_{min} is always reduced in the calculation for p (see p. 291).

Between the depolarizer and the photocell a series of interference filters (Table I) can be inserted as desired by remote control. One of these is a narrow band blue-green element (Balzers Filtraflex B-40); the other five are broad band filters (Balzers Filtraflex Series K). To study the effects of wavelength accurately, the transmission curves of the various colored filters used should be corrected for spectral distribution of the submarine light, which itself varies with h and θ. However, since the influence of λ on underwater polarization is weak, the maximum transmission of each filter for white light is used here. The slight displacement of the observed points relative to λ which

results from the corrections concerned would scarcely affect our conclusions. On the other hand, the effect of λ on the polarizing properties of the Polaroid filter in the instrument is a significant one and is discussed below.

Comparison with Earlier Methods. While nearly all of the present data were obtained with the photoelectric polarimeter, a series of comparative measurements were made both in the field and in the laboratory to contrast this instrument with the two others previously used. The questions of present interest are: first, whether the photographic and visual techniques provide essentially the same information on submarine polarization as does the photoelectric method; second, whether all of these various instruments are equally versatile and accurate in obtaining the desired data.

To the first question the evidence of five parallel series of field measurements made in inshore waters down to 18 m provides essentially an affirmative answer. In general the p determined by each of the three methods under as closely identical conditions as possible showed satisfactory agreement when average values are considered (these varied from 7–22% at the different stations and under the prevailing meteorological conditions). However, the relatively low degree of polarization of the waters studied, and particularly the variable cloudiness of the sky (often inevitable), had an adverse effect on the precision of all of these measurements. Nevertheless, in the only set of data where p was as much as 20%, the differences between the three methods just exceed 5% in absolute value.

These comparative measurements also showed clearly the relative advantages and disadvantages of the three methods. In accuracy the visual and photoelectric techniques were superior to the photographic; in either of the first two techniques the absolute error of a single measurement does not exceed 5% whereas in the photographic technique it may exceed 5%. The photoelectric instrument is more convenient for collecting much data since, unlike the other two, it does not require a SCUBA diver to operate it; this also removes any restriction to relatively shallow depths. On the other hand, the present photoelectric instrument is less versatile than the others because it operates only in a horizontal plane; furthermore, it does not permit measurement of the polarization plane. However, since data on p are particularly needed and since many measurements are required to determine the influence of h and λ on p, this is the instrument of choice for present purposes.

Almost perfect agreement between the visual and photoelectric methods of determining p was found in the laboratory (Fig. 2). Here

a light source whose degree of polarization could be varied by changing the angle of a pile of glass plates in the beam was measured. This suggests that measurements made in the field by these methods are also closely comparable although the difficulties of field work usually increase considerably the variance of such data.

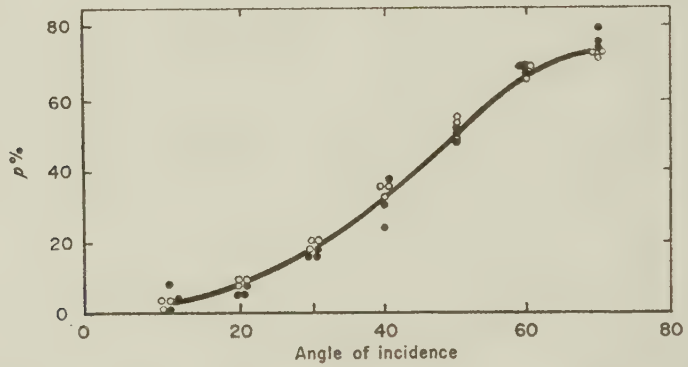

Figure 2. Laboratory comparison of visual and photoelectric methods of measuring degree of polarization (p%). Abscissa shows angle of inclination of a pile of glass plates used to produce partially polarized light. Photoelectric measurements, open circles; visual measurement, solid circles (see text).

Effects of Incomplete Polarization. While these comparative studies were being made, the same laboratory set-up was used with the photoelectric polarimeter to test the influence of the various filters in the instrument on the polarizing properties of its Polaroid P analyzer. Average results of five measurements at one inclination angle of the glass plates are shown in the last column of Table I. The results are between 51.7 and 52.1% without filter and with filters K_2, K_3 and K_5,

TABLE I

Filter	*Approx. max. transmission* λ ($m\mu$)	*Band width for 40% transmission* ($m\mu$)	*% polarization* by Polaroid P analyzer*
K_1 (violet)	415	380–430	48.0
K_2 (blue)	445	430–465	51.8
K_3 (blue green)	490	460–500	51.9
K_4 (yellow green)	550	515–570	50.4
K_5 (orange)	600	580–610	51.7
B–40 (blue green)	500	494–506	50.4
Without filter	—	—	52.1

* See text for explanation of this partially polarized test source.

out at 500 mμ (B-40) and 550 mμ (K_4) the Polaroid's polarizing properies apparently diminish slightly; at 450 mμ (K_1) they definitely liminish.[2] If the Polaroid actually transmits at "extinction" a fracion kI_p of the incident linearly polarized light and if k is zero without ilter as well as with filters K_2, K_3 and K_5, then the above figures give he following coefficients: $k = 0.019$ for K_4 and B-40, $K = 0.052$ for K_1. These permit corresponding corrections to be made in the measured p;[3] this has been done in all data given below.

In the next section the new information obtained with the photoelectric polarimeter serves not only to illustrate the capabilities of the nstrument but to provide quantitative data on several aspects of ubmarine light polarization.

RESULTS

1. General Factors

Two examples of the type of records obtained with the photoelectric olarimeter are shown in Figs. 3 and 4. While the mirror (M) sweeps hrough the horizontal plane (one revolution taking about 4.5 min) nd if the incoming light is polarized linearly, the photocell output o the galvanometer undergoes a series of oscillations from maximum o minimum that arise from rotations of the Polaroid (one turn taking bout 32 sec). If these maxima and minima are plotted, the two urves so obtained in turn oscillate between maxima and minima vhich occur respectively in the bearings of the sun and the anti-sun. Provided the azimuthal position of the polarimeter does not change, he time intervals between these points of zero slope are equal; when hey were not, boat drift was usually responsible; this was minimized, when necessary and possible, by fore and aft anchors. When he mirror faces the metal plate (Fig. 1, III) connecting the lower ressure case of the instrument to the upper one, there is a sudden ecrease in the apparent light level,[4] but this artifact is usually easy o eliminate, as shown in Figs. 3 and 4.

[2] The decreased polarization of violet light by the filter used is in accord with ie average data published by its manufacturer although the slight dip at 500 and 50mμ is not. The latter, however, is not crucial for our argument.

[3] The increased submarine polarization at the extreme violet end of the spectrum as not noticed in the first measurements with the photoelectric polarimeter (Ivanoff, 957b) because the decreased polarizing properties of the Polaroid filter at these avelengths was not considered.

[4] In the earlier version of the polarimeter (Ivanoff, 1957b) three brackets connected ie two main parts of the polarimeter. The resulting three minima in the records ade the analysis of the results more difficult and less certain. The replacement of ie three brackets with a single supporting plate greatly increases the accuracy of ie present measurements.

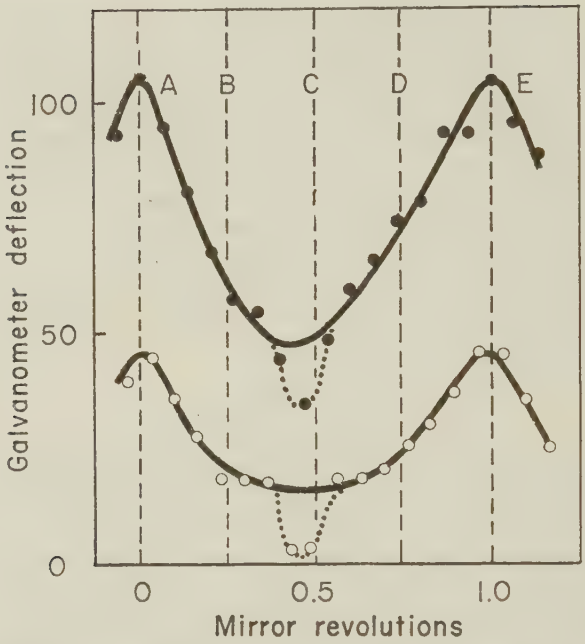

Figure 3. Photoelectric measurements obtained in very clear water with solar zenith angle about 33°. Data taken at 1345, 27 August 1957, St. 1 (Fig. 5); bottom, 2500 m; Secchi disc reading, 50 m. Polarimeter at 16 m using the 500 mμ narrow band filter. Maximal galvanometer readings during rotation of Polaroid, solid circles; minimal ones, open circles. Dotted line indicates shadowing effect of metal plate which connects two chambers of polarimeter. Broken vertical lines A–E indicate five positions of mirror for which the degree of polarization was calculated from equation $p = I_{max} - I_{min}/I_{max} + I_{min}$. The angular difference (θ) between azimuth of instrument's line of sight and sun's bearing is 0° for A and E, ±90° for B and D, and 180° for C. Computations for p are as follows:

A. $p = (106 - 45)/(106 + 45) = 40.4\%$
B. $p = (61 - 20)/(61 + 20) = 50.6\%$
C. $p = (48 - 16)/(48 + 16) = 50.0\%$
D. $p = (74 - 24)/(74 + 24) = 51.0\%$
E. $p = (105 - 46)/(105 + 46) = 39.1\%$

Within errors of measurement, p is the same at this station for $\theta = \pm 90°$ and 180° (av. 50.5%), but it is definitely smaller at $\theta = 0°$ (av. 39.7%). If the effect of wavelength on the polarizing properties of the Polaroid filter is adjusted, the averages become 40.8% for $\theta = 0°$ and 52.0% for $\theta = \pm 90°$, 180°. The ratio of maximal to minimal horizontal radiances which occur at $\theta = 0°$ and $\theta = 180°$ respectively, is $(106 + 46)/(48 + 16) = 2.4$.

For a given θ the ordinates for the two curves connecting the maxima and minima are proportional respectively to $I_{max} = I_{n/2} + I_p$ and $I_{min} = I_{n/2}$, where I_n and I_p are respectively the unpolarized and linearly polarized fractions of the incident light. Hence the polarization factor is

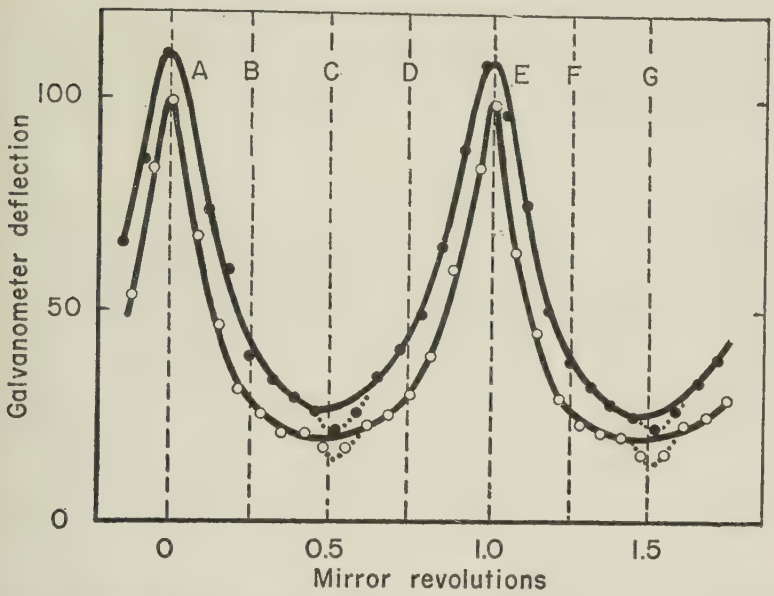

Figure 4. Photoelectric measurements obtained in less clear water (Fig. 5, St. 3) than those in Fig. 3 and with a greater solar zenith distance (about 67°). Data taken at 1630, 26 August 1957. Polarimeter at 5.4 m, using the 500mμ narrow band filter; bottom, 15 m; Secchi disc reading, 10 m. Symbols and method of plotting as in Fig. 3. The corresponding degrees of polarization in various azimuths are: A. 4.7%, B. 18.3%, C. 12.5%, D. 18.4%, E. 4.3%, F. 18.2%, and G. 13.1%. Obviously, although the percent polarization is less over-all, it varies considerably more with azimuth here than in Fig. 3. On an average, $p = 4.5\%$ when $\theta = 0°$, 12.8% when $\theta = 180°$, and 18.3% for $\theta = \pm 90°$. With the λ correction for the Polaroid, these become 4.6%, 13.1% and 18.8% respectively. The ratio of maximal to minimal radiance is $(111 + 101)/(27 + 21) = 4.4$.

$$p = \frac{I_p}{I_n + I_p} = \frac{I_{\max} - I_{\min}}{I_{\max} + I_{\min}} .$$

Theoretically then the two curves allow p to be computed in any horizontal line of sight so long as variation in this parameter is greater than errors of measurement. These curves also indicate the angular distribution of radiance in the horizontal plane, since this is proportional to $I_n + I_p = I_{\max} + I_{\min}$.

Effects of Azimuth. Results have been analyzed mainly for $\theta = 0$, ± 90 and 180°, although for measurements around sunset (Fig. 9) $\theta = \pm 45°$ is also included. Three different patterns are clear in the various series studied. 1) In some cases p is maximal when $\theta = \pm 90°$, intermediate when $\theta = 180°$, and minimal when $\theta = 0°$ (Figs. 8, 11, 13, 15). 2) In other cases $\theta = 0°$ is also minimal, but p is essentially

equal for $\theta = \pm 90°$ and $\theta = 180°$. Consequently these latter two have been averaged (Figs. 7, 10, 12, 14, 16). 3) Still others, mainly in turbid waters, show the same p, within errors of measurement, at all azimuths.

Figure 5. Five stations where measurements of submarine polarization were made. (1) South of Bermuda, with bottom depths greater than 400 m. Secchi disc visibility more than 18 m and as much as 50 m at appreciable distances from the islands. (2) South shore, with bottom depths between 18 and 40 m. Secchi disc readings from 14–18 m. (3) North shore, with bottom depths varying from 15 to 20 m. Secchi disc visibility down to 10–17 m. (4) Harrington Sound; maximum depth about 21 m. Secchi disc visibility 10–13 m. (5) Castle Harbour; maximum depth about 13 m. Secchi disc depths around 6–8 m.

Effect of Transparency. The measurements here reported can be used incidentally to illustrate the influence of the water's clarity on p. The Bermuda area is of considerable interest in this respect since a wide range of transparencies from very clear Sargasso Sea water to highly turbid inshore regions can be conveniently studied. The stations occupied in the present measurements are numbered from 1 to 5 on a scale of increasing turbidity (see Fig. 5). Since transparency measurements were not a primary part of our 1957 summer program, Secchi disc readings provide the only information available on water

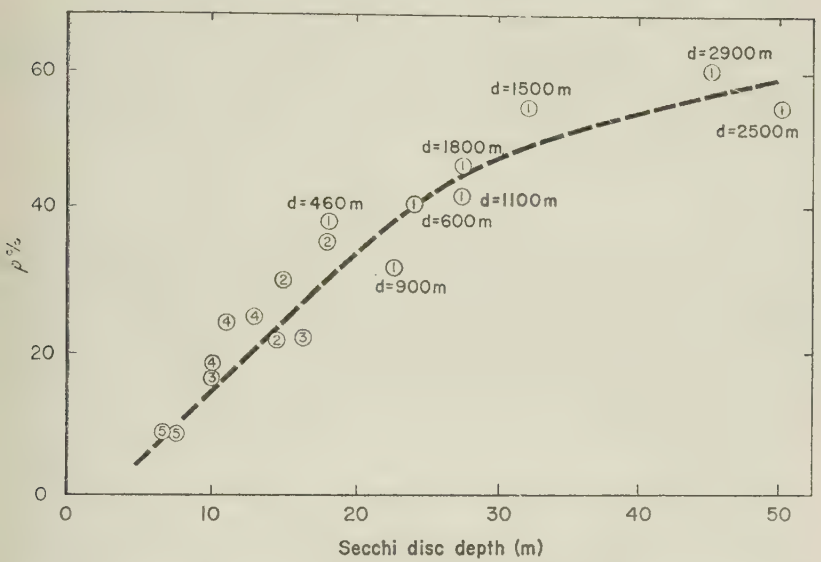

Figure 6. Maximum p measured at 9 m depth using the 500mμ narrow band filter as a function of ecchi disc depth (S). Circled numbers indicate water types in Fig. 5. Bottom depths (d) are shown or stations in area 1. Clarity of water increases, on an average, with bottom depth d.

ransparency at the time of polarization measurements (Fig. 6). As s well known, such data are limited among other things by the ob- erver, the state of the water surface, and the relative solar bearing *e.g.*, the sunny side of the ship in one instance gave a reading of 19 m, he shady side 25 m; in another case the readings were 45 and 58 m espectively). Nevertheless, the correlation between Secchi disc eadings and degree of polarization is striking.

Note that, to provide reasonably comparable data, the results plotted re limited to $h = 9$ m and $\lambda = 500$ mμ. At other depths somewhat ifferent results would be expected. In deeper more turbid water the ecrease in p with h is probably greater so that the average curve ould bend still more. If h is less than 9 m, a straighter curve would kely be found to fit the data. In addition, measurements in Fig. 6 nclude only the case when $\theta = \pm 90°$. Usually this is maximal, but s already noted, it may be equalled under certain conditions at $= 180$ or even 0°.

Influence of Cloud Cover. Whenever possible, measurements were nade while the sun was shining (Figs. 3–21). However, there usually re some scattered clouds in the sky in Bermuda so that the measure-

ments were frequently disturbed by the passage of a cloud in front of the sun. This always decreases p, but the actual effects, both on p and on the plane of polarization, depend on the resulting change in directionality of underwater illumination, which varies with different optical conditions of the sky.

2. Effect of Depth

In addition to the direct effect of h on p, a secondary influence arises where the bottom is close enough to affect significantly the light that is present. As earlier observations showed (Waterman, 1958), p decreases near the bottom, and more so if the latter is light rather than dark. For this reason the present data fall into two categories: a) where there is no bottom influence; b) where there is bottom influence.

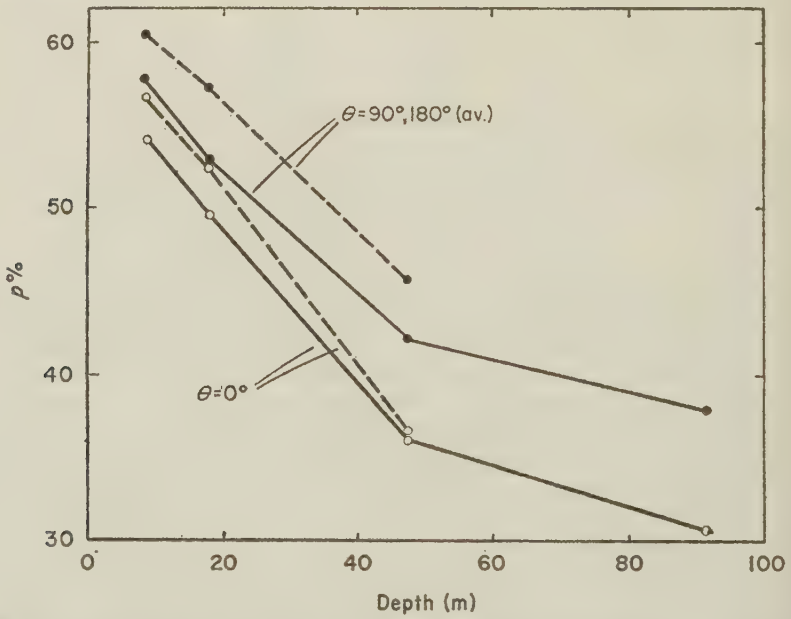

Figure 7. Influence of h on p in clear water at St. 1 (Fig. 5); bottom, 2900 m; no Secchi disc reading; solar zenith distance (i) = 60–78°. Solid lines connect points determined without colored filter; broken lines connect points measured with the 500mμ narrow band filter. The points indicated for $\theta = \pm 90$ and 180° are averages of the two. Data of 22 July 1957.

Far from Bottom. Two series of measurements were made in 2500–3000 m of water where the optical effect of the bottom is certainly negligible (Figs. 7 and 8). Some of these data were taken without colored filters to increase the instrument's sensitivity to the low in-

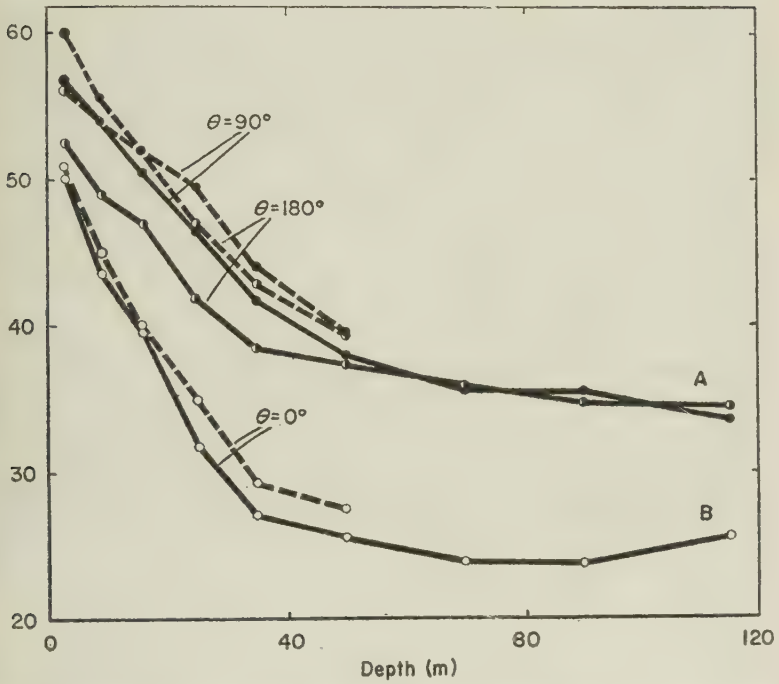

Figure 8. Influence of h on p in clear water at St. 1 (Fig. 5); bottom, 2500 m; S = 50 m; i between 29 and 33°. Broken and solid lines as in Fig. 7. Data of 27 August 1957.

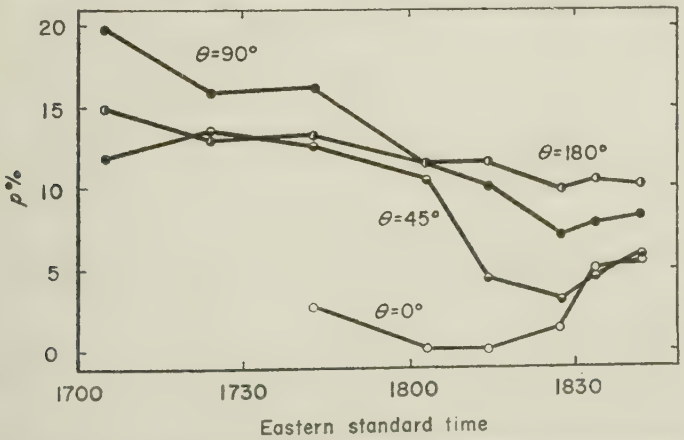

Figure 9. Degree of polarization around sunset at St. 2 (Fig. 5); measured at 5.4 m without filter in moderately turbid water; bottom about 12 m. Sun's altitude at 1700 was 18°50′; sunset occurred at 1852. At 1815 the solar disc was dim enough to look at with the naked eye; after 1845, the underwater light was too weak for measurement with the polarimeter. Data of 26 August 1957.

tensities present; the rest were taken with the 500 mμ filter (narrow band) which reduces the influence of depth on the band width error. In Fig. 7, where the sun's zenith distance was less than 20° throughout the measurements, the percent polarization is the same within the errors of measurement at both 90 and 180° to the sun's bearing, but it is clearly less in the solar bearing. The data in Fig. 8, which extend down to 115 m, show in addition that at this depth maximal and minimal radiance in the horizontal plane differ by a factor of two toward and away from the sun, with i between 40 and 45°. The degree of polarization follows the same general trend as in the previous case, but in addition it illustrates two new points.

1) While the differences in p when $\theta = 90$ and 180° do not exceed the experimental errors at depths greater than 60 m, polarization at 180° becomes weaker than at ±90° in shallower depths. This point is discussed later in relation to the effects of azimuth on polarization.

2) Down to 90 m p decreases more and more slowly when $\theta = 0°$, but at greater depths it appears to increase again. This matter will also be discussed later where it is shown to be similar to some phenomena observed around sunset (Fig. 9).

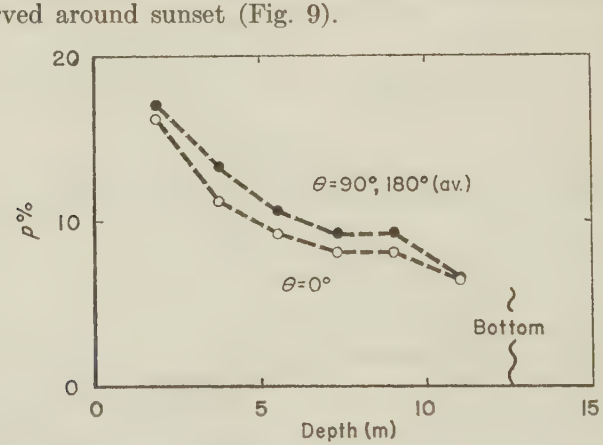

Figure 10. Effect of h on p in turbid water at St. 5 (Fig. 5); bottom, 12.5 m; 500mμ narrow band filter used; $S = 6.5$ m; i between 17 and 32°. Note that decrease in p with h accelerates slightly beyond 9 m, probably as a result of increased turbidity. Data of 19 August 1957.

Near Bottom. Several series of measurements (Figs. 10–13) indicate that in shallow water, when p is determined in a narrow spectral band centered at 500mμ, it decreases sharply close to bottom. The extent and degree of this polarization decrease probably depend on the clarity of the water, the albedo of the bottom, and the fact that turbidity often increases near the latter. The effect of transparency

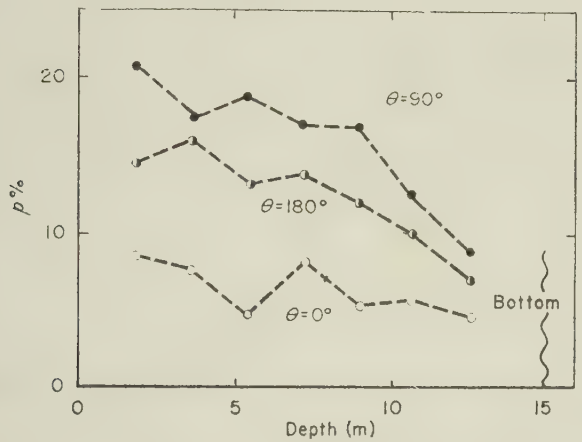

Figure 11. Effect of h on p in moderately turbid water at St. 3 (Fig. 5); bottom, 15 m; measured th 500mμ narrow band filter; S = 10 m; i between 55 and 57°. Note that decrease in polarization ith depth is accelerated at depths greater than 9 m, at least when $\theta = \pm 90$ or 180°. Data of 26 ugust 1957.

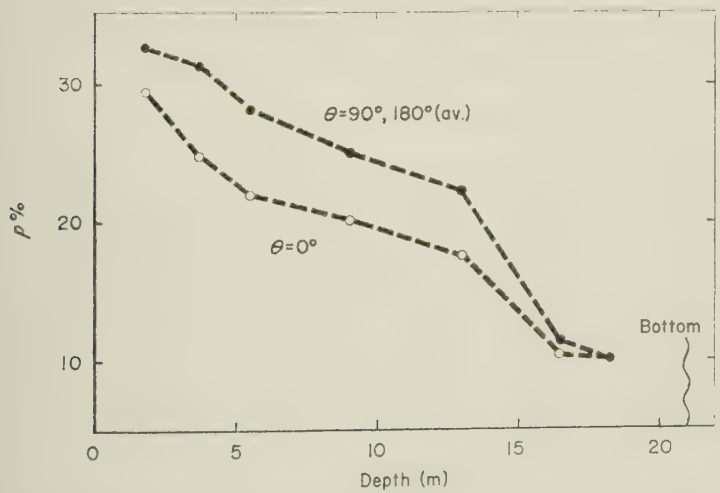

Figure 12. Effect of h on p in moderately turbid water at St. 4 (Fig. 5); bottom, 21 m; measured th 500mμ narrow band filter; S = 11 m; i between 16 and 22°. Decrease in p with depth clearly celerates with depths in excess of 13 m. At about 18 m, submarine illumination appears to reach equilibrium condition where p becomes nearly independent of azimuth. Data of 17 August 1957.

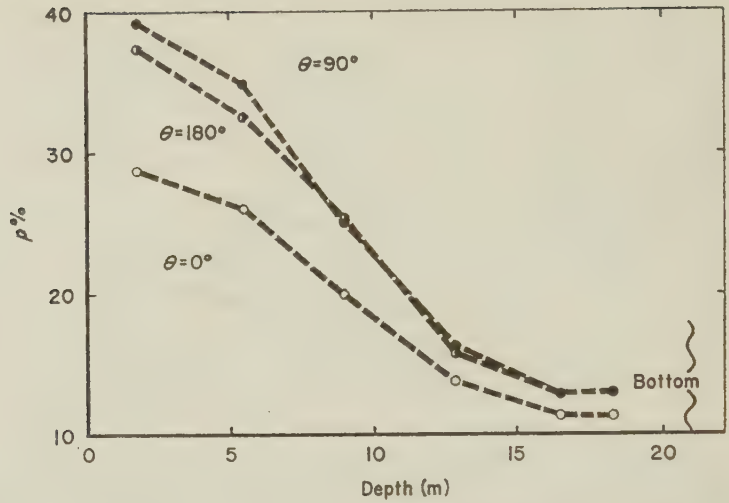

Figure 13. Effect of h on p in moderately turbid water at St. 4 (Fig. 5); bottom, 21 m; measured with 500mμ narrow band filter; S = 13 m; i between 27 and 32°. Decrease in p with h accelerates below 6 m. At about 16 m, submarine illumination appears to reach an equilibrium and p stops decreasing. Data of 30 August 1957.

may be seen by comparing the above figures where the extent of the bottom influence ranges from 3.5 to 15 m. Close to the bottom p seems to approach a constant value (Figs. 12 and 13).

3. Effect of Wavelength

In general, measurements of p as a function of λ (Figs. 14–16; Table II) show that p is greater at the two ends of the visible spectrum, with our highest readings usually at 600mμ. The minimum occurs between 445 and 500mμ, with the actual $p_{\min}$ apparently being correlated with the color of the water mass concerned. Thus the blue waters of the Sargasso Sea (Fig. 14, St. 1) and of Castle Harbour (Table II, St. 5) have $p_{\min}$ near 450mμ, while the waters of Harrington Sound (Figs. 15, 16, St. 4), which appear greener, have $p_{\min}$ close to 500mμ. The data also show that the change in p due to λ, (Δp), is apparently greatest where p is large, that is, in clear water and near the surface. As would be expected from these facts, the variation of $\Delta p/p$ as a function of λ, which averages 0.2, seems to be practically independent of turbidity and depth.

In addition, the ratios of maximal ($\theta = 0°$) to minimal ($\theta = 180°$) radiance measured in various azimuths decrease toward the short

wavelengths. Although the variations of i in the different series of data prevent a quantitative analysis, the ratio appears to decrease toward shorter wavelengths down to the lower spectral limit of our filters. This should be compared with the fact that the ratio of submarine irradiance coming from above to that coming from below is known to pass through a minimum at a λ shorter than that of maximum transparency (Jerlov, 1951).

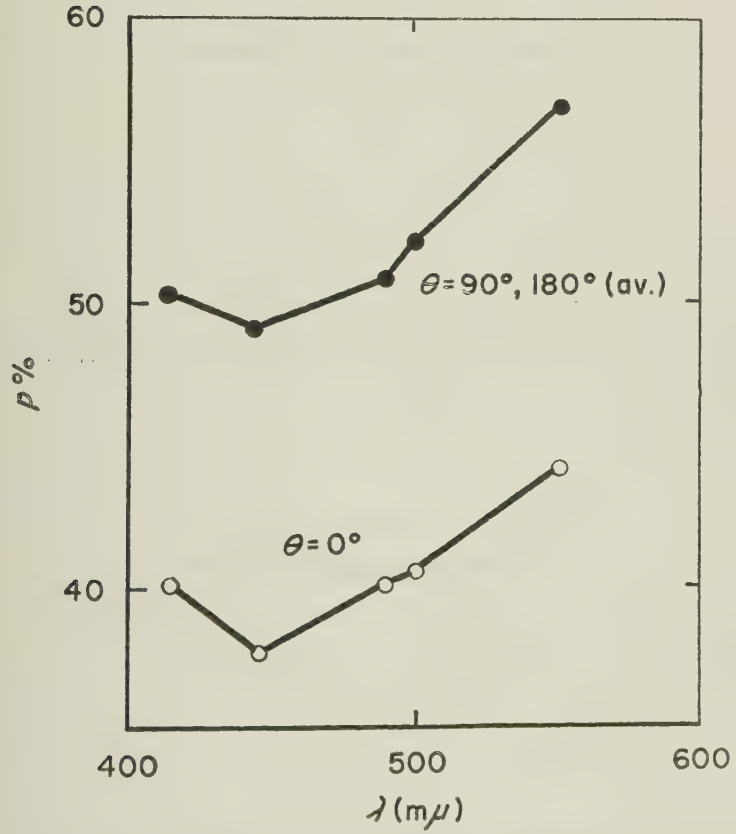

Figure 14. Effect of λ on p when h is 16 m in clear water at St. 1 (Fig. 5); bottom, 2500 m; S = m; i between 29 and 33°. Without colored filters, p at $\theta = 0°$ was 39.8%, and at $\theta = \pm 90$ and 0° p was 49.4% (av.). Data of 27 August 1957.

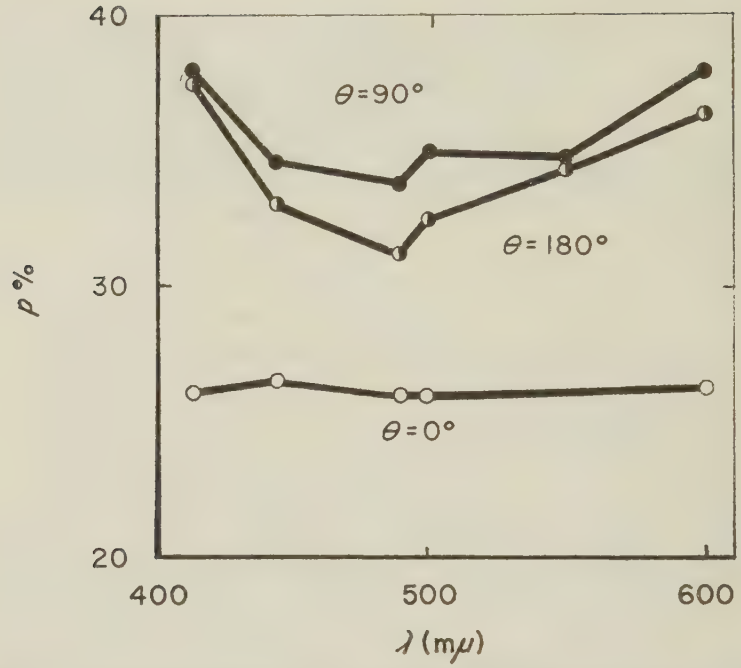

Figure 15. Effect of λ on p when h = 5.5 m in moderately turbid water at St. 4 (Fig. 5); bottom, 21 m; S = 13 m; i about 24°. Without colored filters, p at θ = 0° was 25.7%, and at θ = $\frac{90}{180}$ ±90 and 180° p was 34.3% (av.). Data of 30 August 1957. *Cf.* Fig. 16, where conditions were essentially the same except for h.

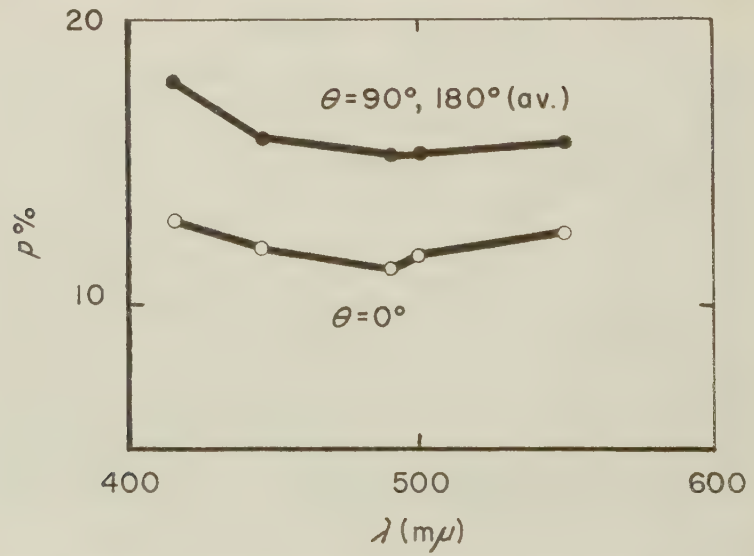

Figure 16. Effect of λ on p when h = 14.5 m in moderately turbid water at St. 4 (Fig. 5); bottom, 21 m; S = 13 m; i about 25°. Without colored filters, p at θ = 0° was 12.4%, and at θ = ±90 and 180° it was 15.8% (av.). Data of 30 August 1957.

TABLE II. SUMMARY OF THE EFFECTS OF λ ON p

*Station**	*Bottom depth* (*m*)	*h* (*m*)	*Clarity*	*S*** (*m*)	*i* (°)	*p (no filter)* $\theta = 0°$ (%)	$\theta = 90°,180°$ (*Av.* %)	p_{min} (%)	$p_{415m\mu}$ (%)	$p_{550m\mu}$ (%)	Δp† (%)	$\Delta p/p_{min}$
1 (Fig. 14)	2500	16	clear	50	29–33	39.8	49.4	48.9 (at 445mμ)	50.2	56.8	9.2	0.19
1	2900	18	clear	45	21–23	—	—	52.2 (at 445mμ)	54.0	60.7	10.3	0.20
4 (Fig. 15)	21	5.5	moderately turbid	13	24	25.7	34.3	33.7 (at 490mμ)	37.8	34.6	5.0	0.15
4 (Fig. 16)	21	14.5	moderately turbid	13	25	12.4	15.8	15.3 (between 490 and 500mμ)	17.8	15.6	2.8	0.18
4	21	5.5	moderately turbid	11	20	25.8	29.1	28.1 (at 500mμ)	33.2	30.4	7.4	0.26
4	20	9	moderately turbid	10	44–54	—	—	18.0 (at 500mμ)	19.5	20.2	3.7	0.21
4	16	14.5	moderately turbid	—	23–34	9.1	10.1	10.2 (between 445 and 500mμ)	10.8	11.1	1.5	0.15
5	12.5	9	turbid	6.5	28	—	—	7.6 (at 445mμ)	8.2	9.3	2.3	0.30

* See Fig. 5.

** Secchi disc reading in meters.

† $\Delta p = (p_{415m\mu} - p_{min}) + (p_{550m\mu} - p_{min})$.

DISCUSSION

The preceding data may be discussed from several points of view; probably the most important points relate to 1) the angular distribution of p underwater, and 2) the angular distribution of submarine light itself.

1. *Effects Dependent on the Angular Distribution of* p. The angular distribution of percent polarization in the sea is still poorly known since the photographic (Ivanoff, 1956b, 1957a) and visual (Waterman and Westell, 1956; Waterman, 1958) measurements which have been made are few and quite incomplete. However, the function may roughly approximate Rayleigh's equation, at least beyond the critical angle. If so, $p = \sin^2 \alpha / 1 + \cos^2 \alpha$, where α is the angle between the parallel rays of underwater sunlight and the direction of scattering (*i.e.*, line of sight). Provided this equation holds and if only horizontal lines of sight are considered (as in the above measurements), p should be maximal for all solar zenith distances when $\theta = \pm 90°$ and it should be minimal for $\theta = 0$ and 180°, except when $i = 0°$ and when p is the same for all azimuths. At both minima, percent polarization should be equal and directly related to the sun's altitude above the horizon. The difference between maximal and minimal p is least when three parameters have particular values: 1) The zenith distance must be minimal so that the axis of best symmetry[5] of submarine illumination makes a maximal angle with the horizontal plane. 2) The depth should be great because it is well known that the axis of best symmetry of submarine light's angular distribution approaches the vertical at increasing depths (see Jerlov, 1951). 3) The water must be turbid because this produces vertically symmetrical light distribution at shallower depths.

These various points have largely been verified by measurements in the field. Thus the degree of polarization observed in horizontal directions normal to the sun's bearing is independent of i (Waterman and Westell, 1956: fig. 6), but in the sun's bearing p decreases as i increases (Waterman and Westell, 1956: fig. 7). Similarly, the present results demonstrate that variation in p with azimuth increases as the sun approaches the horizon (for example, compare Figs. 3 and 4), decreases as depth increases (see Fig. 8 at ± 90 and 180° to the sun's bearing), and may become practically zero in turbid water.

[5] The underwater direction of maximum radiance (apparent direction of the sun) may differ from the axis of best symmetry for the angular distribution of submarine illumination, but it is not known whether the direction or the axis is the more significant for underwater polarization. Here the two terms will not be distinguished even though they may not be strictly equivalent.

On the other hand, a relation not predicted by Rayleigh's equation appears again in the present results, namely that lower degrees of polarization occur more consistently in the sun's bearing than they do in that of the anti-sun. This agrees with results obtained previously with the photographic technique (Ivanoff, 1956b: 54; Ivanoff, 1957a: figs. 9 and 10) but not with those found visually (Waterman and Westell, 1956: fig. 8).[6]

In summary then, Rayleigh's equation appears to hold for submarine polarization only as a first order approximation; this we have assumed also in our analysis of underwater elliptical polarization (Ivanoff and Waterman, 1958). It is not surprising that the equation provides only a rough approximation; in the first place, most of the light scattering by sea water is not Rayleigh scattering; in the second place, the combination of sun, sky and ocean have a plane of symmetry which passes through the sun's bearing rather than an axis of symmetry. This plane of symmetry may disappear when the sun's contribution becomes small relative to that of the sky, as in cloudy weather or at sunrise or sunset. The distribution of radiance in the sky must then be important. Thus the percent polarization may be greater at 180° than at ±90° (Fig. 9) when the solar zenith distance is greater than 80°. This could be the effect of some clouds which increased the radiance of the sky in an azimuth different from the sun's bearing.

Much of the problem of angular distribution of submarine polarized light remains to be studied from both experimental and theoretical points of view.

2. *Effects Related to the Angular Distribution of Submarine Light.* As a result of field observations on underwater polarization, a theory was proposed which accounts simultaneously for the effects of tur-

[6] In the latter data the polarization for $\theta = 0°$ did in fact average less than for $\theta = 180°$, but the variation hardly seems significant there, since maxima at +90 and −90° differ by greater amounts.

[7] Recently measurements of the degree of polarization have been made in sea water samples illuminated by a parallel beam of artificial light (Ivanoff, 1958a, 1958b). In these waters, which were collected in the Mediterranean Sea between Nice and Corsica, polarization varied from 45 to 67% for surface waters but was as much as 75, or even 77%, in deep waters. Optically pure water under the same conditions would produce 80% polarization. Furthermore, some samples which were rather turbid and had the milky appearance of a colloidal suspension gave readings of 88% polarization. In certain of these samples, spheroidal particles 1–3μ in diameter were visible under the microscope. Thus the shape of the particles may have an important influence since the degree of polarization is known to be greater for spheroidal particles.

bidity, sky overcast, depth, nearness to bottom, and wavelength (Ivanoff, 1957a). The theory may be summarized as follows: 1) With parallel light, the degree of polarization in light scattered by sea water depends mainly on the optical properties and dimensions of the suspended particles; its actual value increases as the dimensions of the particles decrease.[7] 2) In daylight, submarine polarization decreases for a given water type with the diffuseness of the light.

To support this theory an attempt has been made to derive the variation in the amount of polarization from changes in the angular distribution of submarine illumination. These rough calculations were intended to determine merely whether or not the order of magnitude of the theoretical effect is comparable to the measurements. Such analysis is misleading if it suggests that polarization is dependent on the angular distribution of light. In fact, both phenomena are dependent on the same parameters, such as surface irradiance and optical properties of the water, rather than on each other. However, their variations usually occur together in the same direction. Thus, when underwater illumination becomes more diffuse, the degree of polarization diminishes. This should be the case for more turbid waters, overcast skies, increased depth, greater bottom reflection and the most penetrating wavelength. The data here reported support these predictions of the theory.

Previous work had shown that the degree of submarine polarization may reach 60% in quite clear water at shallow depths (Ivanoff, 1957a), decreasing proportionately at greater turbidities (Waterman, 1954; Waterman and Westell, 1956; Ivanoff, 1957a). This decrease is illustrated from the present data by Fig. 6. These data also seem to show that in the clearest water the percent polarization varies least as a function of the Secchi disc reading. Previous evidence had suggested the contrary, namely that p changes most rapidly in the clearest waters (Ivanoff, 1957a: 50–52). However, to evaluate these discrepancies, one must consider precisely what is meant by clarity and how it is determined. Both the amount of underwater polarization and the Secchi disc reading are complex functions of the optical properties of sea water, and the data in Fig. 6 permit no conclusions to be drawn relative to the way in which these functions are interrelated. All that may be said from present evidence is that, for clear waters, the depth to which the Secchi disc is visible changes more rapidly than does the degree of polarization. Contrary to a previous assumption, p does not seem to provide a particularly sensitive means of distinguishing various clear waters one from another. On the other hand, the measurement of polarization is more precise with greater p, which in fact occurs in the clearest waters.

As mentioned above, a decrease in the degree of polarization was regularly observed whenever the sun was covered by clouds, which agrees with previous findings (Waterman, 1954; Ivanoff, 1957a). Similar effects occur at sunset (Fig. 9) when the relative importance of sky light increases and when irradiance becomes more diffuse. However, it is important to emphasize that, although a completely overcast sky and a blue sky with no sun (at sunrise and sunset, or with a dense cloud covering merely the sun) produce less polarization underwater than does the direct sunlight itself, their influences are not identical. Thus, at angles less than the critical angle, sky polarization is not visible in the former but is visible in the latter case; also, the plane of polarization is more or less horizontal in overcast weather but it may behave in quite a different manner at sunset with a clear sky, possibly as a result of the latter's polarization (Ivanoff and Waterman, 1958).

Our data show that p decreases with depth (irregularities in these measurements being due to either errors in measurement or optical heterogeneity of the water) and approaches a limit of about 30% in very clear sea water. Some previous observations (Waterman, 1955) suggested that polarization in deep water is as great as that near the surface, but the strong interference pattern still recorded in the crystal analyzer at 200 m may have a more likely interpretation in the much narrower deep water light spectrum (Ivanoff, 1957a: 41). Other measurements made by the visual method (Waterman, 1958) indicated a slight increase in the percent polarization at certain depths. On the basis of present data this could be due to an error in measurement, to a change in the sky overcast during measurements, or possibly to the effect of a local increase in the water's clarity. But the last possibility implies that in a clearer layer of water the illumination becomes less diffuse again, which is unlikely.

Wavelength has a definite but small influence on the degree of submarine polarization. Present results agree with the sole previous measurement (made by the photographic method; see Ivanoff, 1957a) and with the fact that it is for the most penetrating wavelengths that underwater light is most diffuse (Johnson and Liljequist, 1938). Since diffuseness of illumination and polarization by scattering are inversely related, one would thus expect that minimum polarization in very clear sea water would occur near 475mμ. The apparent correlation observed between the λ for p_{min} and the color of the water in the present results is mentioned above.

Two circumstances have already been cited which influence the degree of polarization in the sun's azimuth in a special way involving both the angular distribution of p and that of submarine radiance. In deep water, p for the sun's bearing passes through a minimum and then

increases again (Fig. 8). The same thing happens at sunrise or sunset (Fig. 9), when this has also been observed at $\theta = \pm 45°$. Such phenomena could result from opposing effects of an increase in the diffuseness of underwater illumination, which decreases polarization, and a reduced obliquity in the light, which augments polarization in the sun's bearing.

Actually the diffuseness of the light increases with depth and with the sun below the horizon while the axis of best symmetry of the angular distribution of radiance tends toward the vertical with depth and with i near 0°. Hence the degree of polarization would decrease while the first of these effects predominated and would then increase again when the second factor became predominant. In Fig. 8, curves A and B may come together horizontally where the angular distribution of submarine illumination becomes a symmetrical figure of rotation around the vertical. Degree of polarization would then be independent of azimuth regardless of the sun's zenith distance. Unfortunately this equilibrium depth is too great in the Sargasso Sea to be reached with our present instruments.

ACKNOWLEDGMENTS

The authors are grateful to Mr. Eric Kindwall and the crew of the PANULIRUS, especially Mr. Brunell Spurling, for their great assistance in effecting these measurements. Thanks are also due Miss Jeanie Caldwell and Dr. W. H. Sutcliffe, JR., Director of the Bermuda Biological Station, for their constant cooperation.

REFERENCES

IVANOFF, ALEXANDRE

1955. Au sujet du facteur de polarisation de la lumière solaire dans la mer. C. R. Acad. Sci. Paris, *241:* 1809–1811.

1956a. Degree of polarization of submarine illumination. J. opt. Soc. Amer., *46:* 362.

1956b. Facteur de polarisation du résidu sous-marin de lumière du jour. Ann. Geophys., *12:* 45–56.

1957a. Contribution à l'étude des propriétés optiques de l'eau de mer en Bretagne et en Corse, et à la théorie de la polarisation sous-marine. Ann. Géophys., *13:* 22–53.

1957b. Un polarimètre sous-marin à cellule photoélectrique. Premiers résultats obtenus. Bull. d'Infor. C. O. E. C., *9:* 491–499.

1958a. Au sujet de l'utilisation d'un diagramme p-β pour caractériser les masses d'eau océanique. C. R. Acad. Sci. Paris, *246:* 2636–2639.

1958b. Essai d'hydrologie optique entre Nice et la Corse. C. R. Acad. Sci. Paris, *246:* 3492–3496.

IVANOFF, ALEXANDRE AND T. H. WATERMAN
1958. Elliptical polarization of submarine illumination. J. mar. Res., *16* (3): 255–282.
JERLOV, N. G.
1951. Optical studies of ocean waters. Rep. Swedish Deep Sea Exped. 1947–8, *3*(1): 1–59.
JOHNSON (JERLOV), N. G. AND G. LILJEQUIST
1938. On the angular distribution of submarine daylight and the total submarine illumination. Svenska hydrograf.-biol. Komm. Skr., N. S. *14:* 1–15.
WATERMAN, T. H.
1954. Polarization patterns in submarine illumination. Science, *120:* 927–932.
1955. Polarization of scattered sunlight in deep water. Deep-Sea Research, Suppl. *3:* 426–434. Bigelow Festschrift.
1958. Polarized light and plankton navigation. *In:* "Perspectives in Marine Biology". (Ed.: A. A. Buzzati-Traverso) University of California Press, Berkeley. pp. 429–450.
WATERMAN, T. H. AND W. E. WESTELL
1956. Quantitative effects of the sun's position on submarine light polarization. J. mar. Res., *15:* 149–169.

Communication from The International Agency for ^{14}C determination

This Journal has been requested to advise its readers that the above Agency has been established at Charlottenlund Slot, Charlottenlund, Denmark and that standardized ampoules of ^{14}C—activity 0.004 mc.—may be obtained from this Agency at a nominal cost. Other essential equipment and service for radioactive carbon work will also be available.

This Agency is a nonprofit organization which was established in January of 1958 with funds provided by UNESCO. Professor E. Steemann Nielsen is honorary supervisor and Mr. Vagn Hansen directs the daily work. The Danish Institute for Fisheries and Marine Research has provided quarters at Charlottenlund Slot. The working committee which investigated the entire subject and made recommendations leading to establishment of the Agency was chaired by John H. Ryther.

In the communication received it is stressed that the facilities of this Agency are available to all scientific institutions in the world.

The ^{14}C method has been used widely during recent years for measuring the production of organic matter in the sea. It has been employed by many investigators and is in many instances a part of the routine of numerous institutions in gathering oceanographic data. An important factor in the usefulness of the technique for measuring primary production is that the field work does not presuppose any expert knowledge such as that which is required in preparing the ampoules containing the $NaH^{14}CO_3$ and in measuring the radioactivity of the filters containing the samples. This Agency would provide this expert service for those institutions which have no such experts on the staff. Thus this Agency would provide the basic necessities, such as ampoules and other equipment at a nominal fee, the institution would do the field work and, if desired, send the samples back to the Agency, which in time would process the filters containing the samples. The Agency would make a report on its findings to the institution. The half-life of ^{14}C is more than 5000 years, therefore the filters, if properly stored, remain unaltered for a long time.

The most recent description of the different modifications of the ^{14}C method is available in "Contributions to Plankton Symposium, 1957. Measurements of Primary Production in the Sea" (Rapp. Cons. Explor. Mer, Vol. 144, B.2 and B.3, 1958).

Standardized ampoules of ^{14}C—activity 0.004 mc.—may be obtained directly from the Agency, with the institution doing its own processing.

r, if the purchaser wishes, he may buy the ampoules together with umbered membrane filters and have the Agency do the processing; this case special boxes for return of the filters to the Agency will supplied. Prices include packing but not transportation. Direc-ns for use of ^{14}C will be enclosed in each consignment.

mpoules	*Without filters and processing*	*With filters and processing*
or less	D.Kr. 3.25 each	D.Kr. 5.50 each
-99	3.00 each	5.25 each
0 or more	2.75 each	5.00 each

When ordering, the customer must state the salinity of the sea ater. Water from the open ocean may simply be designated as cean water." The photosynthetic rate will be computed by the gency. In the case of brackish or fresh water, the customer must termine the total concentration of carbon dioxide in the water. ater samples for ^{14}C experiments should be taken with a glass, astic or other type of nonmetallic, nontoxic sampler.

Filtration apparatus, water samplers, field kits, filters, special ter holders, and other pertinent equipment are also available. rite to the Agency or to either Dr. John H. Ryther, Woods Hole ceanographic Institution, Woods Hole, Mass., U. S. A. or Prof. laxwell S. Doty, Botany Dept., University of Hawaii, Honolulu, . H.